



UCGE Reports

Number 20311

Department of Geomatics Engineering

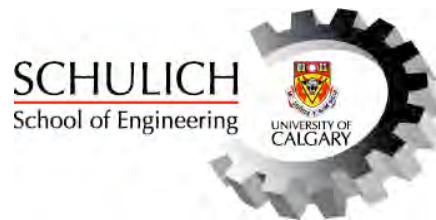
**Reliability of Combined GPS/GLONASS Ambiguity
Resolution**

(URL: <http://www.geomatics.ucalgary.ca/graduatetheses>)

by

Richard Ong

July 2010



UNIVERSITY OF CALGARY

Reliability of Combined GPS/GLONASS Ambiguity Resolution

by

Richard Ong

A THESIS

SUBMITTED TO THE FACULTY OF GRADUATE STUDIES
IN PARTIAL FULFILMENT OF THE REQUIREMENTS FOR THE
DEGREE OF MASTER OF SCIENCE

DEPARTMENT OF GEOMTICS ENGINEERING

CALGARY, ALBERTA

July 2010

© Richard Ong (2010)

Abstract

This thesis presents an analysis of the impact of combining GPS and GLONASS on the reliability of phase ambiguity resolution (fixing). The rate of correct fixes (i.e. the actual success rate) is investigated, as well as the identification of those fixes as correct or incorrect. Two reliability indicators – the predicted success rate and the F-test – are evaluated.

The processing software PLANSoft™ was developed to do GPS/GLONASS ambiguity resolution. GLONASS is incorporated either by partial fixing (only GPS) or full fixing (both GPS and GLONASS). Single- and dual-frequency strategies are also investigated.

Static analysis reveals that GLONASS full fixing increases actual success rate, fix reliability (using the F-test) and solution availability. The L1/L2 strategy similarly improves success rate and reliability. Widelane is effective for longer baselines due to the smaller effect of phase errors. Testing under overhead foliage induces cycle slips which decrease the observability of the ambiguities.

Acknowledgements

I would like to acknowledge the following persons and parties for their invaluable contributions to this thesis:

1. First and foremost, my family: my parents William and Nancy, my brother Jan, and my fiancée Leslie. Nothing in this world would be possible or worthwhile without your endless love, support and encouragement.
2. My supervisor, Professor Gérard Lachapelle. My internship, graduate studies and various research projects under your guidance and support have opened many doors, both to wisdom and to opportunity. Thank you for sharing your knowledge and your advice and your stories, and for giving me countless opportunities to push myself and develop new skills.
3. My co-supervisor, Professor Mark Petovello. I am grateful to you for both the volume of knowledge you passed on to me as well as the patience, perseverance and guiding hand with which you passed on that knowledge.
4. Research associates, past and present, from the PLAN Group with whom I have collaborated: Dr. Cillian O'Driscoll, Dr. Daniele Borio, Dr. Tom Williams, Dr. Valerie Renaudin, Mr. Rob Watson, Mr. Saurabh Godha and Mr. John Schleppe.

Many of the skills that I required for this research have been developed in one way or another through my collaborations with these individuals.

5. Those individuals involved with the STEALTH™ project for Alpine Canada, General Motors or the Crash Avoidance Metrics Partnership (CAMP): Professor Gérard Lachapelle, Aiden Morrison, Dr. Gerald Cole, James Perks, Dr. Tom Williams, Dr. Paul Alves and Dr. Chaminda Basnayake. Much of my theoretical and practical knowledge of ambiguity resolution has come from my involvement with these projects and individuals.
6. Those individuals who helped me collect data for this research: Professor Gérard Lachapelle, Dr. Tom Williams, Jared Bancroft, Billy Chan, Towfique Ahmed and Michelle Hua. Data collection is more effective and pleasant as a team effort.
7. Professor Kyle O'Keefe and Dr. Glenn MacGougan. Our discussions regarding RTK implementation details were invaluable to the design of PLANSoft™. I am also grateful to Professor Mark Petovello, Mr. Junjie Liu and all other developers of FLYKIN+™, from which much of the structure and implementation of PLANSoft™ was adapted.
8. The National Sciences and Engineering Research Council of Canada (NSERC), and the Alberta Informatics Circle of Research Excellence (iCORE) for their financial support.

Table of Contents

Abstract	ii
Acknowledgements	iii
Table of Contents	v
List of Tables	vii
List of Figures	x
List of Symbols and Abbreviations	xiv
CHAPTER ONE: INTRODUCTION	1
1.1 Background	1
1.2 Objectives	3
1.3 Thesis Outline	5
CHAPTER TWO: AMBIGUITY ESTIMATION AND RESOLUTION	7
2.1 Principles of Navigation and Ambiguity Estimation	7
2.1.1 Measurements	7
2.1.2 Ambiguity Estimation	10
2.1.3 Ambiguity Resolution	12
2.2 GLONASS Ambiguity Resolution	14
2.3 Reliability of Ambiguity Resolution	17
2.4 Ambiguity Resolution Success Rate	20
2.5 Fix Validation and the F Ratio Test	24
CHAPTER THREE: TESTING AND ANALYSIS METHODS	30
3.1 Test Scenarios	30
3.1.1 Static Baselines	30
3.1.2 Vehicle-to-Vehicle Relative Navigation	32
3.1.3 Downhill Ski Runs	35
3.2 Hardware Characteristics	38
3.3 Navigation Methodology: PLANSsoft™	41
3.4 Estimation Strategies	46

3.5 Convergence Time	50
3.6 Generating Integer Fixes.....	51
CHAPTER FOUR: STATIC TESTING RESULTS.....	53
4.1 Positioning Accuracy	54
4.2 Actual Success Rates	67
4.3 Float Estimate Errors before Ambiguity Resolution	71
4.4 Phase Errors	76
4.5 Success Rates under Simulated Reduced Visibility	80
4.6 Reliability Testing: Predicted Success Rate	91
4.7 Reliability Testing: F-Test	100
4.8 Combining Reliability Tests	106
4.9 Probability of Cycle Slip Detection	108
4.10 Reliability under Simulated Reduced Visibility	113
CHAPTER FIVE: KINEMATIC TESTING RESULTS.....	123
5.1 Vehicle-to-Vehicle Relative Navigation.....	123
5.1.1 Actual Success Rates and Reliability Testing	124
5.1.2 Positioning Accuracy.....	133
5.1.3 Signal Tracking and Cycle Slips under Foliage	138
5.2 Downhill Ski Runs.....	148
CHAPTER SIX: CONCLUSIONS AND RECOMMENDATIONS	159
6.1 Conclusions.....	160
6.2 Recommendations.....	163
REFERENCES	165

List of Tables

Table 1 - Errors in ambiguity resolution reliability testing and fault detection.....	19
Table 2 - F-test thresholds from central F distribution (significance level 10%)	29
Table 3 - Signal tracking for V2V in all environments	34
Table 4 - NovAtel OEMV2-G + NovAtel GPS-702-GG hardware: code multipath under open sky	40
Table 5 - Median position errors from correct fixes - 2 km baseline under 5° mask	57
Table 6 - RMS position errors from correct fixes - 2 km baseline under 5° mask	57
Table 7 - Median position errors from correct fixes - 18 km baseline under 5° mask	60
Table 8 - RMS position errors from correct fixes - 18 km baseline under 5° mask	60
Table 9 - Actual success rate probabilities - static baselines under 5° mask.....	68
Table 10 - Horizontal float errors before fix - static baselines under 5° mask	72
Table 11 - Total number of fixes - static baselines under 30° mask.....	81
Table 12 - Actual success rate probabilities - static baselines under 30° mask.....	81
Table 13 - Horizontal float errors before fix - static baselines under 30° mask	83
Table 14 - Predicted success rate results - 2 km baseline under 5° mask.....	92
Table 15 - Predicted success rate results for undifferenced phase 1σ of 6.5 mm - 2 km baseline under 5° mask	97
Table 16 - Predicted success rate results - 18 km baseline under 5° mask.....	98
Table 17 - F-test results - 2 km baseline under 5° mask.....	100
Table 18 - F-test power as a function of number of ambiguities	102
Table 19 - F-test results - 18 km baseline under 5° mask.....	104
Table 20 - Combined reliability testing results - 2 km baseline under 5° mask	107
Table 21 - Combined reliability testing results - 18 km baseline under 5° mask	107
Table 22 - Probability of cycle slip detection results - 2 km baseline under 5° mask....	112

Table 23 - Probability of cycle slip detection results - 18 km baseline under 5° mask ..	113
Table 24 - Predicted success rate results - 2 km baseline under 30° mask.....	114
Table 25 - Predicted success rate results - 18 km baseline under 30° mask.....	114
Table 26 - F-test results - 2 km baseline under 30° mask.....	118
Table 27 - F-test results - 18 km baseline under 30° mask.....	119
Table 28 - Combined reliability testing results - 2 km baseline under 30° mask	122
Table 29 - Combined reliability testing results - 18 km baseline under 30° mask	122
Table 30 - Total number of fixes - V2V all environments under 5° mask	124
Table 31 - Actual success rate probabilities - V2V all environments under 5° mask	126
Table 32 - Predicted success rate results - V2V open sky under 5° mask	128
Table 33 - Predicted success rate results - V2V foliage under 5° mask	129
Table 34 - F-test results - V2V open sky under 5° mask.....	130
Table 35 - F-test results - V2V foliage under 5° mask	130
Table 36 - Combined reliability testing results - V2V open sky under 5° mask	132
Table 37 - Combined reliability testing results - V2V foliage under 5° mask	132
Table 38 - Median position errors from correct fixes - V2V open sky under 5° mask ..	136
Table 39 - RMS position errors from correct fixes - V2V open sky under 5° mask	136
Table 40 - Median position errors from correct fixes - V2V foliage under 5° mask.....	137
Table 41 - RMS position errors from correct fixes - V2V foliage under 5° mask	137
Table 42 - Signal tracking for V2V in all environments	139
Table 43 - Signal tracking parameters for correct and incorrect L1 + L2 GG fixed GLO fixes - V2V foliage under 5° mask	142
Table 44 - Total number of fixes - downhill ski runs with all masks	149
Table 45 - Actual success rate probabilities - downhill ski runs with all masks	152
Table 46 - Predicted success rate results - downhill ski runs with 5° mask	153
Table 47 - Predicted success rate results - downhill ski runs with 30° mask	154

Table 48 - F-test results - downhill ski runs with 5° mask	155
Table 49 - F-test results - downhill ski runs with 30° mask	156
Table 50 - Combined reliability testing results - downhill ski runs with 5° mask.....	157
Table 51 - Combined reliability testing results - downhill ski runs with 30° mask.....	158

List of Figures

Figure 1 - Static baselines - base station	31
Figure 2 - Static baselines - rover station.....	31
Figure 3 - Vehicle-to-vehicle relative navigation - partly open sky	33
Figure 4 - Vehicle-to-vehicle relative navigation - under foliage.....	33
Figure 5 - Tracking downhill ski runs.....	36
Figure 6 - Vertical consistency of ski runs at checkpoints	37
Figure 7 - NovAtel OEMV2-G + NovAtel GPS-702-GG hardware: code and phase errors under an open-sky zero-baseline configuration.....	40
Figure 8 - NovAtel OEMV2-G + ANTCOM-GG hardware: code and phase errors from an open-sky kinematic test	41
Figure 9 - Example of SD to DD transformation.....	45
Figure 10 - Measurement combinations and fixing strategies	49
Figure 11 - Relationship between fix reliability and convergence time	50
Figure 12 - Data processing method for generating many integer fixes.....	52
Figure 13 - 2D view of position errors, all fixes - 2 km baseline under 5° mask	56
Figure 14 - 2D view of position errors, correct fixes - 2 km baseline under 5° mask	56
Figure 15 - 2D view of position errors, all fixes - 18 km baseline under 5° mask	59
Figure 16 - 2D view of position errors, correct fixes - 18 km baseline under 5° mask....	59
Figure 17 - Horizontal fixed errors vs. ADOP - 2 km baseline under 5° mask	62
Figure 18 - Horizontal fixed errors vs. ADOP - 18 km baseline under 5° mask	63
Figure 19 - Frequency distributions of ADOP - 18 km baseline under 5° mask	63
Figure 20 - L1 DD phase errors - static baselines.....	64
Figure 21 - Horizontal fixed errors vs. phase error standard deviation - 2 km baseline under 5° mask	66

Figure 22 - Horizontal fixed errors vs. phase error standard deviation - 18 km baseline under 5° mask	67
Figure 23 - GLONASS adjusted ambiguity uncertainties for L1 only GG float GLO solution - 2 km baseline under 5° mask	70
Figure 24 - Actual success rate vs. 3D fixed errors - 18 km baseline under 5° mask	70
Figure 25 - Actual success rate vs. median horizontal float errors - static baselines under 5° mask	73
Figure 26 - Actual success rate vs. horizontal float errors - 2 km baseline under 5° mask	75
Figure 27 - Actual success rate vs. horizontal float errors - 18 km baseline under 5° mask	76
Figure 28 - Distribution of phase error standard deviation for L1 only GG fixed GLO solution - 18 km baseline under 5° mask	77
Figure 29 - Actual success rate vs. phase error standard deviation - 2 km baseline under 5° mask	79
Figure 30 - Actual success rate vs. phase error standard deviation - 18 km baseline under 5° mask	79
Figure 31 - Distribution of phase error standard deviation for widelane GG fixed GLO solution - 18 km baseline under 5° mask.....	80
Figure 32 - Relationship between horizontal float error before fix and HDOP using L1 only GPS only solution - 2 km baseline	83
Figure 33 - Distribution of number of ambiguities for L1 only GPS only solution - 2 km baseline under 5° mask	85
Figure 34 - Distribution of number of ambiguities for L1 only GPS only solution - 2 km baseline under 30° mask	86
Figure 35 - Distribution of number of ambiguities for L1 only GG float GLO solution - 2 km baseline under 30° mask.....	86
Figure 36 - Distribution of number of ambiguities for L1 only GG fixed GLO solution - 2 km baseline under 30° mask.....	87
Figure 37 - Actual success rate vs. number of ambiguities - 2 km baseline under 30° mask	88
Figure 38 - Actual success rate vs. number of ambiguities - 18 km baseline under 30° mask	89

Figure 39 - Actual success rate vs. ADOP - 2 km baseline under 30° mask	90
Figure 40 - Actual success rate vs. ADOP - 18 km baseline under 30° mask	90
Figure 41 - Distribution of predicted success rate for L1 only GPS only solutions - 2 km baseline under 5° mask	94
Figure 42 - Predicted success rate as a function of <i>a priori</i> phase uncertainty	95
Figure 43 - Distribution of predicted success rate for widelane GG fixed GLO solution - 18 km baseline under 5° mask	99
Figure 44 - Distribution of F-test result for L1 only GPS only solution - 2 km baseline under 5° mask	103
Figure 45 - F-test correct fix acceptance vs. phase error standard deviation - 2 km baseline under 5° mask	104
Figure 46 - F-test correct fix acceptance vs. phase error standard deviation - 18 km baseline under 5° mask	105
Figure 47 - Time series of probabilities of cycle slip detection for L1 only GPS only solution - 2 km baseline under 5° mask	110
Figure 48 - Distribution of probabilities of cycle slip detection for L1 only GPS only solution - 2 km baseline under 5° mask	110
Figure 49 - Relationship between probability of cycle slip detection and predicted success rate for L1 only GPS only solution - 2 km baseline under 5° mask	111
Figure 50 - Relationship between probability of cycle slip detection and F-test result for L1 only GPS only solution - 2 km baseline under 5° mask	111
Figure 51 - Predicted success rate incorrect fix rejection vs. number of ambiguities - 2 km baseline under 30° mask	116
Figure 52 - Predicted success rate incorrect fix rejection vs. number of ambiguities - 18 km baseline under 30° mask	116
Figure 53 - F-test correct fix acceptance vs. number of ambiguities - 2 km baseline under 30° mask	119
Figure 54 - F-test correct fix acceptance vs. number of ambiguities - 18 km baseline under 30° mask	120
Figure 55 - F-test correct fix acceptance vs. ADOP - 2 km baseline under 30° mask ...	120
Figure 56 - F-test correct fix acceptance vs. ADOP - 18 km baseline under 30° mask .	121

Figure 57 - 2D view of position errors, all fixes - V2V open sky under 5° mask	133
Figure 58 - 2D view of position errors, correct fixes - V2V open sky under 5° mask ...	134
Figure 59 - 2D view of position errors, all fixes - V2V foliage under 5° mask	134
Figure 60 - 2D view of position errors, correct fixes - V2V foliage under 5° mask	135
Figure 61 - L1 DD code and phase errors - V2V all environments.....	140
Figure 62 - Actual success rate vs. lock time - V2V foliage under 5° mask	143
Figure 63 - Relationship between ADOP and convergence time for L1 only GPS only solution - V2V foliage under 5° mask	144
Figure 64 - Relationship between ADOP and convergence time for L1 only GG fixed GLO solution - V2V foliage under 5° mask	145
Figure 65 - Relationship between ADOP and convergence time for L1 + L2 GPS only solution - V2V foliage under 5° mask	145
Figure 66 - Predicted success rate incorrect fix rejection vs. lock time - V2V foliage under 5° mask	147
Figure 67 - Predicted success rate probability vs. lock time - V2V foliage under 5° mask	147
Figure 68 - F-test correct fix acceptance vs. lock time - V2V foliage under 5° mask....	148

List of Symbols and Abbreviations

Symbol	Definition
$\Delta(\bullet)$	Single-difference operator for quantity \bullet
$\nabla\Delta(\bullet)$	Double-difference operator for quantity \bullet
N	Phase ambiguities
Φ	Phase in units of distance
ϕ	Phase in units of cycles
λ	Phase wavelength

Abbreviation	Definition
ADOP	Ambiguity dilution of precision
DD	Double-difference
DOP	Dilution of precision
FDMA	Frequency division multiple access
GG	GPS/GLONASS
GLO	GLONASS
HDOP	Horizontal dilution of precision
ILS	Integer least-squares
LAMBDA	Least-squares ambiguity decorrelation adjustment
PDOP	Position dilution of precision

RTK	Real-time kinematic
SD	Single-difference
V2V	Vehicle-to-vehicle
WL	Widelane
WSSR	Weighted sum-of-squared residuals

Chapter One: Introduction

Differential carrier phase ambiguity resolution is a common technique for achieving sub-decimetre positioning accuracy with Global Navigation Satellite Systems (GNSS). If the ambiguities can be resolved to their correct integer values, the phase measurements can be used for ranging with millimetre-level precision. However, an incorrectly resolved ambiguity results in an undetected position bias. The reliability of positioning is thus directly related to the reliability of ambiguity resolution. This thesis investigates the impact of integrating the Russian Global Navigation Satellite System (GLONASS) with the Global Positioning System (GPS) on the reliability of ambiguity resolution.

1.1 Background

GNSS carrier phase measurements are generally very precise. Spatially correlated effects (such as orbit and atmosphere) and clock effects are removed or reduced by differencing measurements between receivers. The resulting *differential* phase precision is at the millimetre level; however differential ionospheric errors can sometimes exceed the metre level over long distances (over 100 km) between the two receivers when the ionosphere is disturbed (Cosentino et al 2006). However, the phase measurements also contain an unknown number of integer cycles. This *ambiguity* must be resolved (or *fixed*; the terms “ambiguity resolution” and “ambiguity fix” are used interchangeably herein) to the correct integer value before the phase can be used for high-precision ranging.

The importance of resolving the ambiguities correctly must be emphasized. An error of even one cycle on a single phase measurement can result in a position bias of many centimetres or decimetres (depending on the geometry). This bias often goes undetected as the position is generally assumed to be precise if the ambiguity is resolved correctly (even when that is not actually the case). The ambiguities must be highly observable in order to get initial real-valued (“float”) estimates that are accurate enough to be subsequently fixed to the correct integer (“fixed”) values.

The observability of the ambiguities is a fundamental challenge: phase measurements *alone* generally cannot observe them. Code and phase measurements together can observe them but differential code accuracy is at the decimetre level at best (Cosentino et al 2006). Observability of the ambiguities can be improved by using measurements taken over multiple epochs. As the position states converge to the true trajectory, the ambiguities become more observable by both code and phase, and will converge to their correct integer values as well. Observability can also be improved by using code and phase measurements from more satellites. This improves the position geometry and speeds up the convergence of the position and ambiguities. In addition, the accuracy after the ambiguities are resolved is marginally improved by averaging down noise and multipath and improving satellite geometry.

Ambiguity resolution is difficult in signal shaded environments like mountainous areas, and residential and inner city areas where trees and buildings obstruct lines-of-sight to the satellites. This significantly impacts the observability of both the position and the

ambiguities. Consequently, the ambiguities cannot be fixed to their correct integer values as often. GPS is frequently used alone but might not provide the adequate geometry. Other GNSS can be used to increase the number of available code and phase measurements. GLONASS is currently the only GNSS near full operational capability. Ambiguity resolution using GPS and GLONASS together has been widely investigated (e.g. van Diggelen 1997, Keong & Lachapelle 2000, Habrich et al 1999, Wang 2000). The focus of much of the literature is on algorithms for integrating GLONASS phase measurements (e.g. Wang 2000), or the effect of GLONASS on position accuracy and fix performance (e.g. van Diggelen 1997). It has generally been found that the addition of GLONASS improves positioning accuracy.

1.2 Objectives

It is difficult to resolve the phase ambiguities correctly all of the time and in all environments and field conditions, even when GPS and GLONASS are integrated. The consequence of resolving the ambiguities incorrectly is undetected position biases, hence it is critically important not to accept incorrect fixes. In that light, this thesis investigates the impact of adding GLONASS to GPS on the reliability of the ambiguity resolution process itself. *Reliability* in this context refers to the ability to reject incorrect ambiguity fixes, such that they do not introduce position biases. However the identification and acceptance of correct fixes is also important to achieve precise positioning. The objectives of this research are the following:

1. Determine how adding GLONASS impacts the rate of correct ambiguity fix. This is often referred to as the *actual success rate*. This effect is important to study as one way to reduce the rate of incorrect fix acceptance is to just reduce the rate of incorrect fixes.
2. Determine how adding GLONASS impacts the rate of acceptance of correct fixes and rejection of incorrect fixes. The *predicted success rate* and *F-test* reliability tests are described herein as methods of discriminating the correctness of fixes. The impact of GLONASS on the performance of these tests is investigated.
3. Characterize the factors that influence success rate and reliability. Different environments, restricted satellite visibility and the effect of ionosphere over longer inter-receiver distances are explored.

Much of the previous research in fix reliability has characterized it theoretically or using simulations (e.g. Teunissen 1998, Teunissen and Verhagen 2004, Teunissen et al 1999, Verhagen 2004, 2005, O'Keefe et al 2006). The scope of this research is fix reliability in three *real-world* scenarios: 1.) static baselines under open sky; 2.) platform-to-platform relative navigation under open sky and foliage; and 3.) tracking downhill skiers. Inter-receiver distances range from 10 m to 18 km (at which point ionosphere effects are studied). Restricted satellite visibility conditions are simulated by imposing circular elevation masks of up to 30°. Ambiguity resolution is performed repeatedly by fixing and then resetting the ambiguities. Special processing software (PLANSsoft™) was developed

to do the GPS/GLONASS ambiguity resolution, as well as generate the predicted success rate and F-test result. These tests are evaluated by determining how often they correctly identify correct and incorrect fixes.

The contribution of this research is characterizing the exact impact of GLONASS on fix reliability. This is evaluated by comparing the performance of GPS alone to that of GPS/GLONASS (GG). GPS and GLONASS are integrated in two ways: 1.) partial fixing of only GPS ambiguities; and 2.) full fixing of both GPS and GLONASS ambiguities. Different subsets of phase measurements – L1 only, L1 and L2 used separately, and L1 and L2 in the widelane combination – are also explored. To accomplish the above, PLANSoft™ was developed by the author and significant field testing was conducted.

1.3 Thesis Outline

This thesis consists of six chapters. Chapter One introduces the motivation and objectives of this thesis. The scope and contributions of the research are defined.

Chapter Two presents an overview of ambiguity estimation and resolution. The reliability of ambiguity resolution is discussed in detail. The predicted success rate and the F-test are introduced and their role in ambiguity estimation is discussed.

Chapter Three describes the testing, data processing and analysis methods. Three test scenarios are proposed: 1.) static baselines under open sky; 2.) platform-to-platform

navigation in urban environments; and 3.) downhill skiers on an open ski slope. The GLONASS navigation and ambiguity resolution algorithm (implemented in PLANSoft™) is described, and various strategies for incorporating measurements into ambiguity estimation are outlined. The methods and visual displays used to derive and analyze the ambiguity resolution results are also defined.

The results of the static baseline testing are presented in Chapter Four. This chapter investigates the impact of GLONASS and dual-frequency measurement combinations on the success rate, as well as the acceptance of correct fixes and the rejection of incorrect fixes. The causative and related factors are then investigated in detail, including: float solution errors; phase errors; number of ambiguity states; ambiguity dilution of precision; and the probability of cycle slip detection. These are illustrated to visually facilitate interpretation. An analysis of the fixed-ambiguity positioning accuracy is also provided.

The results of the two kinematic tests are presented in Chapter Five. This chapter gives an overview of the success rate and reliability of ambiguity resolution in these scenarios. The impact of foliage, particularly in terms of how signal tracking affects ambiguity resolution, is further investigated.

Chapter Six concludes this thesis and presents the major findings from the previous chapters. Recommendations for future research in this area are finally made.

Chapter Two: Ambiguity Estimation and Resolution

This chapter presents an overview of phase ambiguity estimation. The role of code and phase measurements in navigation using ambiguity estimation is described in detail. A review of ambiguity resolution methods from the literature is then presented, both in general and specific to the use of GLONASS. The reliability of ambiguity resolution is also discussed.

2.1 Principles of Navigation and Ambiguity Estimation

2.1.1 Measurements

GNSS provides two types of measurements for ranging and position estimation: code and phase measurements. These measurements have different properties:

1. Code measurements are derived from the pseudo-random noise (PRN) code overlaid on the carrier signal. Correlating the incoming PRN code with a locally generated replica gives an estimate of the signal delay. This delay can be converted into the satellite-to-user range; however it is affected by satellite and receiver clock errors. Atmosphere effects and orbit determination errors also impact the accuracy of the code measurement. The latter effects are spatially correlated, and are reduced by differencing measurements between two nearby GNSS receivers (often designated as *base and rover receivers or stations*). This

single-differencing (SD) technique also removes the satellite clock errors. Further refinement is done by differencing SD measurements between satellite pairs to remove receiver clock errors. Usually all of the satellite pairs share a common satellite, designated as the *base satellite*. The resulting *double-differenced* (DD) code measurement is parameterized as

$$\nabla\Delta P = \nabla\Delta R + \varepsilon_{\nabla\Delta P}$$

where “ $\nabla\Delta$ ” is the double-differencing operator,

$\nabla\Delta P$ is the DD code measurement,

$\nabla\Delta R$ is the DD satellite-to-user range, and

$\varepsilon_{\nabla\Delta P}$ is the DD code error.

The DD code measurement directly observes the DD satellite-to-user range, which is used to derive the vector between the base and rover receivers. Spatially correlated effects like the atmosphere are reduced in this manner. However, measurement noise and multipath do not cancel out; instead, they are additive when expressed as variances (Lachapelle 2008). The exact level of noise and multipath is highly dependent on receiver technology, signal strength and reflector type. However, code chips are generally hundreds of metres long, ultimately limiting the precision of the derived signal delay. Conley et al (2006) gives a typical stand-alone error budget of 10 cm and 20 cm for noise and

multipath, respectively. For SD or DD processing these budgeted errors must be multiplied by $\sqrt{2}$.

2. Phase measurements are derived from the Doppler frequency of the carrier signal itself. Correlating the incoming carrier with a locally generated replica gives an estimate of the carrier's Doppler frequency. This frequency is a measure of the satellite-to-user relative velocity. The Doppler frequency induces a change in the phase of the carrier; integrating these phase changes over time gives the total *change* in the satellite-to-user range since the start of integration. Therefore the phase does not measure the *absolute* range, but contains an *ambiguity* that (when expressed in carrier cycles) is integer in nature.

Like the code, the phase is affected by clock errors, atmospheric effects and incorrect orbit determination. The double-differenced parameterization (which removes or reduces these effects) is expressed as

$$\nabla\Delta\Phi = \nabla\Delta R + \lambda_i \nabla\Delta N + (\lambda_i - \lambda_{base}) \Delta N_{base} + \varepsilon_{\nabla\Delta\Phi}$$

where “ Δ ” is the single-differencing operator,

$\nabla\Delta\Phi$ is the DD phase (expressed in units of distance),

$\nabla\Delta N$ is the DD phase ambiguity,

ΔN_{base} is the base satellite's SD phase ambiguity,

λ_i is the wavelength of the signal from the i^{th} satellite

λ_{base} is the wavelength of the signal from the base satellite, and

$\varepsilon_{\nabla\Delta\Phi}$ is the DD phase error.

The precision of DD phase measurements is much better than that of the code measurement due to the shorter carrier wavelength. Phase noise is nominally on the order of 1-2 mm, while the typical phase multipath 1σ level is around 2 cm in benign environments (Lachapelle 2008).

If velocity estimation is required, it can be achieved either by differentiating positions over time, or using the un-integrated Doppler frequency of the carrier.

2.1.2 Ambiguity Estimation

To use phase measurements for positioning, it is necessary to estimate the phase ambiguities. Ideally they are estimated as integers in the process of *integer ambiguity resolution* or *ambiguity fixing*. However they can also be estimated as real or “floating-point” values in the process of *float ambiguity estimation*. There are two approaches to ambiguity estimation (e.g. O’Keefe et al 2009):

1. *Geometry-based approach.* The DD measurements are used to estimate the position (more correctly, the vector between the base and rover receivers) along with the ambiguities until the latter can be resolved.
2. *Geometry-free approach.* Each DD measurement is used to estimate the corresponding DD satellite-to-user range and ambiguity. Different DD measurements are treated independently until the ambiguities can be resolved, at which point the DD phase measurements are used to estimate the positions.

In both approaches, the phase measurements generally cannot be used alone to estimate the ambiguities since they cannot simultaneously observe the position and ranges. The code measurements must be used in conjunction, which is a limiting factor in ambiguity estimation. Even with sub-metre code noise and multipath, a single epoch of code and phase measurements is generally not enough to do float ambiguity estimation to better than half a wavelength (e.g. for the L1 band, less than 10 cm; for the L2 band, less than 13 cm). As a rule of thumb, this is the accuracy required to resolve the ambiguities correctly and reliably. This problem is overcome by taking advantage of the fact that phase ambiguities remain constant over time if phase lock is maintained, i.e. there are no cycle slips. Thus the ambiguities can be estimated using measurements over multiple epochs.

The estimation is more effective if there is also *a priori* knowledge of the position or the satellite-to-user ranges. For kinematic applications the position (or range) and

ambiguities can both be constrained in a filter (such as a Kalman filter) designed and tuned for the expected dynamics. Within such a filter, the position (or range) and ambiguity estimates are said to *converge* to their true values as the measurement errors are smoothed out.

2.1.3 Ambiguity Resolution

Ambiguity resolution is an *integer estimation* problem. Therefore, standard linear estimators such as parametric least-squares cannot be used to estimate the integer ambiguities. Solving for the integer ambiguities is conceptually defined as a three-step process (Teunissen 2003): 1.) estimate the float ambiguities; 2.) map the float ambiguities to integer values, and validate those integers; and 3.) adjust the float estimate of the position. If the integer ambiguity estimate is correct, then the phase measurements can directly observe the satellite-to-user ranges (and consequently the user's position) with up to millimetre-level precision.

The most basic ambiguity resolution methods are *integer rounding* and *bootstrapping*. In integer rounding, each real-valued ambiguity is rounded to the nearest integer. Bootstrapping is a variation of integer rounding: after one ambiguity is rounded to the nearest integer, the real-valued estimates of the remaining unrounded ambiguities are corrected according to their correlation with the first ambiguity (Teunissen 2003).

More sophisticated ambiguity resolution methods have been listed and classified by Yang et al (2006). The most common class of ambiguity resolution method is the *search* method. Han & Rizos (1996) define searching techniques in three domains: 1.) the measurement domain; 2.) the position domain; and 3.) the ambiguity domain. In each case a “search space” of candidate values is defined for the parameter in the search domain. The candidates in the search space are discriminated (according to some criteria) and the one corresponding to the “best” estimate of the integer ambiguities is chosen.

The *integer least-squares* (ILS) method has been demonstrated as the optimal search method in terms of maximizing the probability of correct fix (Teunissen 2001a, 2003). Float estimation with a geometry-based model is used to initialize a search space over the integer ambiguities. ILS then seeks to minimize the weighted sum of squared *ambiguity residuals*, or the distances between the (initial) float and (final) integer ambiguity estimates (Teunissen 2000b). Other search methods include the ambiguity function method (Counselman & Gourevitch 1981, Mader 1992), the Fast Ambiguity Search Filter (FASF) (Chen & Lachapelle 1995), and the Fast Ambiguity Resolution Approach (FARA) (Frei & Butler 1990).

Pre-processing of the ambiguities has also been investigated with positive results in terms of reducing search spaces. The most important of these is the Least-Squares Ambiguity Decorrelation Adjustment (LAMBDA), which applies a linear transformation to the ambiguities to decorrelate them for more efficient searching (Teunissen 1995). Cholesky

decomposition of the variance-covariance matrices was also proposed by Landau & Euler (1992) as a way to reduce the search space.

2.2 GLONASS Ambiguity Resolution

Resolving GLONASS phase ambiguities is difficult due to the frequency division multiple access (FDMA) structure of the GLONASS signal. The DD phase parameterization is reiterated here:

$$\nabla \Delta\Phi = \nabla \Delta R + \lambda_i \nabla \Delta N + (\lambda_i - \lambda_{base}) \Delta N_{base} + \varepsilon_{\nabla \Delta\Phi}.$$

For GPS measurements, the term $(\lambda_i - \lambda_{base})$ is zero since each satellite transmits on the same frequency. The term $\nabla \Delta N$ is the only ambiguity that needs to be estimated. This is the DD phase ambiguity and is integer in nature. For GLONASS this is not the case since each satellite transmits its signals on a different frequency. The maximum wavelength difference between signals from different satellites is 0.9 mm (in the L1 band) and 1.1 mm (in the L2 band). Therefore, there are two ambiguity terms to consider: $\nabla \Delta N$, the DD phase ambiguity; and ΔN_{base} , the SD phase ambiguity of the GLONASS base satellite. Both ambiguities are integer in nature. However, if the frequency division of the signals is ignored, then the base satellite SD ambiguity is effectively absorbed by the DD ambiguity and the resulting quantity $(\lambda_i \nabla \Delta N + (\lambda_i - \lambda_{base}) \Delta N_{base})$ is *not* integer in nature.

Several methods to overcome this problem have been presented in the literature. Some of the major results and innovations include:

- Keong & Lachapelle (2000) investigated GPS/GLONASS real-time kinematic (RTK) processing for short-baseline attitude determination. The primary innovation was the use of a common oscillator to drive both GNSS receivers. This made double-differencing unnecessary as the clock errors between the two receivers were only separated by a constant offset. Once the offset was calibrated (using the residuals), SD measurements were used estimate and resolve the SD phase ambiguities.
- Wang (2000) attempted to estimate the SD ambiguity of the GLONASS base satellite using code-minus-carrier. This rough estimate was refined by doing a search over the adjacent integers, using test statistics to choose the integer.
- Habrich et al (1999) used SD measurements to do float ambiguity estimation in a geometry-based approach – i.e. the position and ambiguities were estimated together with the latter estimated as real values. This produced an estimate of the SD ambiguity of the GLONASS base satellite. DD ambiguities were then derived by a linear transformation of the SD ambiguities.
- van Diggelen (1997) compared two RTK approaches: dual-frequency GPS-only and single-frequency GPS/GLONASS. It was found that the GPS/GLONASS

approach resulted in faster ambiguity resolution for baselines less than 1 km in length, while the dual-frequency approach was faster for longer baselines.

- Takac (2009) noted that the sensitivity to errors in the estimate of the GLONASS base satellite SD ambiguity is low. For the GLONASS L1 band, the worst-case error in the DD ambiguity is 4.6 mm per metre of error in the base satellite SD ambiguity. It follows that at least 40 m of error in the base satellite ambiguity can be tolerated before inducing a half-cycle error in the DD ambiguity.
- Other methods that have been proposed include scaling the GLONASS phase measurements to the GPS wavelength (Kozlov & Tkachenko 1998), scaling the measurements to “common” wavelengths on the order of μm (Rossbach 2000), and introducing a constant “system bias” for single-differenced phase measurements (Leick et al 1998). Leick (1998) gives an overview of some of these workarounds.

Another side effect of GLONASS FDMA is that all GNSS measurements contain frequency-dependent biases related to the hardware or receiver architecture (Takac 2009, Boriskin & Zyryanov 2008, Kozlov et al 2000). These are often calibrated and minimized by receiver manufacturers. Any residual biases will cause problems in double-differencing as the biases will not cancel out, leaving *inter-frequency biases*. This becomes a concern when using receiver types of different brands, as the biases can have a

larger effect than noise and multipath (Kozlov et al 2000) and can exceed one half-cycle in some cases (Takac 2009).

Pre-mission calibration of receiver pairs over a zero baseline has been proposed by Takac (2009); however this does not address residual biases caused by inconsistency between units. Kozlov et al (2000) suggests partial fixing of the ambiguities known to be unbiased, which implies fixing only GPS ambiguities. Inter-frequency biases have a minimal impact in this thesis as only one family of receivers is used; however the idea of partial fixing will be investigated in great detail.

2.3 Reliability of Ambiguity Resolution

The correctness of the integer ambiguity estimates is a paramount factor in ambiguity resolution. However, the *reliability* of the ambiguities is also an important consideration. Ambiguity resolution can be evaluated by various *reliability tests* that indicate (to a certain level of confidence) how likely it is that a correct integer estimate could be found, or whether or not an actual estimate is thought to be correct. Two of these reliability tests are described in subsequent sections.

Evaluating the reliability of ambiguity resolution can be thought of as a hypothesis test (although not all reliability tests are statistical tests). The null hypothesis is that the correct integer estimate cannot be determined. That is, no candidate integer set is *sufficiently more likely* to be correct than any other candidate integer set. The alternative

hypothesis is the logical negation of this null hypothesis. This gives rise to two types of errors that reliability testing might not detect:

1. A Type I error occurs when a true null hypothesis is rejected. For reliability testing, this occurs when a correct integer estimate really cannot be determined (the true null hypothesis) but the reliability test indicates that a correct estimate can be found (the rejection of the hypothesis). *As a result*, the user will proceed to find a “correct” estimate, which is overwhelmingly likely to be actually incorrect (only one integer set out of the many candidates can be correct). The user has false confidence in the incorrect ambiguities and accepts an *undetected bias* in the position.
2. A Type II error occurs when a false null hypothesis is accepted. For reliability testing, this occurs when a correct integer estimate really can be determined (the false null hypothesis) but the reliability test indicates that a correct estimate cannot be found (the acceptance of the hypothesis). *As a result*, the user will not try to find an integer estimate at all (even though a correct estimate can be found). The ambiguities are not used to refine the position estimate, and it remains a “float” estimate. The user accepts a *loss of precision* in the position.

The end results of Type I and II errors are described by Verhagen (2004) as “failure” and “false alarm”, respectively. These are similar to the results of measurement fault detection: undetected biases from not detecting a present fault, or loss of precision from

detecting an absent fault. Table 1 shows the relationship between the errors that can be made in reliability testing for ambiguity resolution and fault detection for navigation.

Table 1 - Errors in ambiguity resolution reliability testing and fault detection

	Fix reliability testing	Fault detection
Error: Undetected biases ("failure")	A correct integer estimate really cannot be determined ... But reliability test indicates a correct estimate can be found ... <i>As a result,</i> (incorrect) integer estimate is identified and used	There is actually a measurement fault present ... But fault detection test does not detect the fault ... <i>As a result,</i> faulty measurement is used
Error: Loss of precision ("false alarm")	A correct integer estimate really can be determined ... But reliability test indicates a correct estimate cannot be found ... <i>As a result,</i> correct integer estimate is not identified and used	There is no measurement fault present ... But fault detection detects a fault anyway ... <i>As a result,</i> measurement with detected fault is rejected

It is impossible to minimize both undetected biases and loss of precision. From a navigation reliability point of view, an undetected bias is highly detrimental because the estimated accuracy of the position is often much higher than the actual accuracy. For ambiguity resolution this is compounded by two factors: 1.) incorrect fixes can be common especially in more challenging signal environments; 2.) applications that use ambiguity resolution often require centimetre-level accuracy, so there is very little tolerance for biases.

The reliability tests used in this thesis – predicted success rate and the F-test – can be tuned to reject more incorrect fixes, i.e. detect and reject more biases. However, this comes at the expense of rejecting more correct fixes, i.e. more loss of precision. This may lengthen the time to successful ambiguity resolution, which is a fairly important consideration especially for kinematic applications. Although only a single successful fix is required in the absence of cycle slips, in some environments cycle slips can happen frequently. In this thesis, both correct fix acceptance and incorrect fix rejection will be considered when evaluating reliability testing.

2.4 Ambiguity Resolution Success Rate

Success rate is another term for the rate of correct ambiguity resolution. In the context of navigation reliability, it would be ideal to know how often the ambiguities are correctly fixed. This implies knowledge of the *actual* success rate. However, since it is impossible to detect all instances of incorrect fix (without an external truth solution with sub-decimetre accuracy), the actual success rate for any field test is unknown.

However, whenever the ambiguities are about to be resolved, the success rate of that instance of ambiguity resolution can be predicted. Conceptually, this quantity – the *predicted* success rate – comes from integrating over the probability density function (PDF) of the ambiguities (Teunissen 2000a). The predicted success rate is often expressed as a probability value (i.e. ranging from zero to one) and depends on the following three factors (Teunissen et al 1999):

1. *The measurement model.* The type of model (geometry-based or geometry-free) affects the success rate. For the former, the satellite geometry affects the precision of the estimated positions and ambiguities and impacts the predicted success rate.
2. *The stochastic model.* The predicted success rate is based on the PDF of the ambiguities. This is often represented by the precision of the ambiguities, which can be estimated from the precision of the code and phase measurements.
3. *The integer estimation method.* The success rate is affected by the “pull-in region” of the ambiguities (Verhagen 2005) which is the range over which different float ambiguity estimates will converge to the same integer estimate (Teunissen 2001a). Different integer estimation methods have different pull-in regions and therefore different success rates. Another technique is LAMBDA, which is applied to the ambiguities to de-correlate the ambiguities and reshape their PDF.

Teunissen (1998) has defined an exact formula for predicting the success rate of the bootstrapping method, which has been shown to work nearly optimally when LAMBDA is applied beforehand. Verhagen (2005) uses this as a lower bound for the optimal estimation method (integer least-squares) and shows that it follows the actual success rate to within a probability level of 0.07 over a range of ionospheric standard deviations and different numbers of satellites. This lower bound is defined as

$$P_L = \prod_{i=1}^n \left(2\Phi\left(\frac{1}{2\sigma_{i|I}}\right) - 1 \right)$$

where P_L is the predicted success rate lower bound,

$\sigma_{i|I}$ is the standard deviation of the i^{th} ambiguity after the previous $i - 1$ ambiguities have been fixed, and
 $\Phi(x)$ is the integral of the standard normal distribution from $-\infty$ to x .

Teunissen (2001a) has defined an upper bound for the predicted success rate of integer-least squares, based on the ambiguity dilution of precision (ADOP). This DOP quantity is not the same as other DOP values like horizontal or vertical DOP. Teunissen (2001a) defines it conceptually as the geometric mean of the ambiguity uncertainties, expressed in units of phase. The ADOP is defined as

$$\text{ADOP} = \left(\det(Q_{\hat{N}}) \right)^{\frac{1}{2n}}$$

where $Q_{\hat{N}}$ is the variance-covariance matrix of the real-valued ambiguities, and n is the number of ambiguities.

The ADOP metric essentially combines the precision and geometry of the phase measurements. It also defines the upper bound of the predicted success rate, as

$$P_U = \frac{\left[\frac{n}{2} \cdot \left(\Gamma\left(\frac{n}{2}\right) \right) \right]^2}{\pi(ADOP^2)}$$

where P_U is the predicted success rate upper bound, and

$\Gamma(x)$ is the gamma function at x .

Other approximations of the predicted success rate can be found in Teunissen (1998), Teunissen et al (1999) and Verhagen (2005). Because the predicted success rate is an *a priori* metric, it can be an optimistic measure. Hence this thesis implements the predicted success rate *lower bound* P_L and investigates whether this approximation of the predicted success rate helps to identify which fixes are likely correct, and which are likely incorrect. There are several considerations that must be taken into account when using the predicted success rate:

- The predicted success rate is an *a priori* metric as it only depends on the float ambiguity uncertainties. Therefore the predicted success rate can only be used as a measure of confidence in the ability to *validate* integer ambiguity estimates (as demonstrated in the next section). It cannot actually be used to validate the integer estimate itself.

- The float ambiguity uncertainties are partly a function of differential code accuracy, consisting of noise, multipath and residual atmospheric effects. The non-stochastic, non-Gaussian nature of multipath is not taken into account, which will affect how closely the predicted success rate follows the actual success rate.
- The predicted success rate lower bound is based on the estimated uncertainties of the ambiguities, which should be on the order of fractional cycles when doing integer estimation. If there is a bias in the estimated value of the ambiguities, this will not be reflected in the predicted success rate. For example, the predicted success rate can be very high (even close to one) but the actual success rate with a one-cycle bias is essentially zero. Therefore the predicted success rate does not capture the negative effect of phase biases (Teunissen 2001b).

The rate of *incorrect* fix will occasionally be referred to as *failure rate* for the sake of brevity. For other studies involving predicted success rate with GPS and GLONASS and Galileo, refer to O'Keefe et al (2006, 2009).

2.5 Fix Validation and the F Ratio Test

Fix validation – determining whether the “most likely” integer estimate of the ambiguities is actually correct – is a crucial step in ambiguity resolution. For the ILS estimation method, statistical hypothesis testing of the measurement or ambiguity residuals has been widely used for fix validation. This is valid under the assumption of

measurement data with normally distributed errors which, when passed through a linear estimator results in normally distributed parameter errors. However, this is not the case for integer estimation as the integer parameters are not normally distributed (Verhagen 2005). As well, GNSS measurement errors are generally not normally distributed due to multipath and atmospheric effects.

Regardless, some statistical tests have been developed with satisfactory performance (e.g. Teunissen & Verhagen 2004, Verhagen 2004, 2005). The statistics used for these tests are generally based on computing the weighted sum of squared residuals (WSSR). Verhagen (2004) defines three WSSR quantities. The first two are based on the phase measurement residuals and the third is based on the *ambiguity residuals*, which are the differences between the initial (float) and final (fixed) ambiguities.

$$\hat{\Omega} = \hat{e}^T Q_y^{-1} \hat{e}$$

$$\check{\Omega} = \check{e}^T Q_y^{-1} \check{e}$$

$$R = (\hat{a} - \check{a})^T Q_{\check{a}}^{-1} (\hat{a} - \check{a})$$

where \hat{e} are the phase residuals based on the *float* ambiguities,

\check{e} are the phase residuals based on the *fixed* ambiguities,

$(\check{a} - \hat{a})$ are the ambiguity residuals,

Q_y is the variance-covariance matrix of the phase measurements, and

$Q_{\hat{a}}$ is the variance-covariance matrix of the float ambiguities.

The process of choosing which integer estimates are “likely” to be correct is called *identification*. An example of an identification test based on WSSR quantities is given below (Verhagen 2004). Conceptually, the WSSR quantities of an integer estimate represent the errors associated with that estimate. Therefore an identification test statistic based on WSSR can be thought of as a measure of an integer estimate’s likelihood, with more likely estimates having smaller test statistics. The “most likely” integer estimate should both pass the following identification test and have the smallest test statistic:

$$\frac{\left(\frac{R}{n}\right)}{\left(\frac{\hat{\Omega}}{m-n-p}\right)} < K$$

where m is the number of measurements,

n is the number of ambiguities,

p is the number of position states, and

K is the identification test threshold.

Once the most likely integer estimate is identified, fix validation in the form of *discrimination testing* can be done. Because it is possible for multiple integer estimates to pass the identification test, the most likely estimate must be *sufficiently more likely* than

the “second-most likely” estimate. A comprehensive review of discrimination tests can be found in Verhagen (2004).

The most common class of discrimination test is the F ratio test (or the F-test for short). The concept behind the F-test is that WSSR-based test statistics approximately represent likelihood of correctness. Therefore the ratio between two statistics can be thought of as the difference in likelihood. The standard form of the ratio test is defined by Verhagen (2004) as

$$\frac{\check{\Omega}_2}{\check{\Omega}_1} > K$$

where $\check{\Omega}_1$ is computed from the most likely integer estimate,

$\check{\Omega}_2$ is computed from the second-most likely integer estimate, and

K is the F-test threshold.

An alternate form of the ratio test is the following (Euler & Schaffrin 1990):

$$\frac{R_2}{R_1} > K$$

For both forms of the ratio test, the null hypothesis is that a correct integer estimate *cannot* be determined. That is, $\check{\Omega}_1$ and $\check{\Omega}_2$ (or R_1 and R_2) cannot be discriminated from

one another. Verhagen (2004) develops a basis for hypothesis testing by assuming that if the null hypothesis is true, then the ratio statistic is distributed according to a central F distribution. That is, the weighted phase residuals (for the standard form) or weighted ambiguity residuals (for the alternative form) for both the most likely and second-most likely integer estimates are zero-mean. In practice, this assumption is invalid: Leick (2004) correctly notes that both the numerator and denominator of the ratio statistic are distributed according to non-central χ^2 distributions, so the ratio is distributed according to the doubly non-central F distribution. However, the assumption of centrality is often used for simplicity.

The alternative hypothesis is that a correct integer estimate *can* be determined. That is, $\check{\Omega}_1$ and $\check{\Omega}_2$ (or R_1 and R_2) can be discriminated from one another. The F-test is therefore distributed according to a singly non-central F distribution. That is, the weighted residuals for the most likely integer estimate are zero-mean, and the weighted residuals for the second-most likely integer estimate are *not* zero-mean. The non-centrality parameter of the singly non-central F distribution is defined as

$$\delta_0 = \sum_i^n \left(\frac{\mu_i}{\sigma_i} \right)^2$$

where μ_i is the mean (i.e. bias) in the i^{th} phase measurement or ambiguity, and

σ_i is the uncertainty in the i^{th} phase measurement or ambiguity.

In this thesis, fix validation will be investigated using the alternate form of the F-test, as it is commonly implemented and is easy to generate from the by-products of ambiguity resolution. Verhagen (2004) emphasizes that there are no thresholds with sound theoretical bases. Under the (invalid) assumption of the centrality of the ratio distribution under the null hypothesis, the F-test threshold is taken from the central F distribution at the desired significance level and with degrees of freedom equal to the number of ambiguities. Alternatively, several constant thresholds have been proposed in the literature: e.g. 2.0 (Landau & Euler 1992); 3.0 (Leick 2004); and 4.23 (Verhagen 2004). However, a variable threshold based on the central F distribution is useful as it adapts to the number of ambiguities. Table 2 shows the threshold for various numbers of ambiguities using a significance level of 10%. The ability of the F-test to reject incorrect fixes (or in terms of navigation reliability, *reject and detect biases*) will be particularly highlighted as the F-test results are derived from actual measurement data.

Table 2 - F-test thresholds from central F distribution (significance level 10%)

Number of ambiguities	F-test threshold	Number of ambiguities	F-test threshold
5	3.45	9	2.44
6	3.05	10	2.32
7	2.78	11	2.23
8	2.59	12	2.15

Chapter Three: Testing and Analysis Methods

This chapter describes the testing, data processing and analysis methods used in this thesis. A description of the field testing is given, including the test scenarios that were investigated and the hardware that was used. The processing and analysis methodologies are then explained in detail.

3.1 Test Scenarios

Fix reliability was investigated using real GNSS measurement data collected in the city of Calgary and the surrounding areas. These tests are categorized under the following three scenarios.

3.1.1 Static Baselines

GNSS receivers and antennas were set up on a pair of static points (e.g. see Figure 1 for base station and Figure 2 for rover station). The baseline was surveyed for at least 24 hours, with measurement data recorded at a rate of 1 Hz. The true coordinates of the base station were known, while the true coordinates of the rover station were initially unknown. The latter coordinates (i.e. the “truth” or “reference” solution) were determined with centimetre-level accuracy by computing RTK fixed-ambiguity solutions at every epoch, then averaging all of those position solutions.



Figure 1 - Static baselines - base station



Figure 2 - Static baselines - rover station

Two baselines were surveyed for this thesis. Both shared the same base station (which was under open sky) and had different rover stations (which were both also under open sky). The length of the first baseline was 2 km, while the length of the second baseline was 18 km. Although the baselines were static in this scenario, they were processed in

kinematic mode – that is, epoch-to-epoch processing with the position allowed to move in order to provide a more refined accuracy analysis.

3.1.2 Vehicle-to-Vehicle Relative Navigation

A two-vehicle road test was conducted in the Mount Royal residential area in Calgary. GNSS receivers and antennas were mounted on each vehicle. The application tested here was relative navigation; instead of generating a fixed-ambiguity solution for each vehicle using separate static stations, the *inter-vehicle* vector and velocity were directly estimated in a *moving baseline* approach. The vehicles were separated by a maximum of 300 m. The road test lasted 97 minutes, with measurement data collected at a rate of 2 Hz. There were two major environment sky coverage types encountered in this test:

1. Approximately half of the test (49 minutes) was conducted under open sky conditions. This environment is illustrated by Figure 3. There was some occasional tree coverage that was unavoidable; for example, in Figure 3 there are trees by the side of the road.

2. The other half of the test (49 minutes) was conducted mainly under foliage. This environment is illustrated by Figure 4. Canopies extend above the road, sometimes resulting in near-total coverage.



Figure 3 - Vehicle-to-vehicle relative navigation - partly open sky



Figure 4 - Vehicle-to-vehicle relative navigation - under foliage

Table 3 quantifies the effects of the sky coverage types on signal tracking in this environment. The following observations are made:

- One would expect that the mean C/N₀ would drop under foliage but this is not the case. The hardware that was used was geodetic grade, not high sensitivity. The

mean number of satellites tracked was significantly lower under foliage; this suggests that the weaker signals were simply not tracked.

- The impact of foliage on signal lock is significant. The mean lock time under open sky approached 10 minutes, while the mean lock time under foliage was less than two minutes for all signals. Because signal lock was lost on average every minute or two, the ambiguities were reset very often. This affected the ability to estimate them over time. The rate of detected cycle slips also increased marginally under foliage.

Table 3 - Signal tracking for V2V in all environments

		Partly open sky		Foliage	
		L1	L2	L1	L2
Mean C/N₀ (dB-Hz)	GPS	47	40	47	40
	GLONASS	46	40	47	42
Mean signal lock time (min:sec)	GPS	7:36	7:38	0:57	1:03
	GLONASS	8:20	8:08	1:46	1:52
Rate of cycle slips detected	GPS	0.01%	0.00%	0.05%	0.01%
	GLONASS	0.06%	0.04%	0.02%	0.11%
Mean number of satellites tracked	GPS	7		6	
	GLONASS	4		3	
Mean number of satellites available above 5° elevation	GPS	7		5	
	GLONASS	4		3	

The *reference* or *truth* trajectory (i.e. the true inter-relative vehicle vectors at every epoch) was obtained using a GPS/INS solution. A NovAtel SPAN-CPT integrated GPS/INS (OEMV3 receiver with 20°/hr gyros) was mounted on the lead vehicle; on the trailing vehicle, a Honeywell HG1700 tactical grade inertial sensor integrated with a NovAtel OEM4 receiver was used. Position solutions for both vehicles were generated with the Waypoint Inertial Explorer™ post-processing software using forward-backward smoothing. The individual vehicle solutions were then differenced to form the relative solutions. The availability of solutions with estimated 1σ horizontal accuracies at the sub-decimetre level is 98% under open sky and 72% under foliage.

3.1.3 Downhill Ski Runs

A ski test consisting of a series of seven downhill runs was conducted at the Nakiska ski resort in February 2010. The ski slope used was situated under open sky with mask angles of up to 20° from the slope itself. The skier, shown in Figure 5, wore a backpack with the antenna mounted on his helmet. Each downhill run lasted four to eight minutes, with measurement data collected at a rate of 2 Hz.



Figure 5 - Tracking downhill ski runs

The application tested here was the relative consistency of the ski runs. Two aspects of this application are explained here:

1. A static base station was set up less than two kilometres away from the skier. An average of single-point solutions generated over the course of the test was used for the coordinates of the base station. Due to the proximity of the base to the rover (i.e. the skier), precise coordinates are not required for the base to maintain the precision of the base-to-rover vector. Since the base station is the same for all the ski runs, their consistency can be evaluated by comparing their respective base-to-rover vectors.

2. The truth trajectory (i.e. the base-to-rover vectors) was generated using GPS/GLONASS RTK with forward/backward smoothing. The relative consistency of the ski runs was used to verify this truth trajectory. Checkpoints (consisting of a flagged nail in the snow) were set up at the top and bottom of the ski slope. At the beginning and end of each ski run, the skier stood at these checkpoints for 20 to 30 seconds, and in the same body position, such that the antenna was approximately at the same height. Figure 6 shows that the truth trajectory at the check points was vertically consistent to the sub-decimetre level, validating them *at the top and bottom of the slope*. Additionally, there were no sudden discontinuities in the truth trajectory in between the top and bottom of the slope, validating them *for the entire slope*.

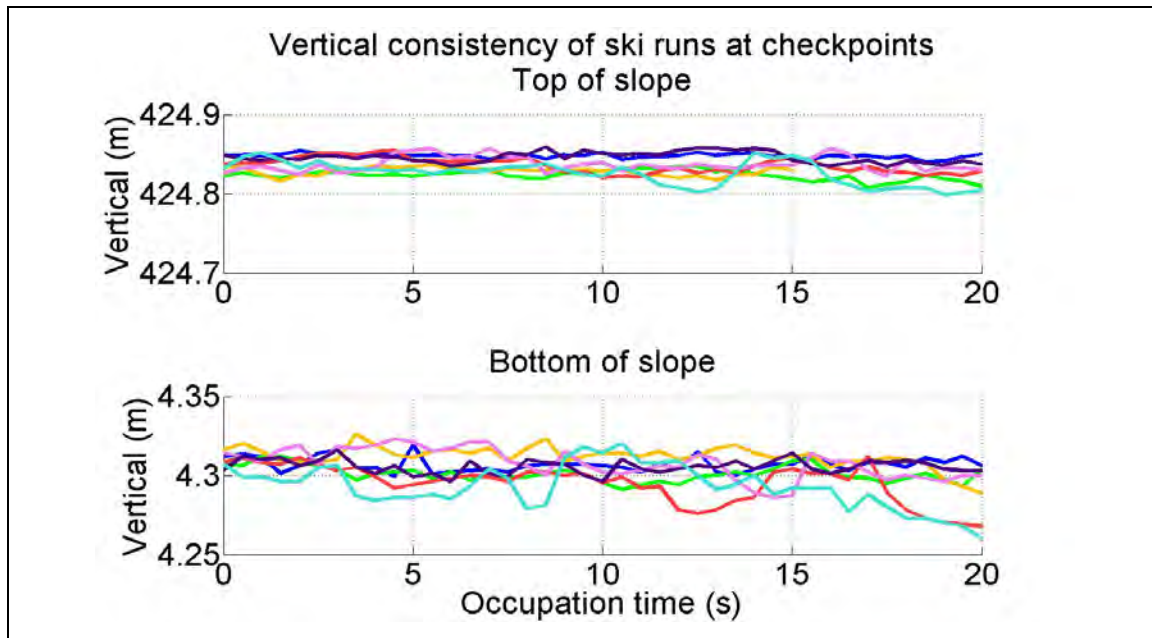


Figure 6 - Vertical consistency of ski runs at checkpoints

3.2 Hardware Characteristics

Field tests were conducted using identical receiver pairs, with base and rover stations both equipped with NovAtel OEMV2-G receivers. These are geodetic-grade GNSS receivers, capable of tracking GPS and GLONASS signals in their respective L1 and L2 bands. The Vision Correlator technology (Fenton & Jones 2005) is implemented to reduce code multipath. Two types of antennas were used with this receiver: 1.) the NovAtel GPS-702-GG antenna, in the static and vehicle navigation test scenarios; and 2.) the ANTCOM-GG antenna, in the downhill ski run test scenario. One of these receivers was housed in a STEALTH™ unit (Lachapelle et al 2009).

The quality of the OEMV2-G + GPS-702-GG receiver-antenna combination was assessed by testing them under open sky in a zero-baseline configuration. The distributions of the double-differenced (DD) code and phase residuals (i.e. errors) are shown in Figure 7. The code multipath was determined using single-point code-minus-carrier, and the RMS values for GPS L1 C/A and GLONASS L1 CA code are shown in Table 4. The following inferences regarding the hardware quality were made:

- The zero-baseline code and phase errors from Figure 7 are mainly determined by the receiver noise level, with the exception of GLONASS phase (addressed below). The code noise is on the centimetre-level while the phase noise is on the millimetre-level, for both GPS and GLONASS. This is indicative of the receiver quality, and suggests that GPS and GLONASS measurements *from these*

receivers can be easily integrated. The reason for the high quality code accuracy is likely carrier phase smoothing in the receiver firmware.

- Code accuracy is a limiting factor in ambiguity resolution. In turn, multipath is a limiting factor in (differential) code accuracy. Code multipath RMS levels were found to be at the sub-metre level for both GPS and GLONASS in the environment tested. The code from both systems is thus accurate to around a few multiples of their respective L1 phase wavelengths, and can provide reasonable initial position estimate with proper measurement weighting and filter tuning. However, it must be noted that these specific values only apply to this environment, which had open sky coverage with relatively few nearby reflectors.
- GLONASS inter-frequency phase biases manifest themselves as multiple peaks in the phase error distribution. Three distinct peaks can be identified in Figure 7; however these peaks are only separated by millimetres. These biases are not expected to significantly affect ambiguity resolution in the scenarios tested herein. However it is important to consider inter-frequency biases when using receivers from different manufacturers.

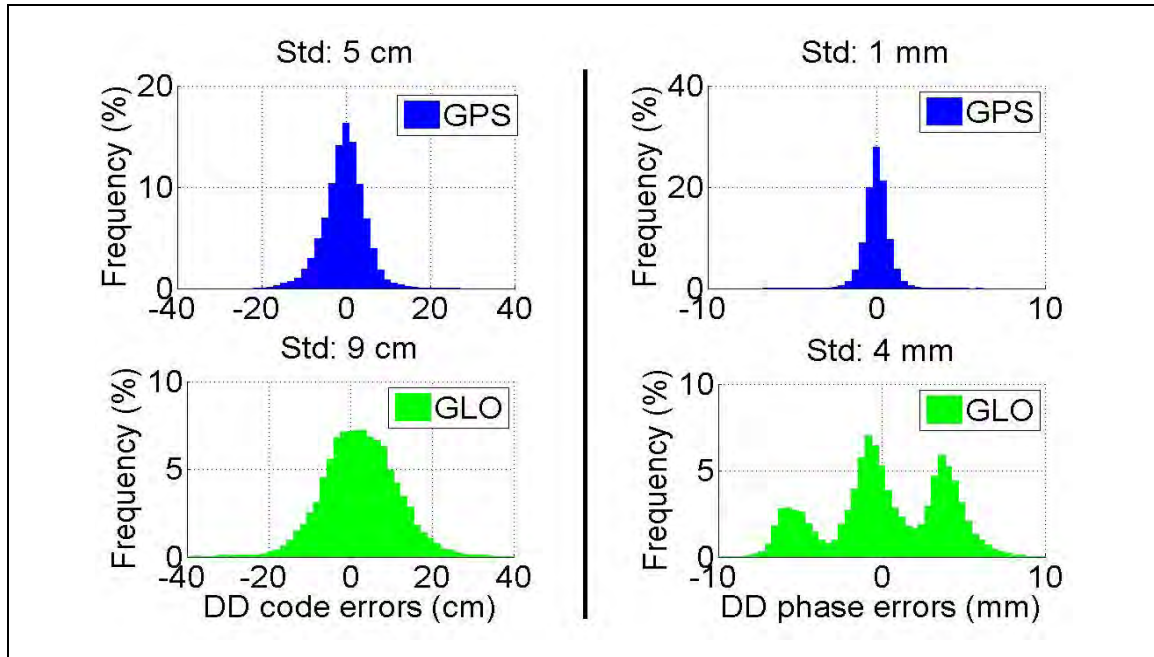


Figure 7 - NovAtel OEMV2-G + NovAtel GPS-702-GG hardware: code and phase errors under an open-sky zero-baseline configuration

Table 4 - NovAtel OEMV2-G + NovAtel GPS-702-GG hardware: code multipath under open sky

	Code multipath RMS (cm)
GPS L1 C/A code	49
GLONASS L1 CA code	61

The quality of the OEMV2-G + ANTCOM-GG receiver-antenna combination was assessed separately in an open sky *kinematic* test. The station in Figure 1 was used as the base station, and then the OEMV2-G + ANTCOM-GG receiver-antenna pair was carried by a pedestrian walking under open sky. The measurement errors were derived by computing fixed-ambiguity solutions and extracting the DD residuals. Their distributions are shown in Figure 8, and they contain both noise and multipath. Figure 8 suggests that the ANTCOM-GG antenna provides lower code and phase quality than the NovAtel

GPS-702-GG antenna. However there are two considerations here: 1.) the test is kinematic and conducted under a different multipath environment (albeit still open sky); and 2.) the measurement errors are larger but still near the same order of magnitude.

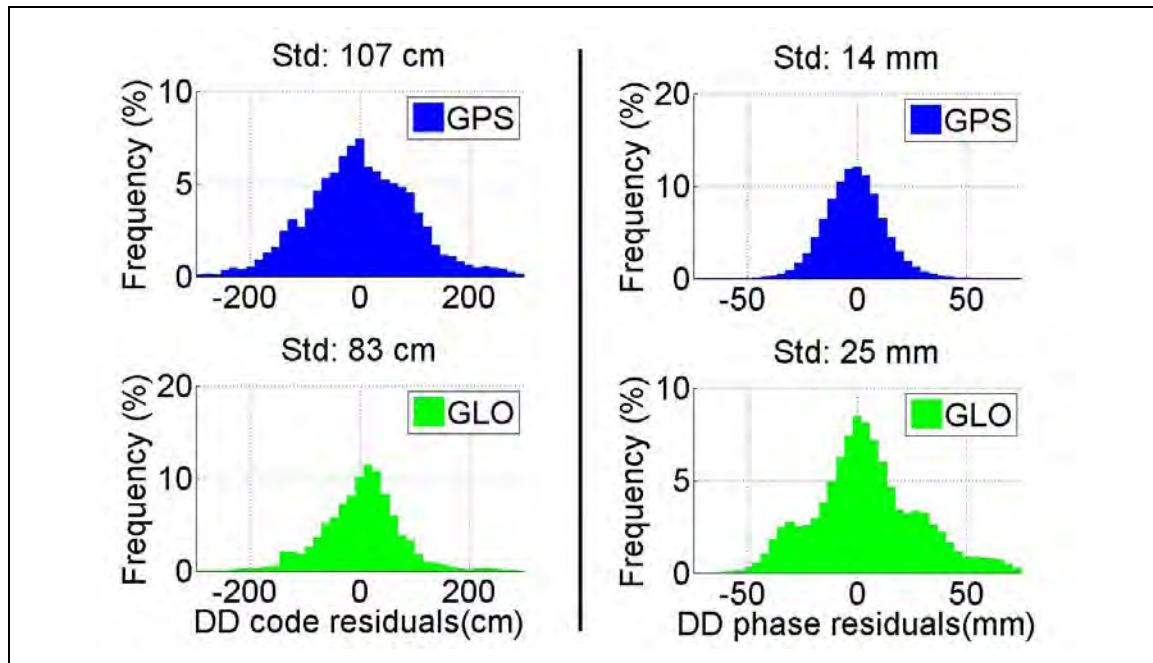


Figure 8 - NovAtel OEMV2-G + ANTCOM-GG hardware: code and phase errors from an open-sky kinematic test

3.3 Navigation Methodology: PLANSoft™

The GPS/GLONASS (GG) ambiguity resolution method used in this thesis is implemented in PLANSoft™, a real-time kinematic (RTK) processing engine developed partly by the author. PLANSoft™ implements geometry-based float estimation in the single-differenced (SD) domain – that is, measurements are single-differenced (between receivers) and then parameterized in terms of the base-to-rover vectors, relative clock

states and SD ambiguities. This is similar to the algorithm used by Habrich et al (1999): the SD ambiguities of all satellites (including the eventually chosen GLONASS base satellite) are observed, albeit coarsely as real values. These parameterizations are given as

$$\Delta P = \Delta R + c\Delta dT + \varepsilon_{\Delta P}$$

$$\Delta \Phi = \Delta R + c\Delta dT + \lambda \Delta N + \varepsilon_{\Delta \Phi}$$

where ΔP is the SD code measurement,

$\Delta \Phi$ is the SD phase measurement in units of distance,

ΔR is the SD satellite-to-user range,

c is the speed of light,

ΔdT is the SD receiver clock offset,

λ is the carrier wavelength,

ΔN is the SD phase ambiguity, and

$\varepsilon_{\Delta P}$ and $\varepsilon_{\Delta \Phi}$ are the SD code and phase errors.

A Kalman filter is implemented as it provides several advantages: 1.) all available measurements are used and the common geometry is taken into account; 2.) multipath can be smoothed out to a certain extent as code measurements are incorporated over time; and 3.) dynamics models can be tuned to smooth the states. The Kalman filter estimates the following state vector:

$$\boldsymbol{x}^{SD} = \left[\left(\boldsymbol{r}_{3 \times 1} \right)^T \quad \left(\boldsymbol{v}_{3 \times 1} \right)^T \quad \left(\boldsymbol{c}_{2 \times 1} \right)^T \quad \left(\boldsymbol{d}_{1 \times 1} \right)^T \quad \left(\boldsymbol{N}_{n \times 1}^{SD} \right)^T \right]^T$$

where \boldsymbol{x}^{SD} is the SD state vector,

\boldsymbol{r} is the base-to-rover position vector,

\boldsymbol{v} is the vector of relative velocity states,

\boldsymbol{c} is the vector of clock offsets,

\boldsymbol{d} is the clock drift, and

\boldsymbol{N}^{SD} is the vector of SD ambiguities.

The float estimates of the base-to-rover vectors and SD ambiguities are *transformed* into the DD domain. Essentially, the base-to-rover vectors are left as-is, while pairs of SD ambiguities from the same GNSS and frequency band are differenced to eliminate the clock effects they have absorbed. The resulting ambiguities are DD ambiguities. A coarse estimate of the GLONASS base satellite SD ambiguity is taken directly from the float solution. The following state vector is the result:

$$\boldsymbol{x}^{DD} = \left[\left(\boldsymbol{r}_{3 \times 1} \right)^T \quad \left(\boldsymbol{v}_{3 \times 1} \right)^T \quad \left(\boldsymbol{N}_{m \times 1}^{GLOBASE-SD} \right)^T \quad \left(\boldsymbol{N}_{n \times 1}^{DD} \right)^T \right]^T$$

where \boldsymbol{x}^{DD} is the DD state vector,

$\boldsymbol{N}^{GLOBASE-SD}$ is the vector of GLONASS base satellite SD ambiguities, and

\boldsymbol{N}^{DD} is the vector of DD ambiguities.

An example of the transformation from the SD to the DD domain is given in Figure 9.

There are three GPS and three GLONASS ambiguities. N_1^{GPS} and N_1^{GLO} correspond to the GPS and GLONASS base satellites, respectively. The transformation is applied as follows:

- The base-to-rover vector and relative velocity are directly copied from the SD to the DD domain.
- The clock states are eliminated completely.
- The two rows in the GPS ambiguity block of the transformation matrix both correspond to the transformation of the GPS ambiguities from the SD to the DD domain. The GLONASS ambiguity block contains a *third* row which copies the coarse estimate of the GLONASS base satellite SD ambiguity. If GLONASS is not being used, then the GLONASS ambiguity block is omitted.

$$\begin{bmatrix} r \\ v \\ \frac{N_{2-1}^{GPS}}{N_{2-1}^{GLO}} \\ \frac{N_{3-1}^{GPS}}{N_{3-1}^{GLO}} \\ N_1^{GLO} \end{bmatrix}_{x^{DD}} = \underbrace{\begin{bmatrix} I & 0 & 0 & 0 & 0 & 0 \\ 0 & I & 0 & 0 & 0 & 0 \\ 0 & 0 & 0 & -1 & 1 & 0 \\ 0 & 0 & 0 & -1 & 0 & 1 \\ 0 & 0 & 0 & 0 & 0 & 0 \\ 0 & 0 & 0 & 0 & 0 & 0 \end{bmatrix}}_{\text{Transformation matrix}} \begin{bmatrix} r \\ \frac{v}{c} \\ d \\ \frac{N_1^{GPS}}{N_1^{GLO}} \\ \frac{N_2^{GPS}}{N_2^{GLO}} \\ \frac{N_3^{GPS}}{N_3^{GLO}} \\ 1 & 0 & 0 \end{bmatrix}_{x^{SD}}$$

Figure 9 - Example of SD to DD transformation

Processing in PLANSOFT™ was done in post-mission, but with all algorithms implementable in real-time – that is, epoch-by-epoch processing with no rewinding or forward/backward smoothing. GLONASS inter-frequency phase biases are not corrected, as they were demonstrated earlier to be very small for the receiver pairs used. Unless otherwise stated, the following processing parameters were used for both GPS and GLONASS:

- Elevation-based measurement uncertainty model: $\sigma = \frac{\sigma_{zenith}}{\sin(\alpha_{elevation})}$.
- Code uncertainty (at zenith) of 50 cm.

- Phase uncertainty (at zenith) of 4 mm.
- Random walk model with velocity spectral densities of $1.0 \text{ (m/s)}^2/\text{s}$ in each direction. This spectral density is sufficient for the kinematic scenarios investigated herein. Although lower (or zero) spectral density values can be used for the static baselines, the same values are used for consistency.
- Fault detection at 0.1% significance level.
- Phase rate cycle slip detection with 4-cycle threshold.
- LAMBDA decorrelation and integer least-squares for ambiguity resolution.

3.4 Estimation Strategies

Section 3.3 defined a framework for navigation estimation and ambiguity resolution within PLANSOFT™. Within that framework, there are several ways to change how the positions and ambiguities are estimated. This thesis investigates the impact of these *estimation strategies* on the success rate and reliability of ambiguity resolution.

The inputs to navigation estimation are the code and phase measurements. Different combinations of these measurements can be used. The choice of combination is motivated by two factors: 1.) if L2 measurements are used, then dual-frequency hardware

is required, and the cost of that hardware is currently affected by the Y-code encryption of the GPS L2 P signal; and 2.) different dual-frequency combinations have different characteristics in terms of measurement noise and performance over varying baseline lengths. Three measurement combinations were investigated:

1. *L1 only.* The code measurements used are GPS L1 C/A and GLONASS L1 CA. The phase measurements used are GPS and GLONASS L1. These are used to estimate the base-to-rover vector and the L1 ambiguities.
2. *L1 + L2.* The code measurements used are GPS L1 C/A and GLONASS L1 CA. Code from L2 is not used. The phase measurements used are GPS and GLONASS L1 and L2. The L1 and L2 phase are *not combined*, but used separately. These are used to estimate the base-to-rover vector and the L1 and L2 ambiguities
3. *Widelane.* The code measurements used are GPS L1 C/A and GLONASS L1 CA. Code from L2 is not used. The phase measurements used are GPS and GLONASS L1 and L2. The L1 and L2 phase are *combined* by forming the quantity $\phi_{WL} - \phi_{L2} - \phi_{L1}$ for each satellite. ϕ_{WL} is referred to as *widelane (WL) phase* and is treated as a phase measurement with a wavelength of $c / (f_{L1} - f_{L2})$. For GPS this wavelength is 86 cm and for GLONASS it is approximately 84 cm for all satellites with differences between satellites of up to 3.9 mm. The L1 and L2 ambiguities are also combined in the manner above to form *widelane ambiguities*.

The L1 code and widelane phase are used to estimate the base-to-rover vector and the widelane ambiguities.

Once the measurement combination was chosen, there were several ways of generating the fixed ambiguity solutions. Three of these fixing strategies were investigated:

1. *GPS only*: only GPS measurements are used to estimate the float solution prior to ambiguity resolution. The chosen measurement combination determines which code and phase measurements are used. The float solution contains only GPS ambiguities. All GPS ambiguities are fixed to integers when possible.
2. *GG – float GLO*: both GPS and GLONASS measurements are used to estimate the float solution prior to ambiguity resolution. The chosen measurement combination determines which code and phase measurements are used. The float solution contains both GPS and GLONASS ambiguities. All GPS ambiguities are fixed to integers, but all GLONASS ambiguities remain as real-valued (float) estimates. The motivation for this approach is discussed in more detail below.
3. *GG – fixed GLO*: both GPS and GLONASS measurements are used to estimate the float solution prior to ambiguity resolution. The chosen measurement combination determines which code and phase measurements are used. The float solution contains both GPS and GLONASS ambiguities. All GPS and GLONASS ambiguities are fixed to integers.

The choice of using GLONASS in a fixing strategy is motivated by hardware requirements: most legacy receivers and many of the current receivers track only GPS. It is also important to investigate the effect of fixing the GLONASS ambiguities, because doing so is more difficult than for GPS. Estimating the GLONASS ambiguities as float values also removes the risk of fixing the ambiguities incorrectly due to GLONASS inter-frequency biases. Some commercial RTK software such as Waypoint's GrafNav™ provide the option to use GLONASS measurements without fixing the ambiguities. Therefore it must be determined whether it is worth fixing the GLONASS ambiguities, or if using the measurements in the float solution is sufficient.

Figure 10 shows the different the estimation strategies and solutions that were generated.

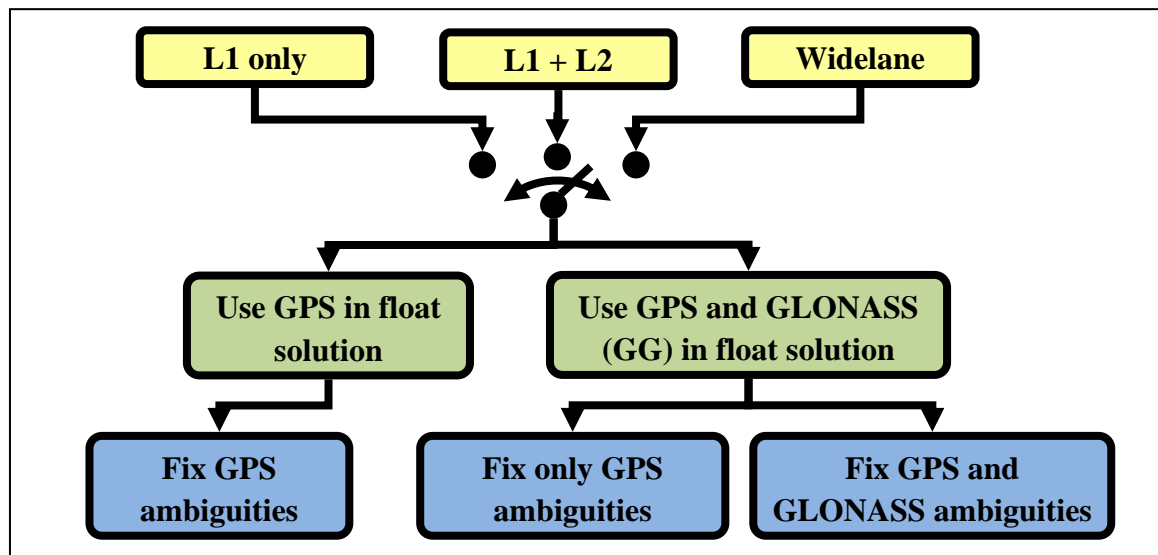


Figure 10 - Measurement combinations and fixing strategies

3.5 Convergence Time

Code accuracy is a major limiting factor for ambiguity resolution; the problem is overcome by using measurements over multiple epochs and constraining the position and ambiguity states so that they can converge to their true values. It must then be decided how much *convergence time* to allow before attempting ambiguity resolution.

The relationship between convergence time and fix reliability is exemplified by Figure 11. Between three and eight GPS and two and six GLONASS satellites were available. Fix reliability in this case is approximately represented by predicted success rates from the vehicle-to-vehicle test. The predicted success rates increase as more convergence time is allowed; this shows how fix reliability improves with more convergence time.

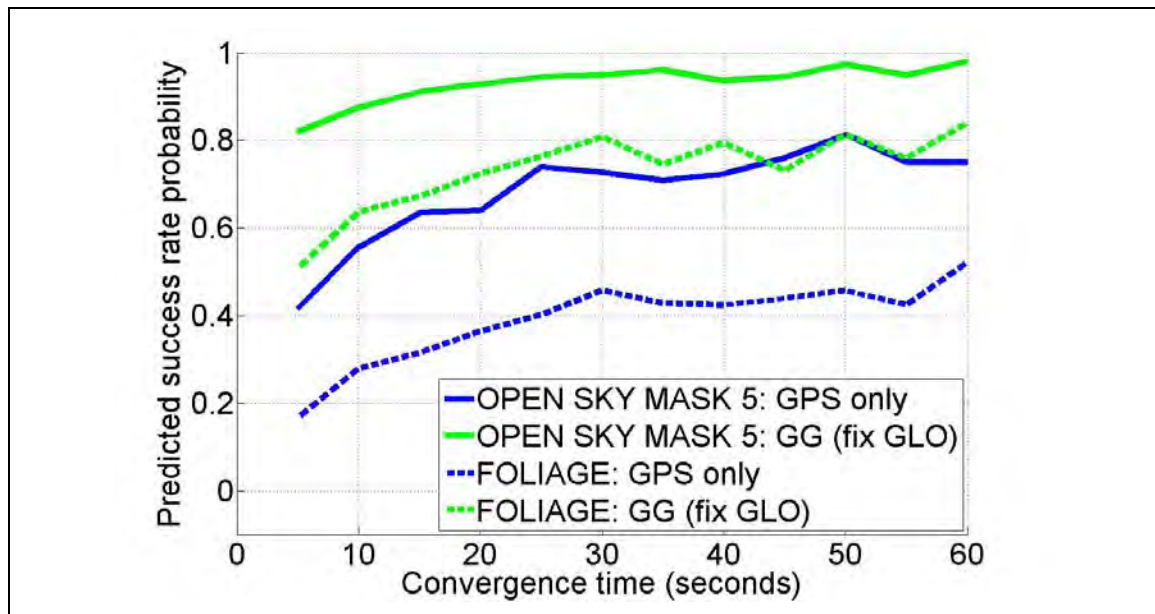


Figure 11 - Relationship between fix reliability and convergence time

For actual field work, convergence time should generally be increased, within reason, to maximize fix reliability. This is often done through a static initialization period when practical. However, the analysis herein requires some fixes to be incorrect so that the reliability tests can be evaluated. In the results presented in this thesis, there was generally no static initialization (unless the test itself was static) and convergence times were chosen through trial and error, such that there were a sufficient proportion of correct and incorrect fixes to analyze.

3.6 Generating Integer Fixes

Navigation methods that implement ambiguity resolution take advantage of the fact that phase ambiguities are constant unless there are cycle slips. The ambiguities are resolved to integers if reliability tests such as the predicted success rate and F-test pass. Once successfully resolved, the integer values of the ambiguities are stored in memory and re-used at every epoch thereafter. Ambiguity resolution is not attempted again unless cycle slips are detected or residual analysis indicates that the original integer fix is incorrect.

However, this approach is not suitable for the analysis in this thesis. A single instance of ambiguity resolution will not yield statistically meaningful results; the process must be conducted many times in order to generate many integer fixes, predicted success rates and F-test results under a wide range of visibility conditions. As well, the performance of the predicted success rate and F-test are being investigated, so they cannot *at the same time* be used to decide whether or not to resolve the ambiguities.

As such, a data processing method has been designed to produce *many* integer fixes. This method is illustrated by Figure 12. There are two key differences between this method and most standard ambiguity resolution implementations: 1.) the ambiguities are forced to be resolved to integers, no matter what the predicted success rate and F-test result indicate; and 2.) after the ambiguities are resolved and the solution recorded, the filter is reset so that another ambiguity resolution process can be conducted.

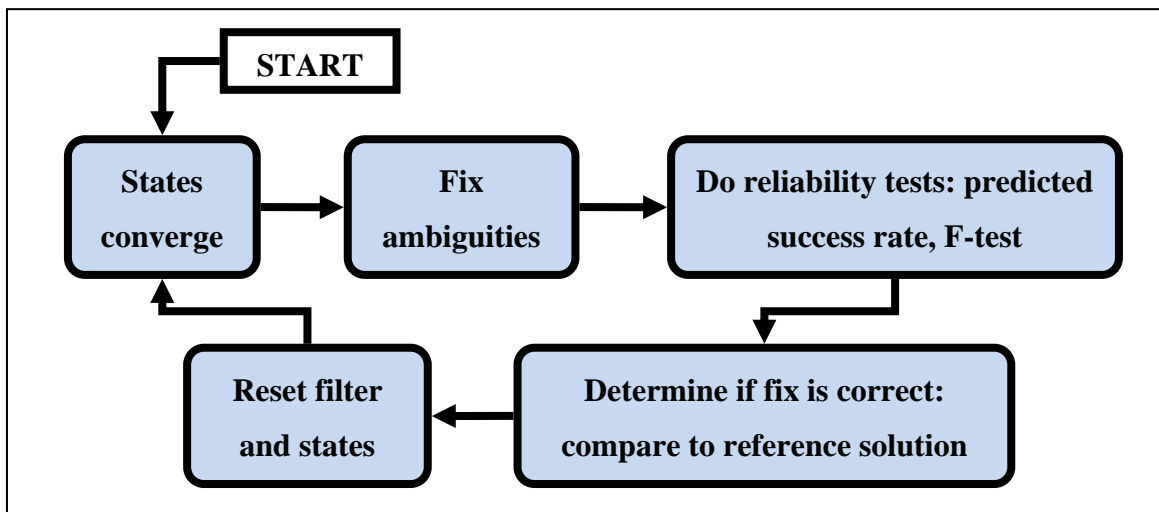


Figure 12 - Data processing method for generating many integer fixes

Chapter Four: Static Testing Results

This chapter presents the analysis and discussion of the reliability of ambiguity resolution for *static* testing. Two static surveys were conducted under open sky conditions, over baselines of 2 km and 18 km respectively. The 2 km baseline was surveyed on March 5-6, 2010, in the city of Calgary. Observations taken on those days from the Meanook Geomagnetic Observatory (450 km north of Calgary) indicate that the geomagnetic *K* index did not exceed 2.0 (Space Weather Canada 2009). This level of *K* index does not suggest a significant ionospheric disturbance (USNOAA 2005). Between seven and 12 GPS and four and eight GLONASS satellites were available. This baseline was surveyed for 39 hours, and a total of 6975 ambiguity fixes were generated (with a convergence time of 20 seconds).

The 18 km baseline was surveyed on August 9-10, 2009, also in the city of Calgary. The *K* index did not exceed 1.0 (Space Weather Canada 2009), indicating no significant ionospheric disturbance. Regardless, the length of the baseline is expected to be a factor due to larger residual atmospheric effects. Between six and eleven GPS and three and seven GLONASS satellites were available. This baseline was surveyed for 26 hours, and a total of 4751 ambiguity fixes were generated (with a convergence time of 20 seconds).

For both baselines, nine types of solutions are investigated. The **L1 only**, **L1 + L2** and **widelane (WL)** measurement combinations are each combined with the **GPS only**, **GG float GLO** and **GG fixed GLO** fixing strategies. Circular elevation mask angles of 5°

and 30° are also applied and investigated. The latter simulates reduced visibility conditions, which are discussed in greater detail in Sections 4.5 and 4.10.

4.1 Positioning Accuracy

An analysis of the solutions in the position domain is first presented. Position accuracies are determined by a comparison to a *truth* or *reference solution*. For both baselines, the reference solution is obtained by computing fixed-ambiguity positions at every epoch, and then taking the average of all of those positions. The 3D precision of the reference solution is better than 2 cm (1σ) for both baselines.

Figure 13 is a 2D representation of the position errors from the 2 km baseline, for both the correct and incorrect fixes. It is clear that incorrect fixes can lead to very large position errors. The characteristics of the positions derived from correct fixes are much more interesting. These are graphically represented in Figure 14 and further summarized in Table 5 (the median errors) and Table 6 (the RMS errors). The actual success rates (fully investigated in Section 4.2) are given to show the availability of these fixed-ambiguity positions, with the actual numbers of correct fixes highlighted in **blue**. The following trends are observed:

- There appears to be little difference in the position errors whether GPS is used alone, or GPS and GLONASS are combined. However, when the GLONASS

ambiguities are fixed (i.e. when the **GG fixed GLO** strategy is used), the cluster of position errors do appear to be visually tighter.

- The position errors do not appear to be affected whether **L1 only** or **L1 + L2** is used. However the spread of errors is much larger when **widelane** is used (highlighted in **red** in Table 5 and Table 6). This is expected because the differential atmospheric effects over a distance of 2 km are generally negligible. Also, the **widelane** solution noise is always higher than in an **L1 only** solution due to the linear combination of observables.
- The spread of position errors is larger vertically than horizontally, and larger north-south than east-west. This is expected: the measurement geometry is weakest in the vertical direction, and then weaker north-south than east-west as the receiver gets farther from the equator (e.g. at Calgary's 51° N latitude).

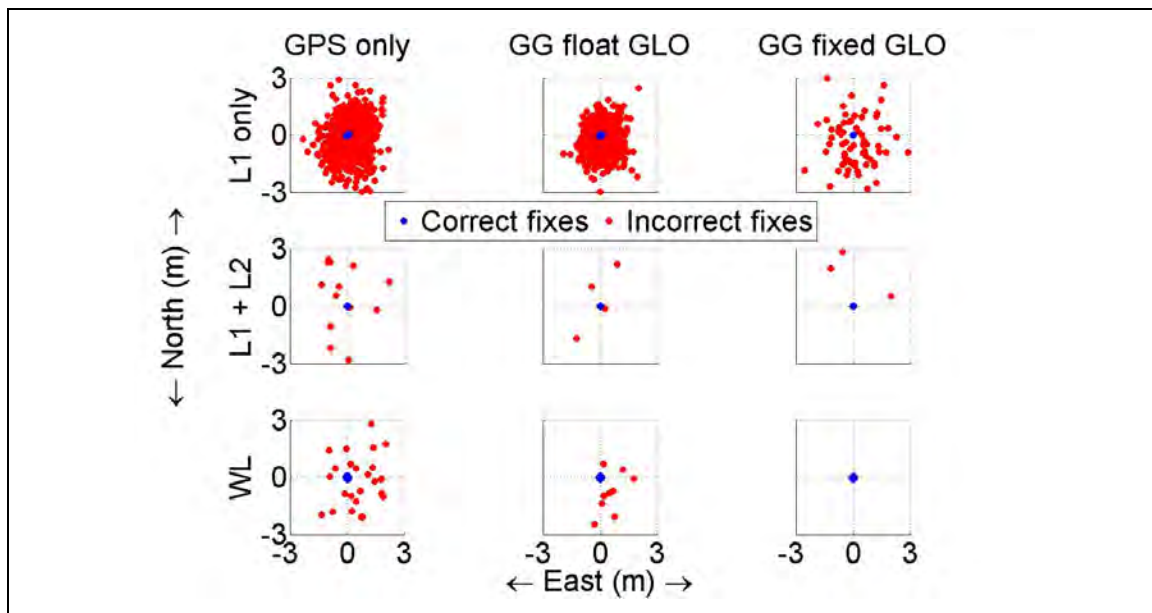


Figure 13 - 2D view of position errors, all fixes - 2 km baseline under 5° mask

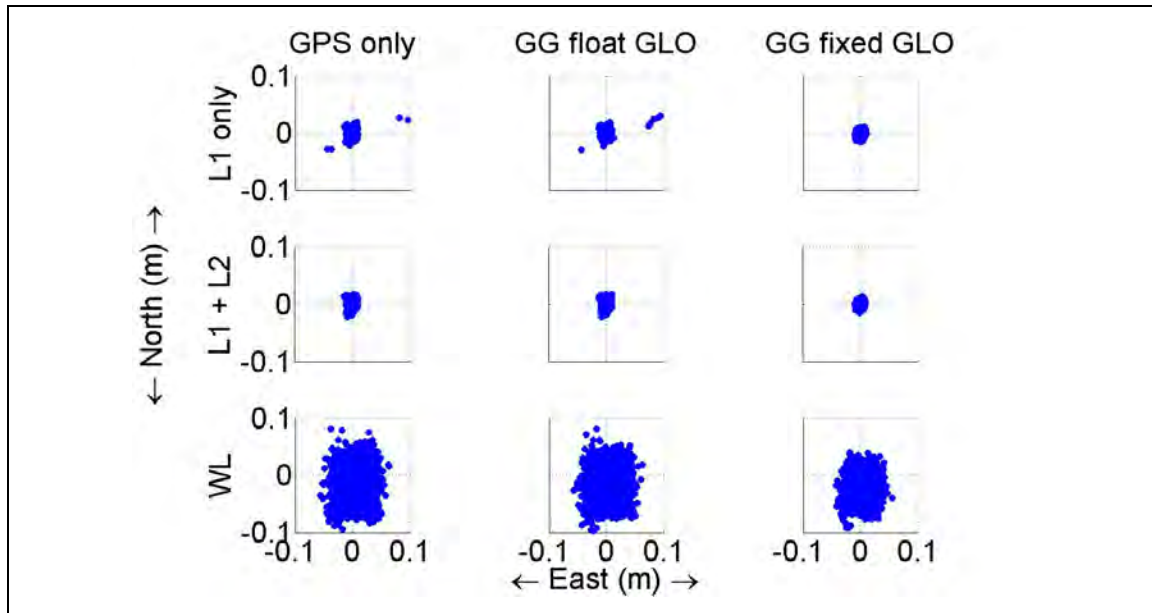


Figure 14 - 2D view of position errors, correct fixes - 2 km baseline under 5° mask

Table 5 - Median position errors from correct fixes - 2 km baseline under 5° mask

		Median errors from correct fixes (cm) – 2 km baseline					Actual success rate probabilities
		East	North	Up	2D	3D	
L1 only	GPS only	0.2	0.3	0.5	0.4	0.7	0.84 (5850) ¹
	GG float GLO	0.2	0.3	0.5	0.4	0.7	0.88 (6156)
	GG fixed GLO	0.2	0.3	0.4	0.4	0.6	0.99 (6901)
L1 + L2	GPS only	0.2	0.3	0.4	0.4	0.7	0.99 (6960)
	GG float GLO	0.2	0.2	0.4	0.4	0.6	0.99 (6969)
	GG fixed GLO	0.1	0.2	0.4	0.3	0.6	0.99 (6972)
WL	GPS only	1.1	1.7	2.3	2.4	3.9	0.99 (6940)
	GG float GLO	1.1	1.7	2.3	2.4	3.8	0.99 (6962)
	GG fixed GLO	0.9	1.9	1.9	2.4	3.5	1.00 (6975)

Table 6 - RMS position errors from correct fixes - 2 km baseline under 5° mask

		RMS errors from correct fixes (cm) – 2 km baseline					Actual success rate probabilities
		East	North	Up	2D	3D	
L1 only	GPS only	0.3	0.5	6.6	0.6	6.6	0.84 (5850)
	GG float GLO	0.4	0.5	7.0	0.6	7.1	0.88 (6156)
	GG fixed GLO	0.3	0.4	0.6	0.5	0.8	0.99 (6901)
L1 + L2	GPS only	0.3	0.4	0.7	0.5	0.9	0.99 (6960)
	GG float GLO	0.3	0.4	0.7	0.5	0.9	0.99 (6969)
	GG fixed GLO	0.2	0.3	0.6	0.4	0.7	0.99 (6972)
WL	GPS only	1.6	2.5	3.7	3.0	4.7	0.99 (6940)
	GG float GLO	1.6	2.5	3.6	3.0	4.7	0.99 (6962)
	GG fixed GLO	1.4	2.5	3.0	2.8	4.1	1.00 (6975)

¹ Number of correct fixes

The position errors from the 18 km baseline are shown in Figure 15 (a 2D view of the errors for the correct and incorrect fixes), Figure 16 (the same view for only the correct fixes), Table 7 (a summary of the median fixed errors) and Table 8 (a summary of the RMS fixed errors). The same trends from the analysis of the 2 km baseline are also observed for the 18 km baseline: the **widelane** positions are less precise (highlighted in **red** in Table 7 and Table 8), and the vertical errors exceed the horizontal errors and the north-south errors exceed the east-west errors. In addition, the positions from this baseline are less precise than those from the 2 km baseline. This is demonstrated in Section 4.4 to be due to larger phase errors over the longer baseline caused by larger differential atmospheric errors. This is mitigated by the **widelane** solutions having a higher probability of fixed success (highlighted in **green** in Table 7 and Table 8), as discussed in Section 4.2. The actual success rates given in Table 9 are also given in Table 7 and Table 8 to show this advantage. The numbers of correct fixes are shown in **blue**.

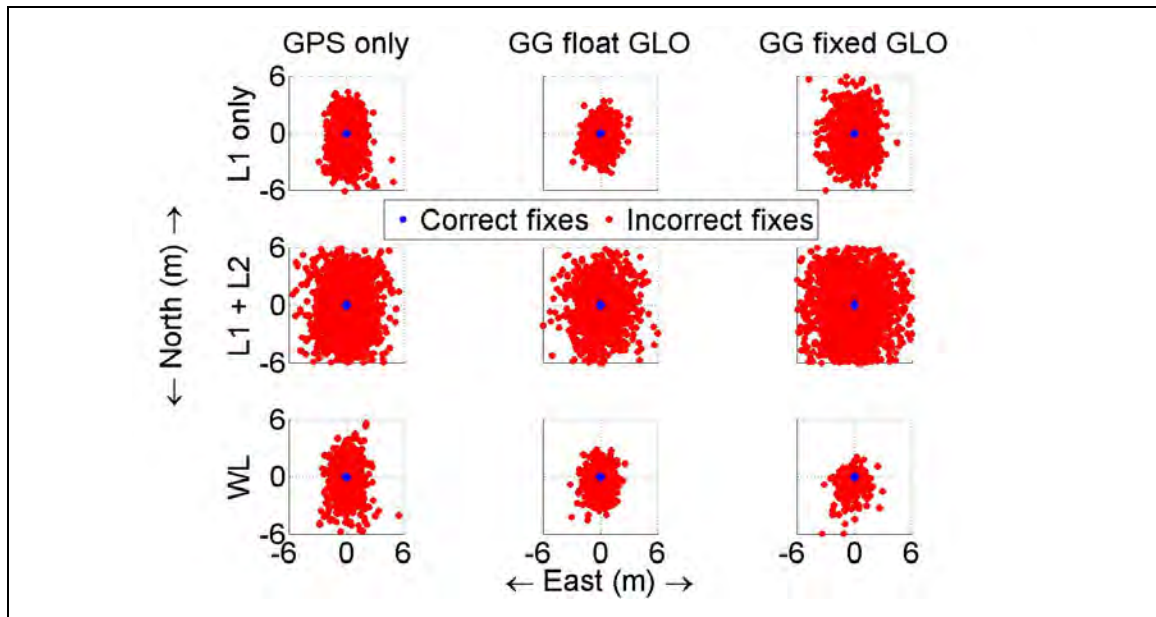


Figure 15 - 2D view of position errors, all fixes - 18 km baseline under 5° mask

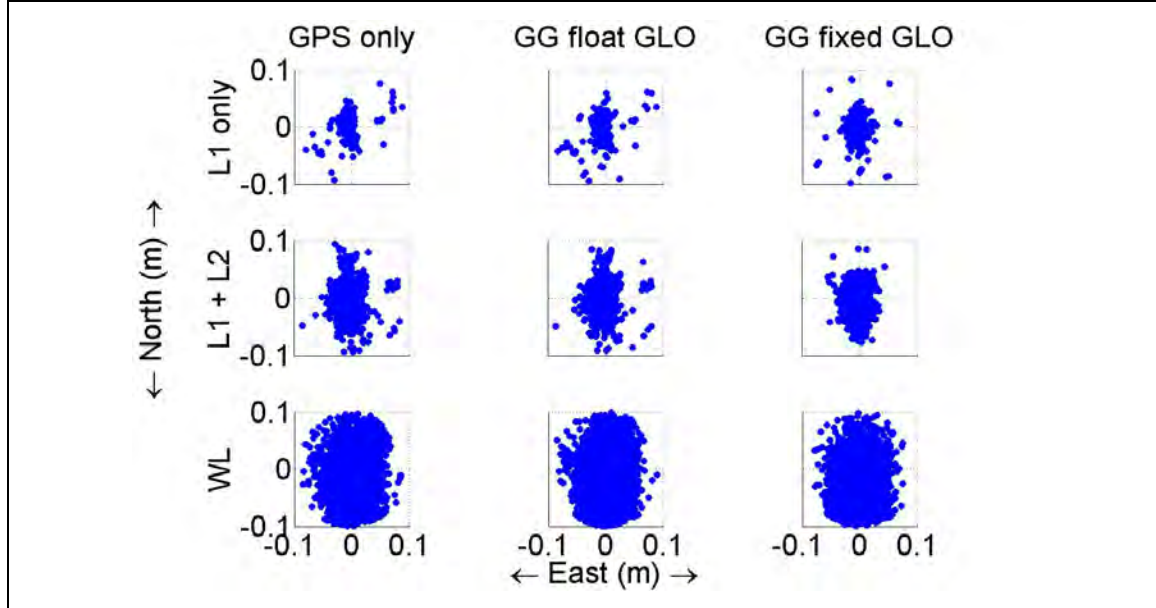


Figure 16 - 2D view of position errors, correct fixes - 18 km baseline under 5° mask

Table 7 - Median position errors from correct fixes - 18 km baseline under 5° mask

		Median errors from correct fixes (cm) – 18 km baseline					Actual success rate probabilities
		East	North	Up	2D	3D	
L1 only	GPS only	0.7	1.4	2.0	1.8	3.0	0.07 (321)
	GG float GLO	0.7	1.4	2.1	1.8	3.1	0.09 (414)
	GG fixed GLO	0.6	1.0	1.9	1.4	2.7	0.17 (826)
L1 + L2	GPS only	0.8	1.4	2.5	1.8	3.5	0.53 (2535)
	GG float GLO	0.8	1.4	2.5	1.8	3.5	0.59 (2782)
	GG fixed GLO	0.8	1.2	2.3	1.7	3.2	0.56 (2651)
WL	GPS only	1.6	2.9	4.8	3.8	6.8	0.66 (3136)
	GG float GLO	1.6	2.8	4.6	3.8	6.7	0.71 (3387)
	GG fixed GLO	1.5	2.5	4.7	3.4	6.4	0.87 (4156)

Table 8 - RMS position errors from correct fixes - 18 km baseline under 5° mask

		RMS errors from correct fixes (cm) – 18 km baseline					Actual success rate probabilities
		East	North	Up	2D	3D	
L1 only	GPS only	1.8	2.1	57.2	2.8	57.2	0.07 (321)
	GG float GLO	1.8	2.2	39.4	2.8	39.5	0.09 (414)
	GG fixed GLO	1.1	1.8	30.6	2.1	30.6	0.17 (826)
L1 + L2	GPS only	1.4	2.2	22.1	2.6	22.2	0.53 (2535)
	GG float GLO	1.4	2.2	15.7	2.6	15.9	0.59 (2782)
	GG fixed GLO	1.2	2.0	5.1	2.3	5.6	0.56 (2651)
WL	GPS only	2.4	4.0	18.8	4.7	19.4	0.66 (3136)
	GG float GLO	2.4	4.0	11.6	4.6	12.5	0.71 (3387)
	GG fixed GLO	2.2	3.8	10.5	4.4	11.4	0.87 (4156)

Ultimately the accuracy of a position derived from correctly fixed phase ambiguities is reliant upon two factors: 1.) the geometry of the phase measurements; and 2.) the quality of those same phase measurements. Conceptually, both of these factors are represented by the ambiguity dilution of precision (ADOP), introduced by Teunissen (2001a). The ADOP was defined in Section 2.4, and is reiterated here:

$$\text{ADOP} = \left(\det(Q_{\hat{N}}) \right)^{\frac{1}{2n}}$$

where $Q_{\hat{N}}$ is the variance-covariance matrix of the real-valued ambiguities, and n is the number of ambiguities.

The ADOP defined above is expressed in units of cycles. However it can also be expressed in units of length by scaling each element of the variance-covariance matrix of the real-valued ambiguities by their corresponding wavelengths. The relationship between the ADOP and the fixed-ambiguity horizontal position errors is shown in Figure 17 and Figure 18 for the 2 km and 18 km baselines, respectively. The following trends are observed:

- The range of ADOPs indicates that **L1 + L2** produces the smallest ADOPs, and **widelane** produces the largest ADOPs. This is expected as **L1 + L2** incorporates more phase measurements. Meanwhile, **widelane** uses phase measurements that are approximately six times coarser than L1 phase due to the scaling of the

wavelength and the addition of the L2 phase (Lachapelle 2008). This explains why the **widelane** positions have larger errors.

- The ADOP and fixed position errors appear to be somewhat correlated. The relationship is obvious for the 2 km baseline; as the ADOP increases, so does the fixed errors. For the 18 km baseline, the median fixed errors appear to increase as the ADOP increases *up to a point*, after which the position errors actually *decrease* as the ADOP increases. This is highlighted by Circles 1 and 2 in Figure 18. However, this is not a real trend: the frequency histograms of the ADOPs in Figure 19 reveal that there are very few fixes with ADOPs greater than 5 cm for **L1 only**, 1 cm for **L1 + L2** or 10 cm for **widelane**. Therefore patterns observed in that range of ADOPs are not statistically significant.

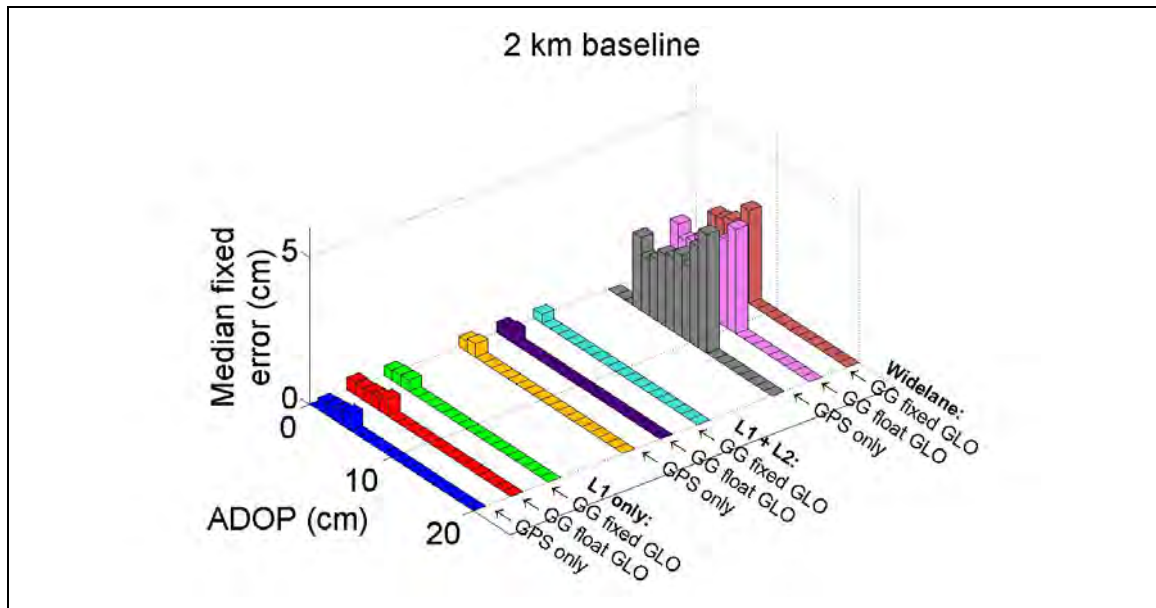


Figure 17 - Horizontal fixed errors vs. ADOP - 2 km baseline under 5° mask

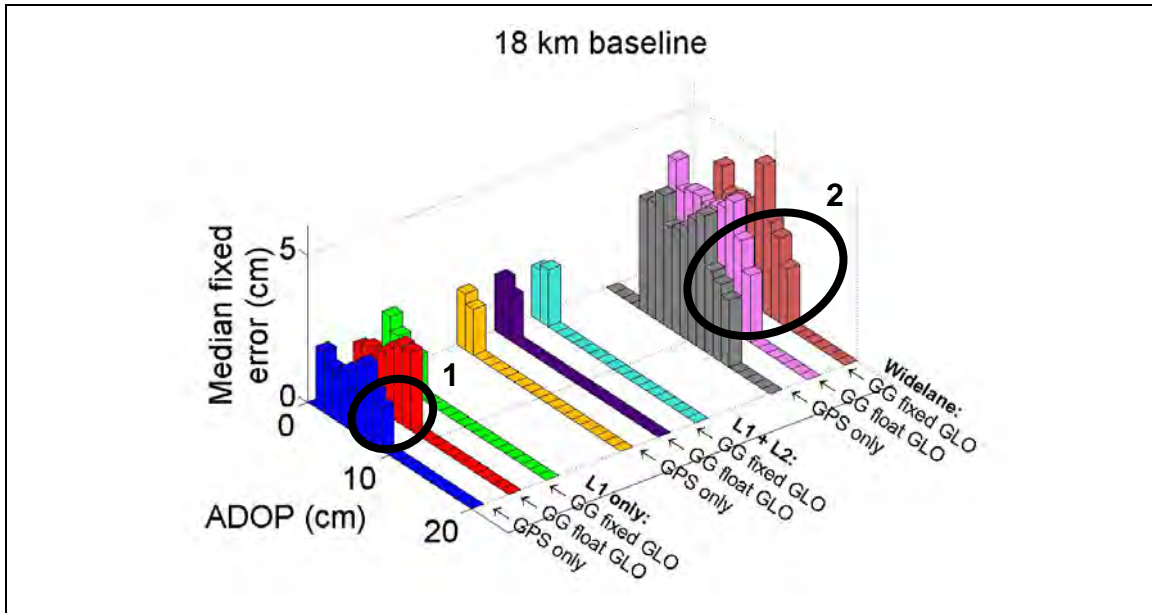


Figure 18 - Horizontal fixed errors vs. ADOP - 18 km baseline under 5° mask

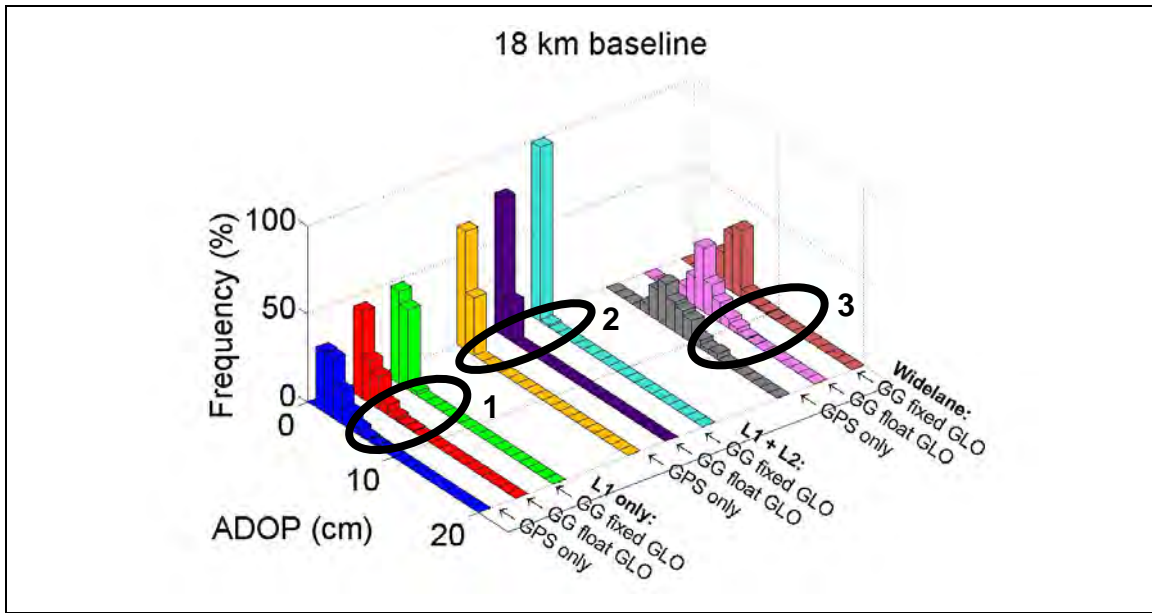


Figure 19 - Frequency distributions of ADOP - 18 km baseline under 5° mask

While the ADOP is a useful metric, it is also an *a priori* quantity; hence it is often not a realistic representation of the *actual* phase accuracy. To analyze the impact of the *true* phase errors, they are first determined herein by computing the DD phase residuals while fixing the base and rover positions to their known coordinates. The result is a combination of phase noise and multipath, as well as any residual atmospheric errors. Figure 20 shows the distributions of the phase errors in the L1 band for both baselines. The phase errors are naturally larger for the 18 km baseline due to the spatial decorrelation of the ionospheric effect over that distance.

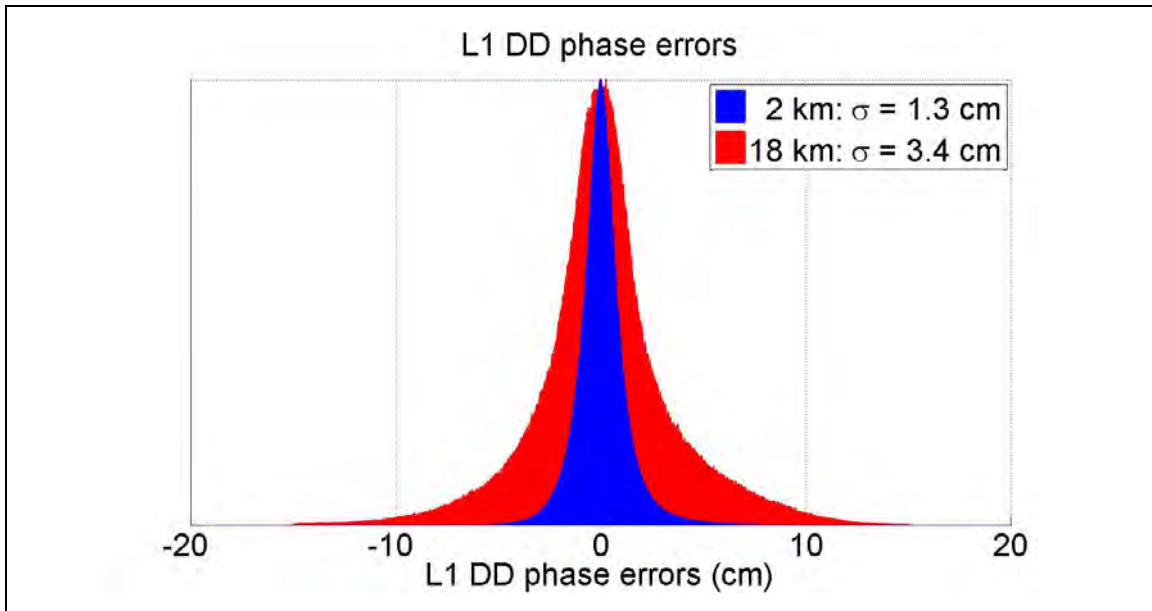


Figure 20 - L1 DD phase errors - static baselines

The impact of the true phase errors on the positioning accuracy is illustrated in Figure 21 and Figure 22 for the 2 km and 18 km baselines, respectively. The level of phase error is characterized for each individual fix by the *standard deviation* of the individual L1 phase errors that correspond with that fix. Figure 21 and Figure 22 are the distributions of the

median horizontal fixed position errors for different phase error standard deviations. There is a trend for the **L1 only** and **L1 + L2** combinations: larger phase errors generally lead to larger position errors. This effect is anticipated since the purpose of ambiguity resolution is to use the phase for positioning. This is also the underlying cause behind the loss of precision in the solutions generated for the 18 km baseline, relative to the 2 km baseline.

The more interesting result is the trend for **widelane**. The dependency of the position errors on the phase errors is actually relatively flat for the **widelane** solutions. This implies that higher levels of phase errors can be tolerated, which can be useful for longer baselines. There are two things to consider about this result:

1. The differential atmospheric effects are very small for the 2 km baseline, and for the 18 km baseline the 1σ value of the phase error distribution is still less than a quarter of an L1 cycle. It is possible that widelane would not tolerate phase errors larger than the ones analyzed here, especially since the effect of the ionosphere is multiplied by 1.28 when using widelane over L1 (Lachapelle 2008). However, the widelane wavelength is also more than four times wider than L1, suggesting that the *final* effect of the ionosphere when using widelane is less than half the effect when using L1.
2. There is a problem when specifically considering positioning accuracy: even though the relationship between position and phase errors is nearly flat, the

position errors are larger to begin with and little benefit is gained. However this property of widelane – to tolerate larger phase errors – manifests itself in other aspects of ambiguity resolution. This is demonstrated later in this chapter (Sections 4.4 and 4.7).

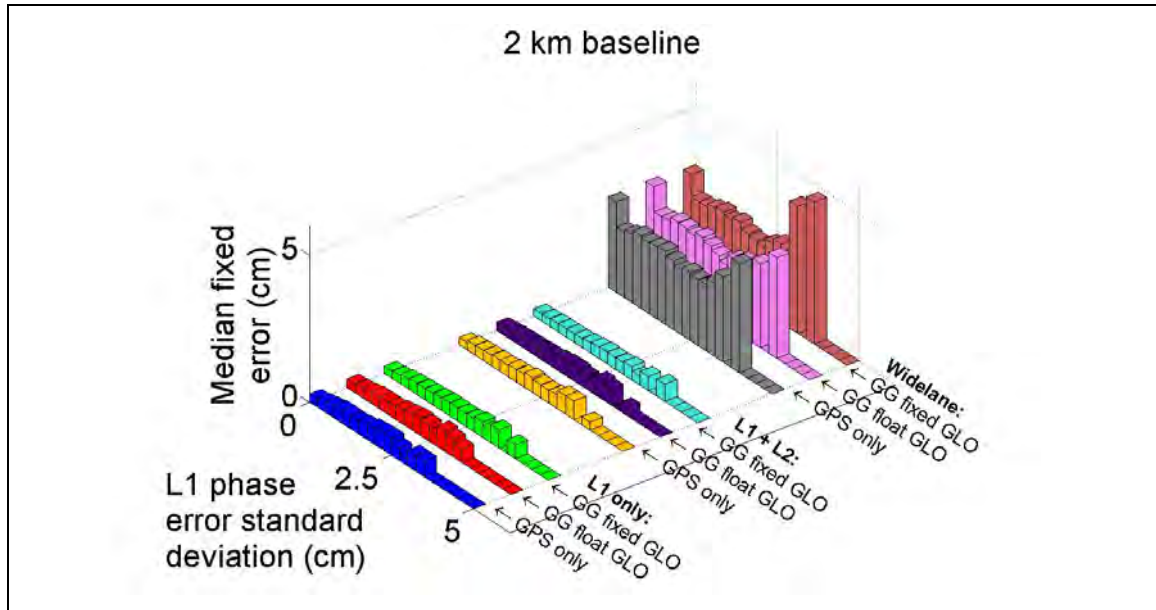


Figure 21 - Horizontal fixed errors vs. phase error standard deviation - 2 km baseline under 5° mask

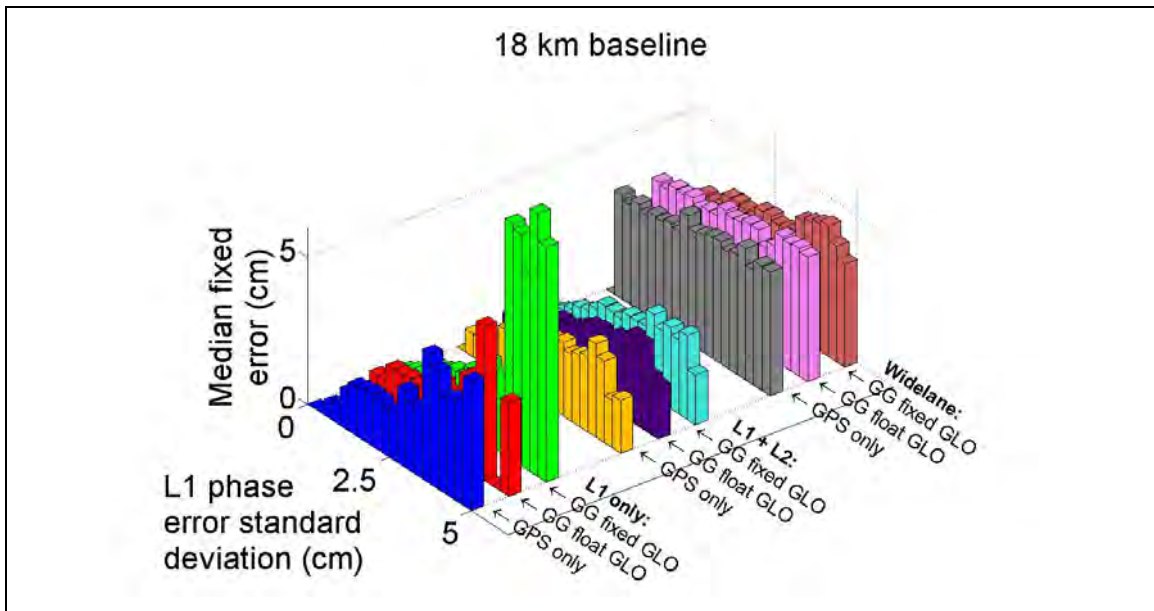


Figure 22 - Horizontal fixed errors vs. phase error standard deviation - 18 km baseline under 5° mask

4.2 Actual Success Rates

The actual success rates, or the rate of correct fixes, are investigated in this section. The correctness of fixes is determined by comparing the fixed-ambiguity position to the reference solution. The fix is taken to be correct with a horizontal agreement of better than 10 cm and incorrect otherwise. Table 9 shows the actual success rates of every estimation strategy for both baselines. The corresponding numbers of correct fixes are highlighted in **blue**, with 6975 *total* fixes for the 2 km baseline and 4751 for the 18 km baseline. All of the solutions are processed using a circular elevation mask angle of 5° – that is, a mask angle used only to mitigate multipath and differential atmospheric effects, not to simulate reduced visibility conditions.

Table 9 - Actual success rate probabilities - static baselines under 5° mask

		Actual success rate probability	
		2 km baseline	18 km baseline
L1 only	GPS only	0.84 (5850)	0.07 (321)
	GG float GLO	0.88 (6156)	0.09 (414)
	GG fixed GLO	0.99 (6901)	0.17 (826)
L1 + L2	GPS only	0.99 (6960)	0.53 (2535)
	GG float GLO	0.99 (6969)	0.59 (2782)
	GG fixed GLO	0.99 (6972)	0.56 (2651)
Widelane	GPS only	0.99 (6940)	0.66 (3136)
	GG float GLO	0.99 (6962)	0.71 (3387)
	GG fixed GLO	1.00 (6975)	0.87 (4156)

The following trends are observed:

- The **GG** strategies are more effective at fixing ambiguities correctly than the **GPS-only** strategy. This is highlighted in **green** in Table 9. This is especially noticeable for the 18 km baseline as the actual success rates are lower and there is more room for improvement.
- Furthermore, the actual success rates are maximized when the GLONASS measurements are incorporated and the ambiguities are *also* fixed. There is one exception – the 18 km baseline, when using the **L1 + L2** measurement combination. In the **GG float GLO** mode, the GLONASS float ambiguities and their uncertainties are adjusted along with the positions when the fixed GPS

ambiguities are applied. This is illustrated in Figure 23, which shows the adjusted 1σ uncertainties of the GLONASS float ambiguities for the **L1 only GG float GLO** solution from the 2 km baseline. Most of the uncertainties are less than 1 cm, which suggests that fixing only the GPS ambiguities would yield adjusted GLONASS float ambiguities that are close to integers. However, it is important to note that *actually* fixing the GLONASS ambiguities yields more correct fixes.

- The use of dual-frequency combinations is beneficial. Again this trend is most noticeable for the 18 km baseline due to the overall lower actual success rates and thus the larger room for improvement; in this scenario the **widelane** combination proved to be more effective. For the 2 km baseline it is clear that dual-frequency is advantageous, but the question of which combination (**L1 + L2** or **widelane**) is better overall is investigated under simulated reduced visibility in Section 4.5.

- The actual success rates from the 18 km baseline are all lower than those from the 2 km baseline. It is demonstrated in Section 4.4 that this is caused by the increased residual ionospheric effects on the phase measurements. Furthermore, the errors given in Table 7 and Table 8 suggest that the fixed positions may not always achieve decimetre-level accuracy – this is confirmed by Figure 24, which shows the distributions of the actual success rates over various 3D fixed position errors. The **widelane** positions have the lowest precision, with correct ambiguity resolution resulting in a range of 3D fixed errors up to 20 cm.

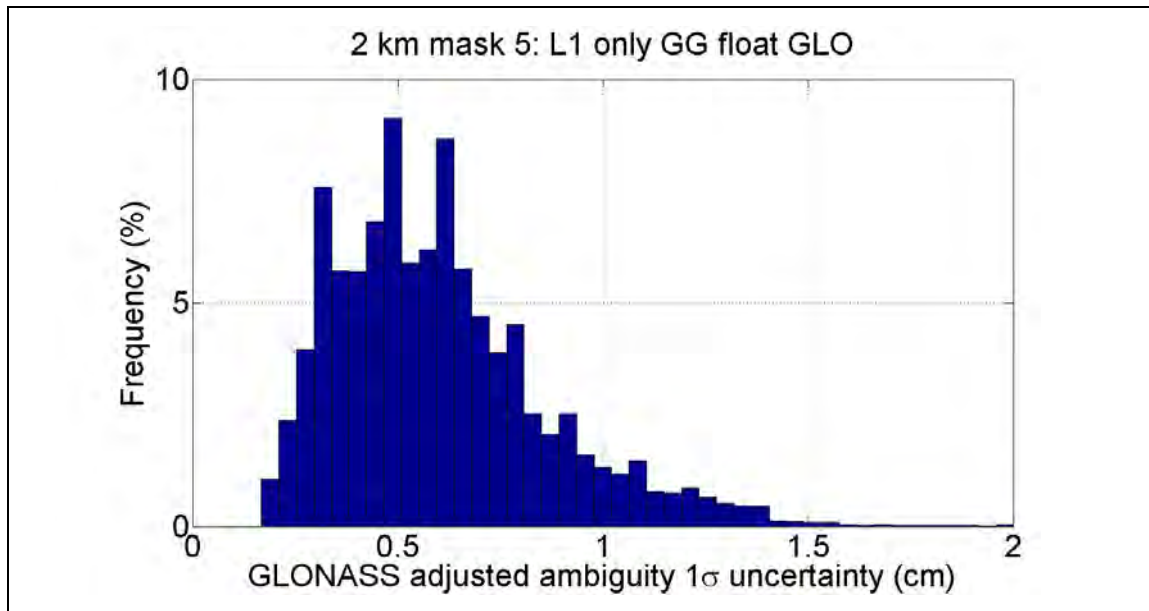


Figure 23 - GLONASS adjusted ambiguity uncertainties for L1 only GG float GLO solution - 2 km baseline under 5° mask

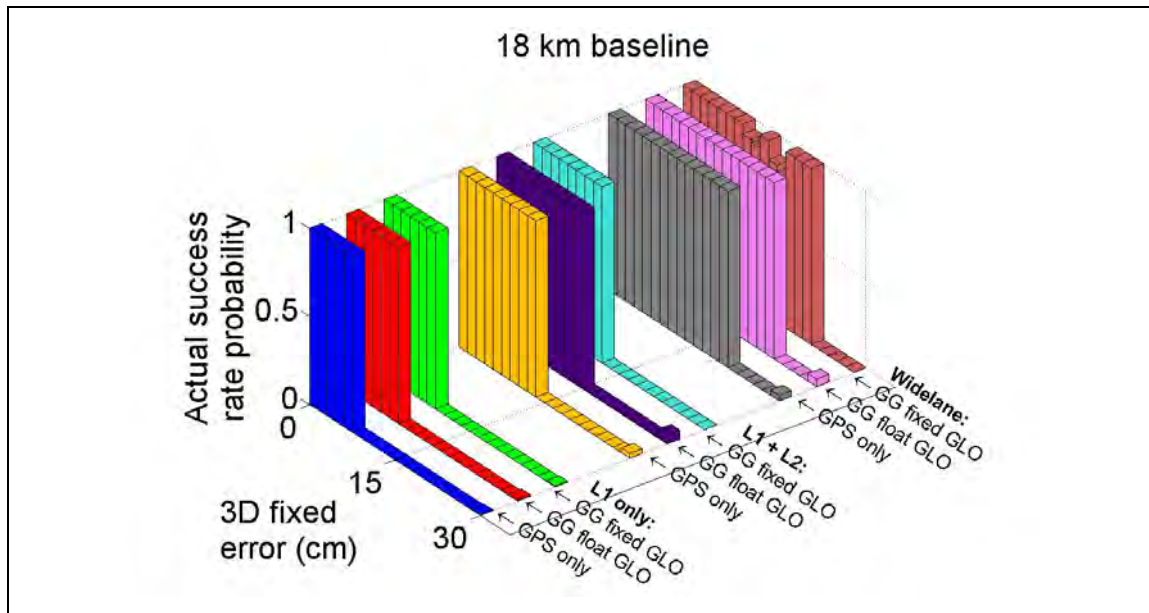


Figure 24 - Actual success rate vs. 3D fixed errors - 18 km baseline under 5° mask

4.3 Float Estimate Errors before Ambiguity Resolution

The trends in the actual success rate are ultimately driven by a number of underlying factors. The first of these is the error in the *float* estimate of the position (referred to as “float errors” herein), just prior to ambiguity resolution. Recall the parameterization of the double-differenced (DD) phase measurement:

$$\nabla\Delta\Phi = \nabla\Delta R + \lambda_i \nabla\Delta N + (\lambda_i - \lambda_{base}) \Delta N_{base} + \varepsilon_{\nabla\Delta\Phi}$$

An error in the float estimate of the position will affect the range term $\nabla\Delta R$, which in turn affects the float estimates of the ambiguities $\nabla\Delta N$ and ΔN_{base} . The effect of the float errors on the ambiguity resolution process is investigated here. Table 10 shows the median horizontal float errors for all of the integer fixes together, and also the correct and incorrect fixes separately.

Table 10 - Horizontal float errors before fix - static baselines under 5° mask

		Median horizontal float errors before fix (cm)					
		2 km baseline			18 km baseline		
		All fixes	Correct fixes	Incorrect fixes	All fixes	Correct fixes	Incorrect fixes
L1 only	GPS only	49	46	67	87	62	89
	GG float GLO	40	39	56	69	48	72
	GG fixed GLO	40	40	61	69	57	73
L1 + L2	GPS only	48	48	68	86	82	92
	GG float GLO	40	40	28	69	65	75
	GG fixed GLO	40	40	42	69	66	72
WL	GPS only	50	50	119	88	73	130
	GG float GLO	41	41	86	71	62	106
	GG fixed GLO	41	41	—	71	68	109

There is a slight correlation between the median float errors before ambiguity resolution, and the actual success rate probability of ambiguity resolution (see Table 9). Figure 25 illustrates this for both baselines. The actual success rate goes up as the median float errors decrease. This trend is different between the baselines, and confined to solutions that use the same measurement combination. For instance the actual success rates are much higher for the **L1 + L2** and **widelane** combinations than for the **L1 only** combination, despite similar median float errors.

An interesting observation is that the float errors do not change significantly between different measurement combinations. The combinations use different subsets of phase

measurements, but the same code measurements (GPS L1 C/A and GLONASS L1 CA).

This suggests that code accuracy is a major determinant of float errors, as expected.

The median float errors *do* improve when GLONASS measurements are added (i.e. switch from **GPS only** to **GG float GLO**). This is highlighted in **green** in Table 10. The improvement is on the decimetre-level, but the corresponding increase in actual success rate probability is only 0.06. Fixing the GLONASS ambiguities (i.e. using **GG fixed GLO**) does not improve the float errors – this is expected as float estimation happens *before* integer estimation.

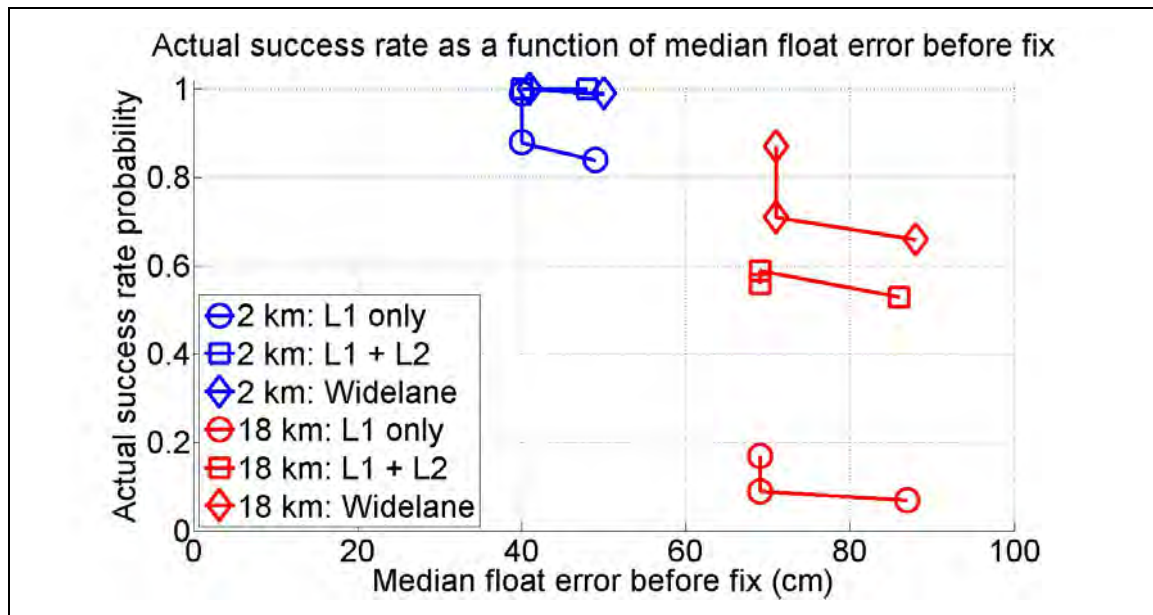


Figure 25 - Actual success rate vs. median horizontal float errors - static baselines under 5° mask

The general trend for both baselines is that correct fixes have smaller median float errors than incorrect fixes. This suggests that ambiguity resolution can only be consistently

successful with a precise initial float estimate. The dependence on the float estimate accuracy is further illustrated by Figure 26 and Figure 27 for the 2 km and 18 km baselines, respectively. These are the distributions of the actual success rate probability for various levels of float errors before fix.

The actual success rate does not significantly change whether GPS is used alone or combined with GLONASS. Hence, the role of the GLONASS measurements appears to be to *provide more accurate float estimates* in the first place, rather than to change the distribution of the actual success rate. From these distributions, it is also clear why the **GG float GLO** strategy does not have a big impact on the actual success rate in this case: decimetre-level improvements in float errors do not improve the actual success rate probability by more than 0.10.

However, the actual success rates tend to be higher when the GLONASS ambiguities are fixed. This implies that estimating the GLONASS *ambiguities* improves the overall ambiguity resolution process, beyond just decreasing the float errors by virtue of having more measurements in float estimation. This is explored in greater detail in Section 4.5.

As well, the actual success rates (for the same levels of float error) are much higher when *dual-frequency* measurement combinations are used. **Widelane** has the highest actual success rate distributions – this is expected as its ambiguity has a longer wavelength than either L1 or L2 and is thus inherently more observable with the coarser code measurements. For **L1 + L2** there are other factors that are investigated in Section 4.5.

The above findings are valid for the case when the differential atmospheric errors are benign. As to the question of whether they would be the same under a high level of ionospheric activity with differential effects reaching or exceeding 10 ppm, that can be better assessed when GPS/GLONASS data can be collected under such conditions.

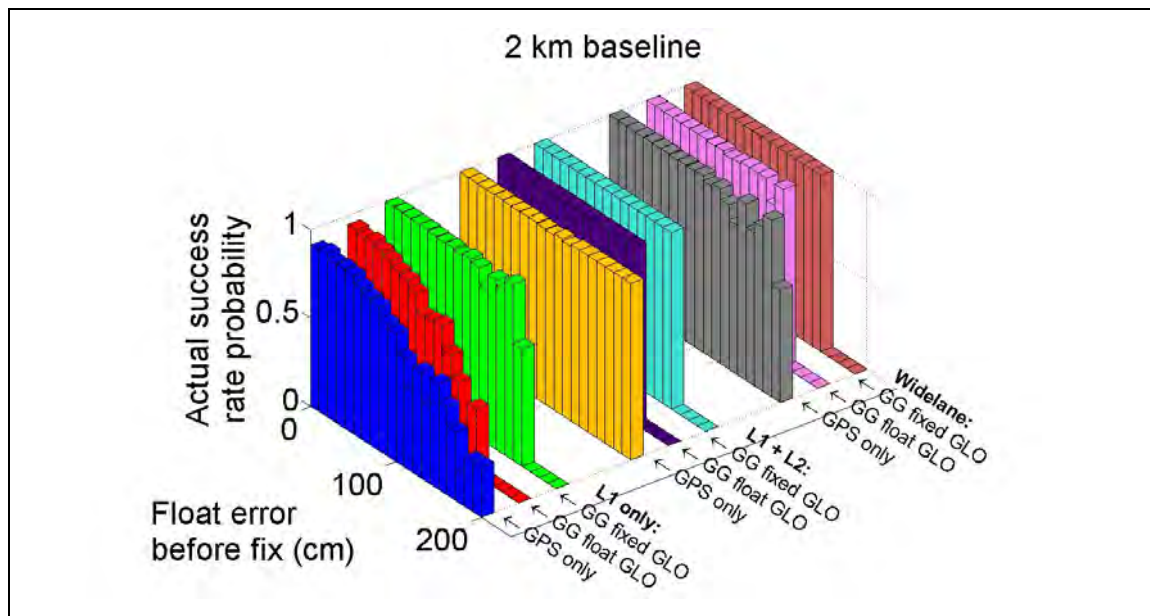


Figure 26 - Actual success rate vs. horizontal float errors - 2 km baseline under 5° mask

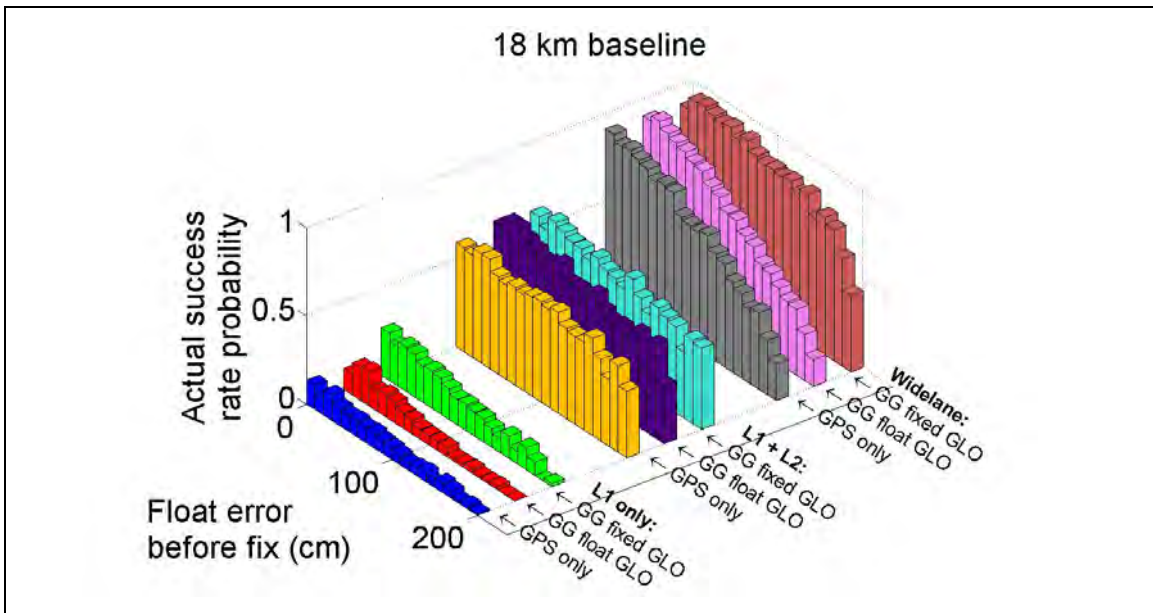


Figure 27 - Actual success rate vs. horizontal float errors - 18 km baseline under 5° mask

4.4 Phase Errors

It was demonstrated in Section 4.3 that errors in the float solution, prior to ambiguity resolution, will affect the actual success rate. Comparisons between different measurement combinations suggested that the code measurements contribute heavily to the float estimate accuracy, and consequently to the actual success rate.

The phase errors from both the 2 km and 18 km baselines were previously shown in Figure 20, and were shown to impact fixed-ambiguity positioning accuracy. The phase accuracy *also* contributes to determining the actual success rate: the phase is more accurate for the 2 km baseline than for the 18 km baseline, and consequently the actual success rates are higher. This is illustrated by Figure 28. Each *individual* fix is associated

with a set of phase residuals, characterized by their standard deviation. Figure 28 is the distribution of the phase error standard deviations for every **L1 only GG fixed GLO** integer fix for the 18 km baseline. Note that this solution is only chosen for illustrative purposes – results for *all* of the solutions are presented afterwards.

For this particular solution, the phase error standard deviations are clearly larger for the incorrect fixes than the correct fixes. The median phase error standard deviation is 1.7 cm for the correct fixes and 2.8 cm for the incorrect fixes. Additionally, there are many incorrect fixes with phase error standard deviations in the range of 3 to 5 cm, which indicates that there are *individual* phase errors with larger magnitudes. This suggests that the level of phase errors has an effect on ambiguity resolution.

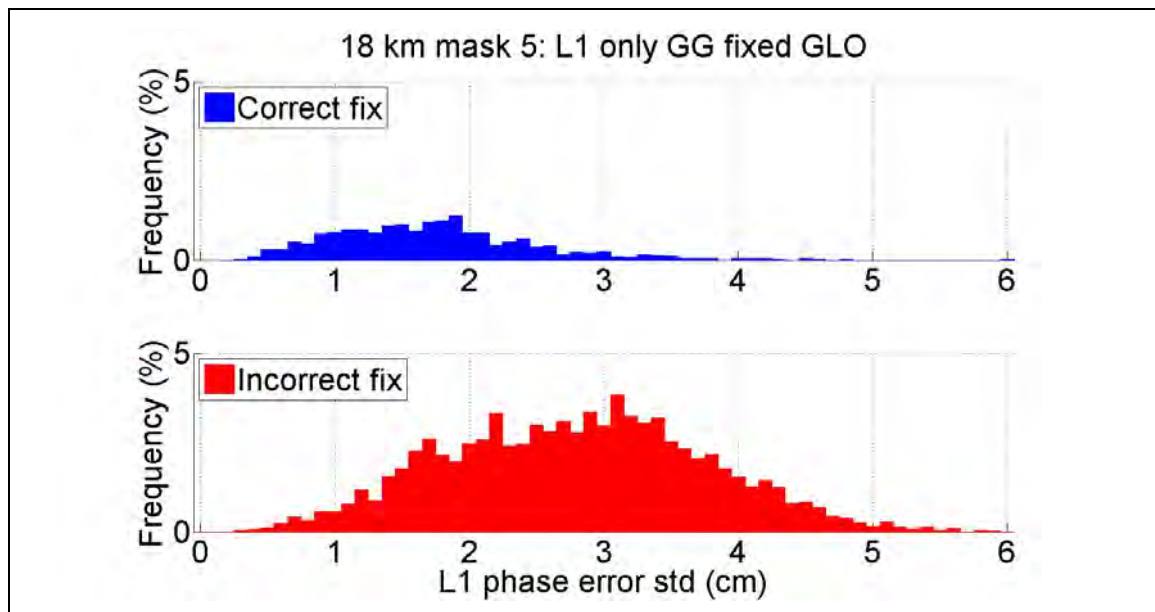


Figure 28 - Distribution of phase error standard deviation for L1 only GG fixed GLO solution - 18 km baseline under 5° mask

Further investigation reveals the nature of this relationship. The distributions of the actual success rate for various levels of phase errors (as represented by the L1 standard deviations) are shown in Figure 29 and Figure 30 for the 2 km and 18 km baselines, respectively. There is a negative trend: as the phase error standard deviation increases, the actual success rate decreases. Hence the phase errors have a proven impact on ambiguity resolution.

The **widelane** combination has an interesting feature. The distribution of the actual success rate for **widelane** does decrease with increasing phase error levels, but is much flatter than either **L1 only** or **L1 + L2**. This is corroborated by Figure 31, which shows the distribution of the phase error standard deviations for the **widelane GG fixed GLO** integer fix from the 18 km baseline. The distributions appear very similar whether the fix is correct or not, suggesting that widelane solutions can sustain fairly consistent actual success rates *even as the phase errors increase*, as anticipated. This is an advantageous feature in scenarios where the phase errors are high, such as long baseline surveys.

The effect of GLONASS here is similar to that for the float errors. The distributions of the actual success rates for the same levels of phase errors are similar whether GLONASS measurements are used or not (i.e. **GPS only** vs. **GG float GLO**) but improve when the GLONASS ambiguities are fixed (i.e. **GG fixed GLO**).

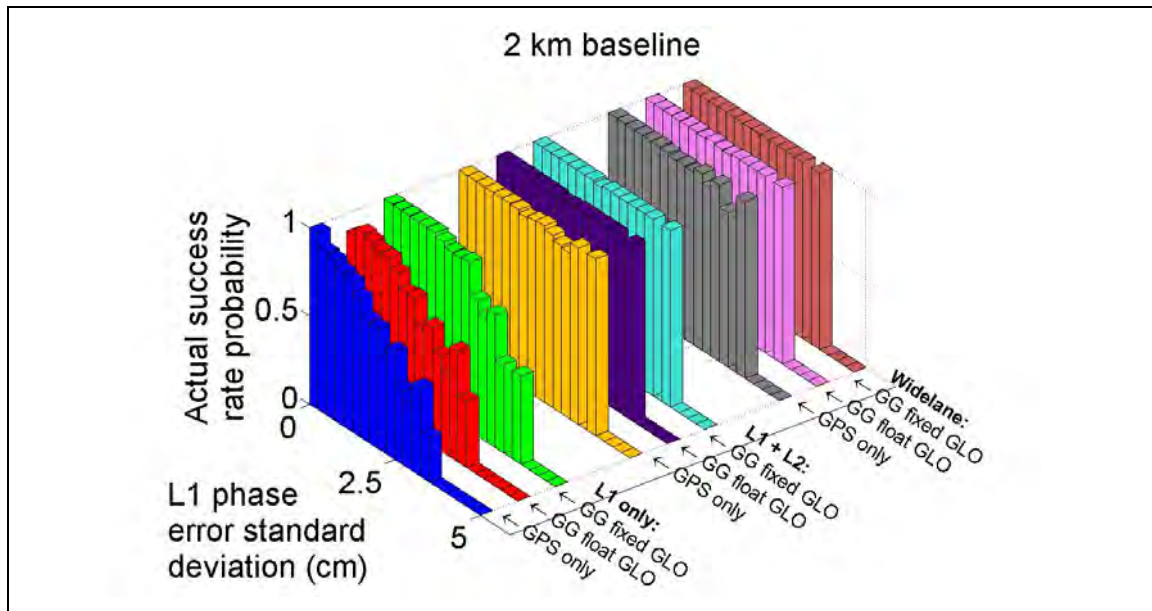


Figure 29 - Actual success rate vs. phase error standard deviation - 2 km baseline under 5° mask

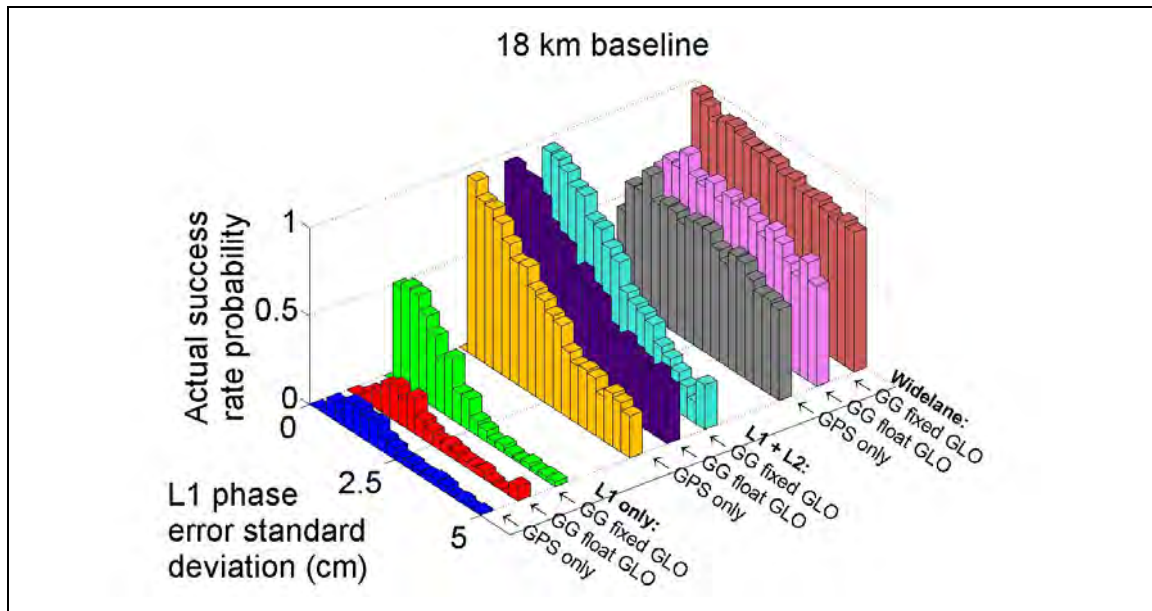


Figure 30 - Actual success rate vs. phase error standard deviation - 18 km baseline under 5° mask

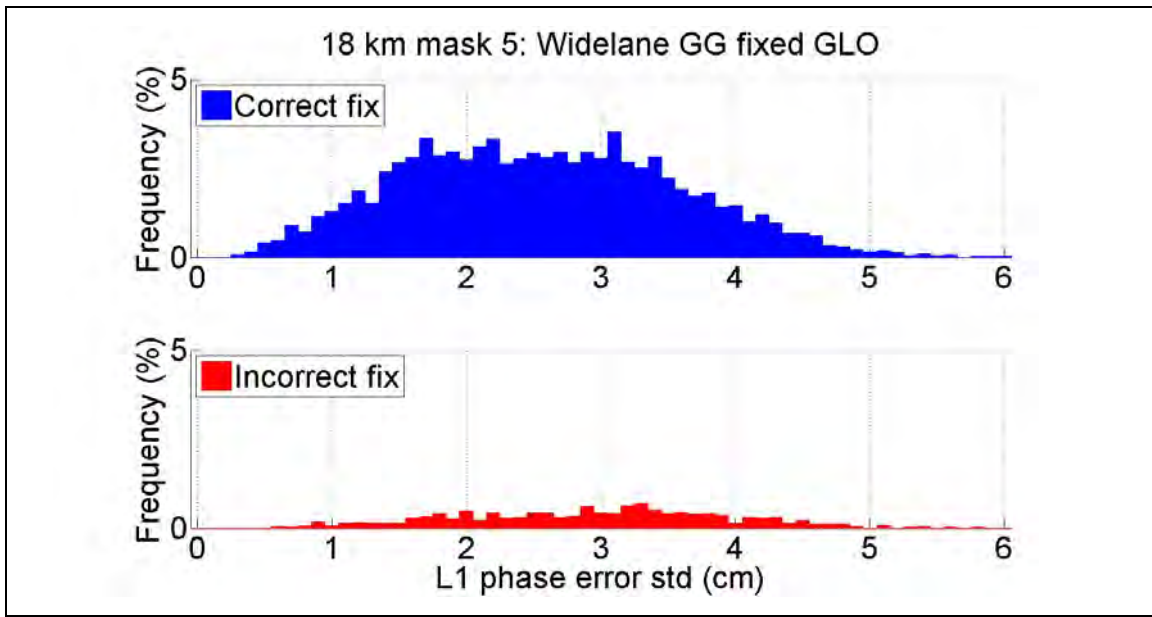


Figure 31 - Distribution of phase error standard deviation for widelane GG fixed GLO solution - 18 km baseline under 5° mask

4.5 Success Rates under Simulated Reduced Visibility

The effect of reduced satellite visibility on the actual success rate is investigated in this section. A reduced visibility scenario is simulated by increasing the mask angle of the circular elevation mask from 5° to 30°. The higher elevation mask reduces the availability of solutions, and consequently the number of integer fixes that are generated is reduced. Table 11 shows the number of *total* integer fixes generated, using GPS alone or GPS and GLONASS together. Table 12 then shows the actual success rates for both baselines in this scenario, with the numbers of correct fixes highlighted in **blue**.

Table 11 - Total number of fixes - static baselines under 30° mask

		Total number of fixes	
		2 km baseline	18 km baseline
Under 5° mask		6975	4751
Under 30° mask	GPS only	5745	4012
	<i>Availability relative to 5° mask</i>	(82.3%)	(84.4%)
	GPS/GLONASS	6952	4736
	<i>Availability relative to 5° mask</i>	(99.7%)	(99.7%)

Table 12 - Actual success rate probabilities - static baselines under 30° mask

		Actual success rate probability	
		2 km baseline	18 km baseline
L1 only	GPS only	0.18 (1057)	0.04 (152)
	GG float GLO	0.20 (1403)	0.05 (260)
	GG fixed GLO	0.59 (4105)	0.13 (617)
L1 + L2	GPS only	0.90 (5168)	0.62 (2492)
	GG float GLO	0.88 (6131)	0.63 (2999)
	GG fixed GLO	0.98 (6831)	0.66 (3112)
Widelane	GPS only	0.58 (3321)	0.47 (1900)
	GG float GLO	0.59 (4095)	0.49 (2337)
	GG fixed GLO	0.87 (6037)	0.74 (3491)

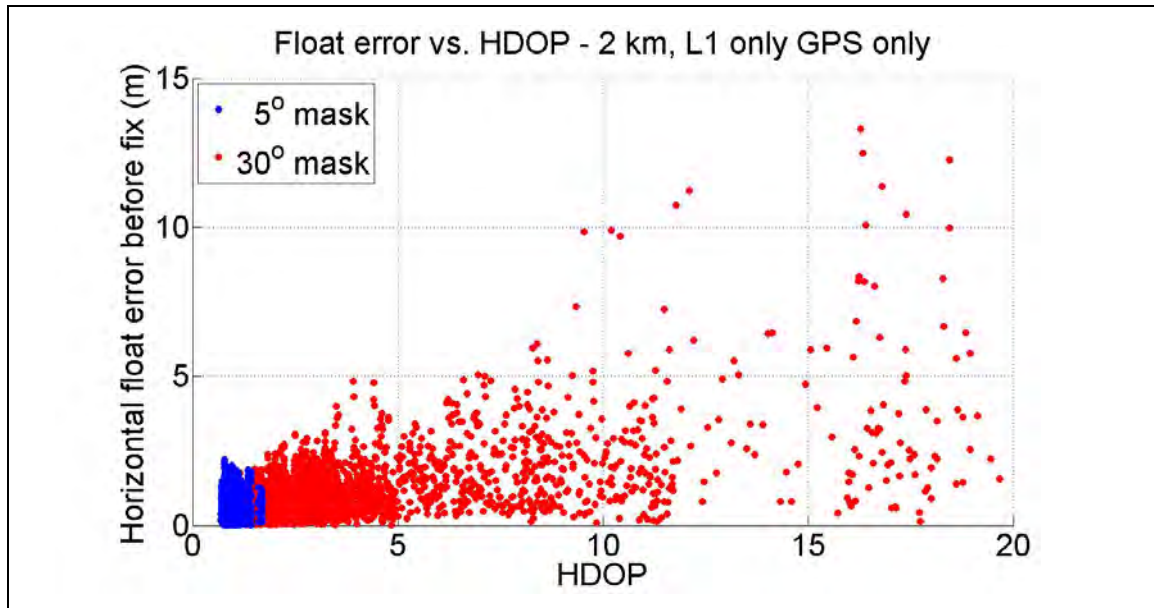
Table 11 highlights one of the advantages of adding GLONASS to GPS: the availability of fixes under the 30° mask is almost 100%, relative to the number of fixes under the 5° mask. For the fixes that *are* generated, the actual success rates are all much lower under the 30° mask than under the 5° mask, as anticipated. This decrease is especially evident for the 2 km baseline, as the actual success rate probabilities were previously very close

to one. One of the reasons is that the errors in the float estimate, just prior to ambiguity resolution, are higher under a 30° mask than a 5° mask. Table 13 shows the median horizontal float errors for all of the fixes together as well as the correct and incorrect fixes. The float errors are larger due to the poorer satellite geometry, as illustrated in Figure 32 using the **L1 only GPS only** solution from the 2 km baseline.

Under the normal 5° mask, there was a correlation observed between the median float errors and the actual success rate. Under this reduced-visibility 30° mask, this relationship is very weak. Table 13 shows that adding GLONASS measurements (i.e. going from **GPS only** to **GG float GLO**) does decrease the float errors. However, Table 12 indicates that adding those same GLONASS measurements barely affects the success rate – the maximum increase in actual success rate probability is 0.02. What *does* improve the actual success rate significantly is when the GLONASS ambiguities are fixed (as highlighted in **green**).

Table 13 - Horizontal float errors before fix - static baselines under 30° mask

		Median horizontal float errors before fix (cm)					
		2 km baseline			18 km baseline		
		All fixes	Correct fixes	Incorrect fixes	All fixes	Correct fixes	Incorrect fixes
L1 only	GPS only	71	41	79	95	44	98
	GG float GLO	57	37	63	72	36	75
	GG fixed GLO	57	47	77	72	52	76
L1 + L2	GPS only	70	65	135	95	84	114
	GG float GLO	56	53	95	71	66	81
	GG fixed GLO	56	55	165	71	69	76
WL	GPS only	72	54	106	97	69	136
	GG float GLO	59	47	81	75	57	97
	GG fixed GLO	59	54	105	75	66	112

**Figure 32 - Relationship between horizontal float error before fix and HDOP using L1 only GPS only solution - 2 km baseline**

The independence of the success rate from the float errors and the difference between the **GG float GLO** and **GG fixed GLO** strategies both point to an underlying factor related to the integer ambiguity estimation that is impacting the success rate. This underlying factor is the *number of ambiguities* estimated as integers within the ambiguity resolution process: the actual success rate is higher with more ambiguities in the ambiguity resolution process (not the float estimation process). To illustrate this relationship, the distributions of the number of ambiguities are analyzed for a series of solutions from the 2 km baseline. The results are shown as follows:

- Figure 33: Under the **5° mask**, the **L1 only GPS only** fixes have between six and eleven ambiguities. With the abundance of ambiguities, most of the fixes are correct.
- Figure 34: When the **30° mask** is applied for the same **L1 only GPS only** solution, the number of ambiguities decreases to between three and seven. Most of the fixes are now incorrect.
- Figure 35: Under the same **30° mask**, the number of ambiguities stays the same when the estimation strategy is switched to **L1 only GG float GLO**. Because there are still so few ambiguities, most of the fixes are still incorrect.
- Figure 36: Finally, under the same **30° mask**, the number of ambiguities increases substantially when the estimation strategy is switched to **L1 only GG fixed GLO**.

Correspondingly, there are more correct fixes. However, as illustrated in Figure 36 (as well as the Figure 34 and Figure 35), a significant proportion of the fixes use between three to five ambiguities, and most of these fixes are incorrect.

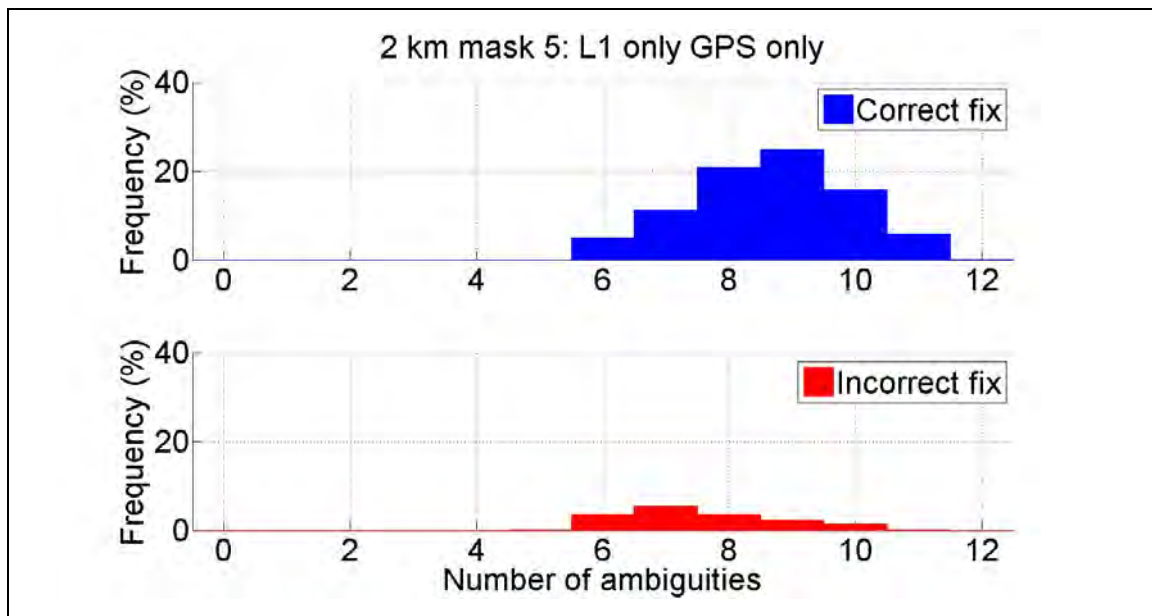


Figure 33 - Distribution of number of ambiguities for L1 only GPS only solution - 2 km baseline under 5° mask

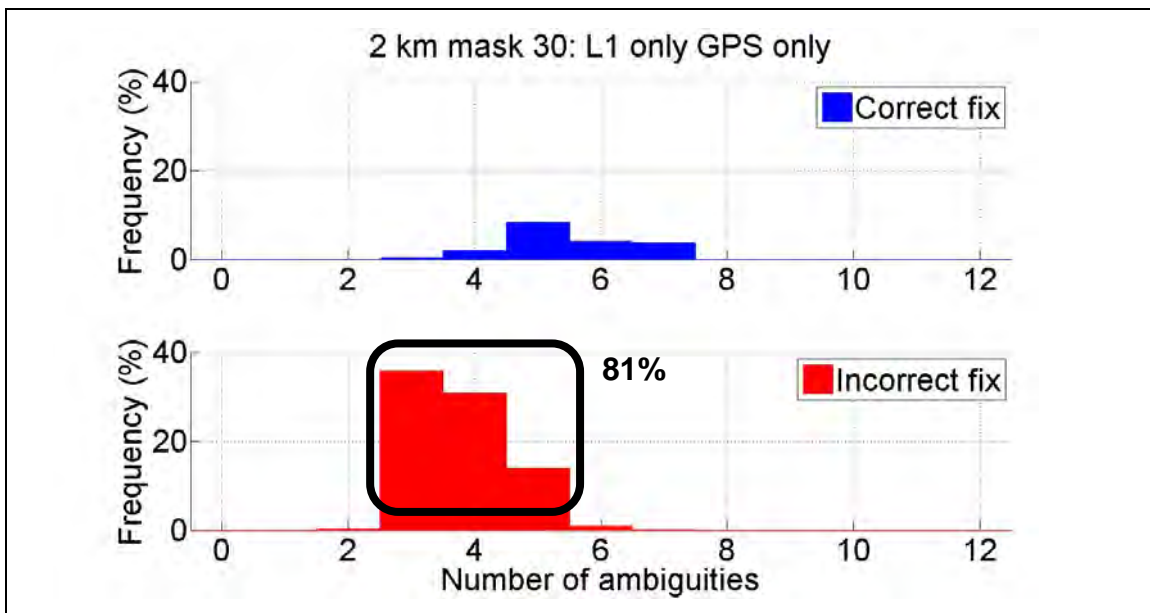


Figure 34 - Distribution of number of ambiguities for L1 only GPS only solution - 2 km baseline under 30° mask

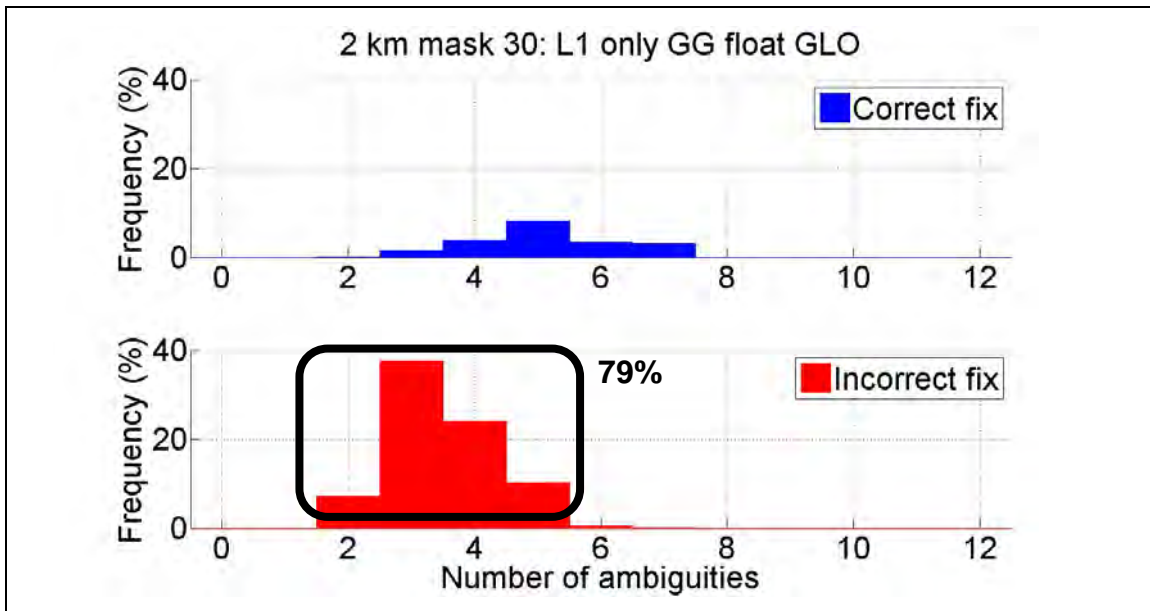


Figure 35 - Distribution of number of ambiguities for L1 only GG float GLO solution - 2 km baseline under 30° mask

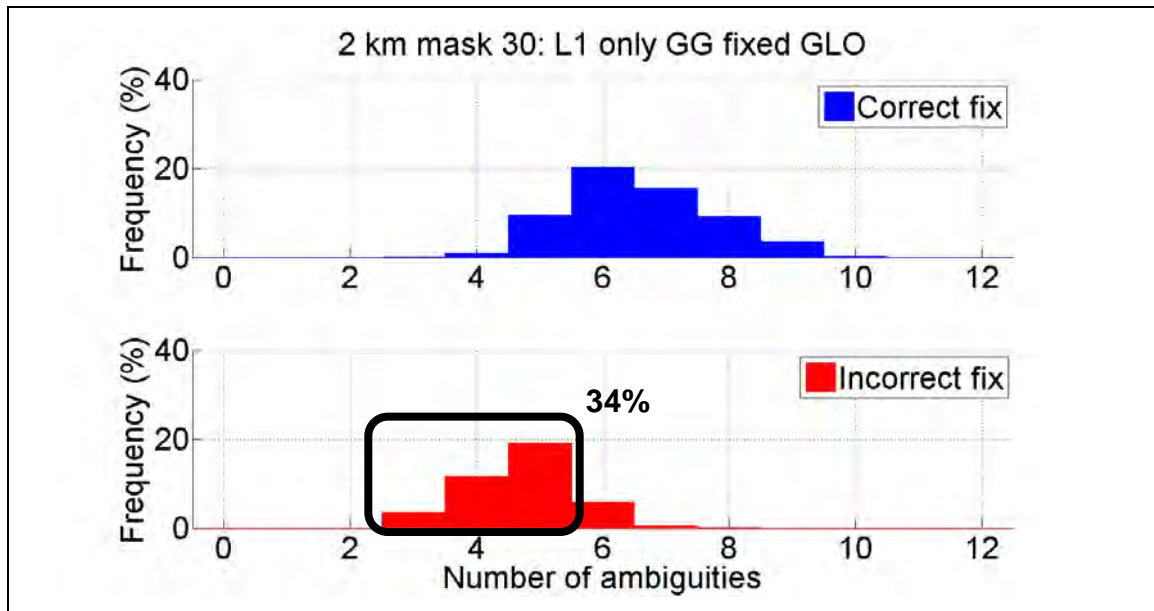


Figure 36 - Distribution of number of ambiguities for L1 only GG fixed GLO solution - 2 km baseline under 30° mask

The effect of the number of ambiguities on ambiguity resolution is fully illustrated in Figure 37 and Figure 38 for the 2 km and 18 km baselines, respectively, with all solutions processed under a 30° elevation mask. These are distributions of the actual success rates for various numbers of ambiguities. There is a positive trend: the more ambiguities there are, the higher the actual success rate. This is the primary way that the **GG fixed GLO** and **L1 + L2** strategies impact the actual success rate.

However, there is a limit to how much improvement can be achieved by adding more ambiguities. For the 2 km baseline, fixes with more than six ambiguities have actual success rates close to one. For the 18 km baseline, fixes with more than nine ambiguities have actual success rates greater than 0.60.

This raises a number of considerations. Under open sky conditions it is reasonable to expect between six and nine ambiguities from a strategy such as **L1 only GPS only**, and consequently higher actual success rates. From the analysis here, this may suffice for shorter baselines. When satellite visibility is reduced, the number of ambiguities naturally drops and therefore augmentation by either the **GG fixed GLO** strategy and/or the **L1 + L2** combination should be considered. **Widelane** can also be considered for longer baselines because it can withstand larger phase errors. In fact, the most effective strategy for the 18 km baseline under the 30° mask is **widelane GG fixed GLO**.

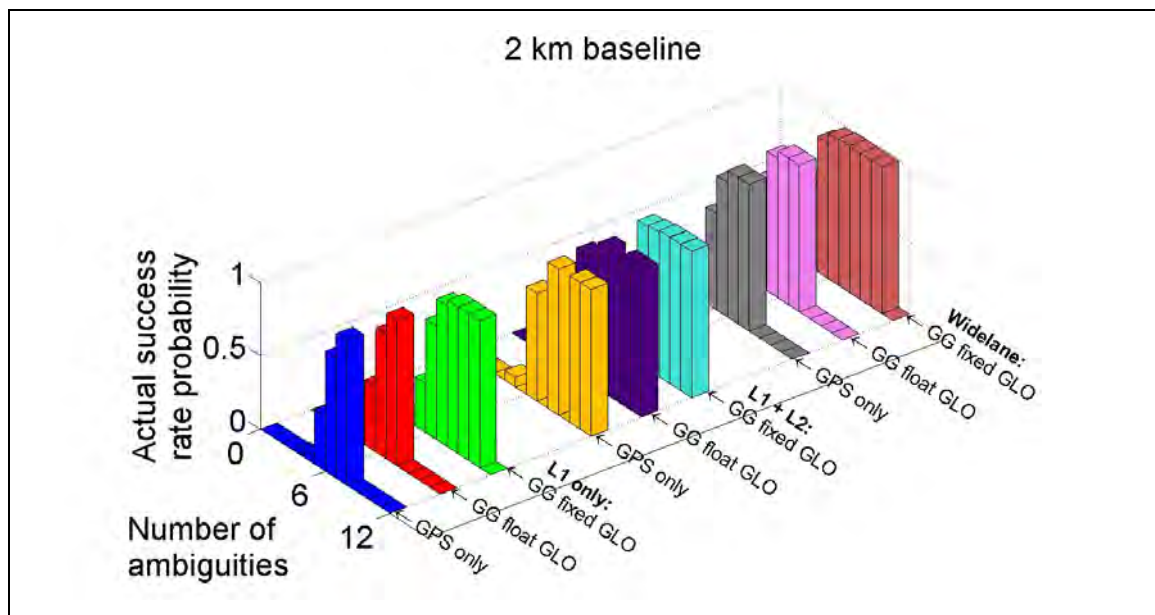


Figure 37 - Actual success rate vs. number of ambiguities - 2 km baseline under 30° mask

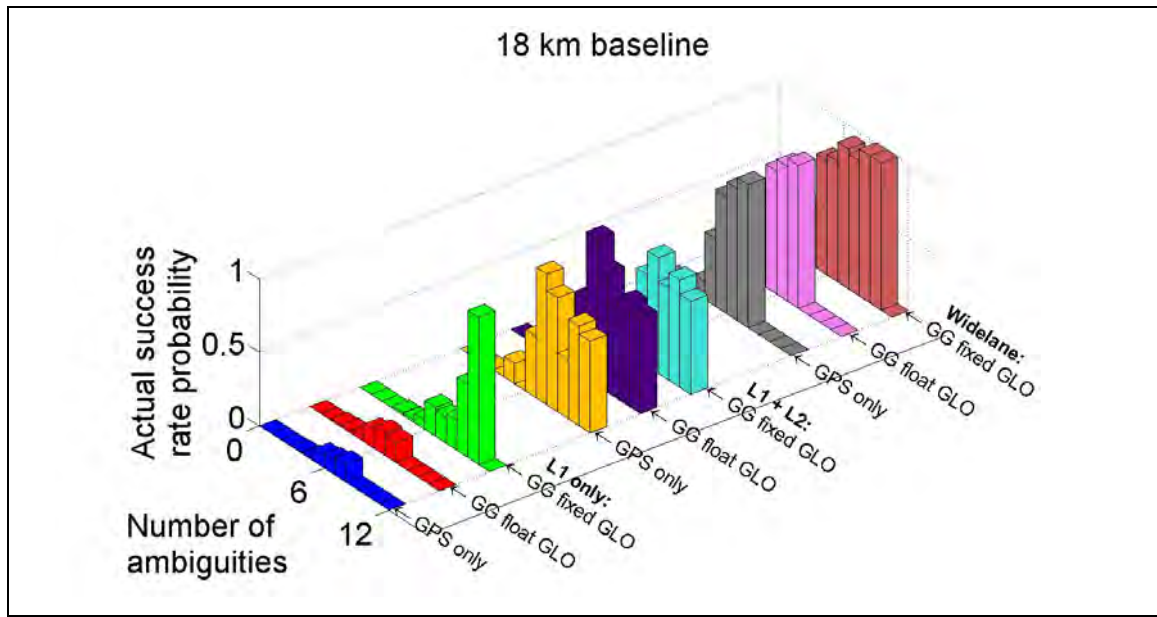


Figure 38 - Actual success rate vs. number of ambiguities - 18 km baseline under 30° mask

The number of ambiguities is naturally connected to the geometry of the integer ambiguity estimation – that is, the ADOP. The effect of reducing the visibility on the ADOP is shown in Figure 39 and Figure 40 for the 2 km and 18 km baselines, respectively, with all solutions processed with a 30° elevation mask. The pattern is obvious: reduced satellite visibility increases the ADOP, which correlates strongly with the number of incorrect fixes. This is anticipated since poor geometry often leads to less precise position solutions. The range of ADOPs under the 30° mask is larger than the range of ADOPs under the 5° mask (shown by Figure 17 and Figure 18) – for example, the ADOPs for the 2 km baseline **L1 only** solutions do not exceed 5 cm under the 5° mask but go up to 10 cm or more under the 30° mask. It is not surprising then that the actual success rates are lower under the 30° mask.

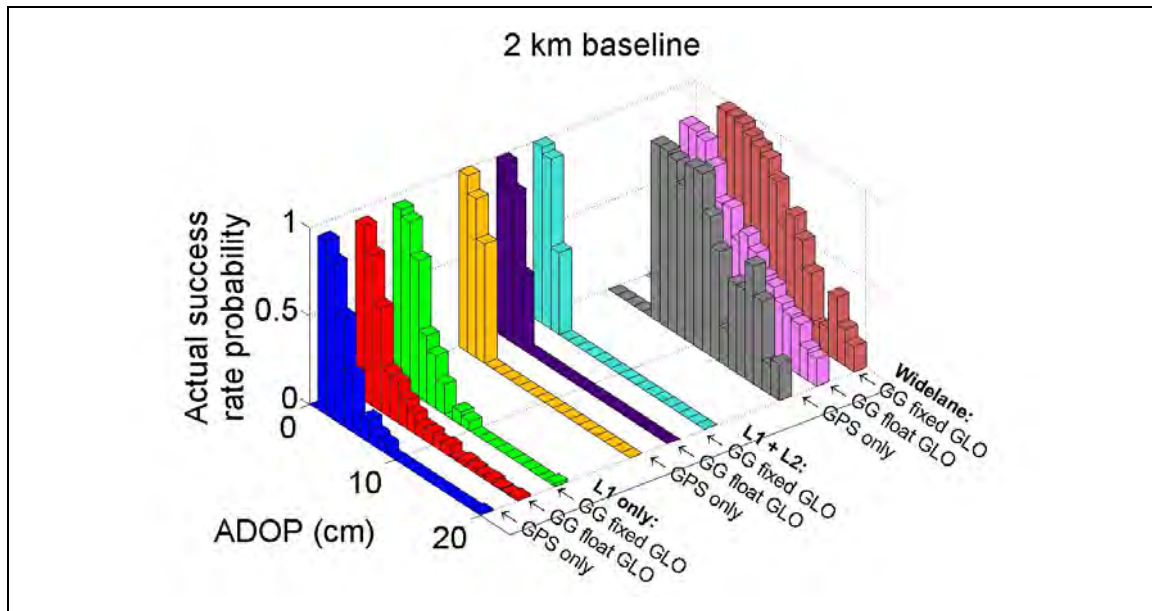


Figure 39 - Actual success rate vs. ADOP - 2 km baseline under 30° mask

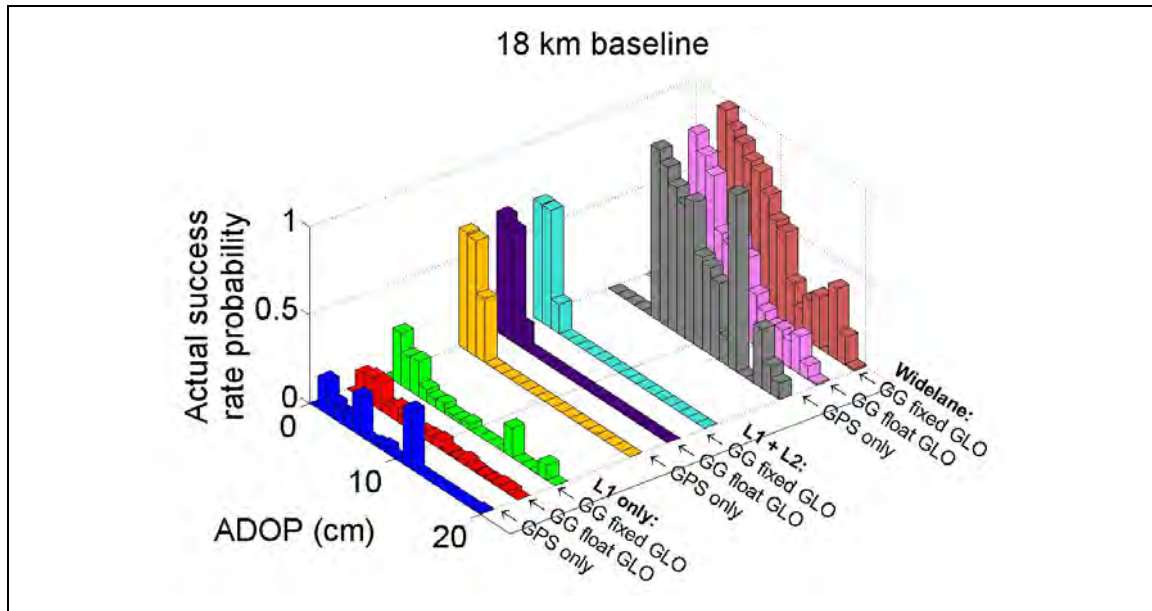


Figure 40 - Actual success rate vs. ADOP - 18 km baseline under 30° mask

4.6 Reliability Testing: Predicted Success Rate

The effectiveness of the predicted success rate as a test or indicator of reliability for ambiguity resolution is investigated here. Table 14 shows four categories of results from applying the predicted success rate for the 2 km baseline. A probability threshold of 0.95 was set for the predicted success rate – the integer fix was accepted if it exceeded this value and rejected otherwise. The results are separated into the correct and incorrect fixes; within each group of fixes, the rates of acceptance and rejection are then presented. Correct fixes should be accepted and incorrect fixes rejected; otherwise an *error* is said to occur. No incorrect fix results are presented for the solutions with too few incorrect fixes to compute meaningful acceptance and rejection rates. The numbers of fixes corresponding to each result are highlighted in **blue**.

Table 14 - Predicted success rate results - 2 km baseline under 5° mask

		Predicted success rate (0.95 threshold) – 2 km baseline			
		Correct fix		Incorrect fix	
		Accept	Reject	Reject	Accept
L1 only	GPS only	97.5% (5703)	2.5% (147)	12.7% (143)	87.3% (982)
	GG float GLO	98.6% (6068)	1.4% (88)	7.1% (58)	92.9% (761)
	GG fixed GLO	99.1% (6841)	0.9% (60)	— —	— —
L1 + L2	GPS only	97.5% (6786)	2.5% (174)	— —	— —
	GG float GLO	97.7% (6806)	2.3% (163)	— —	— —
	GG fixed GLO	97.4% (6793)	2.6% (179)	— —	— —
WL	GPS only	94.5% (6558)	5.5% (382)	— —	— —
	GG float GLO	94.8% (6599)	5.2% (363)	— —	— —
	GG fixed GLO	94.6% (6599)	5.4% (376)	— —	— —

For this baseline, the predicted success rate generally appears to accept fixes too often.

For the solutions that have enough incorrect fixes to analyze, the rate of incorrect fix acceptance is very high, as highlighted in red in Table 14. There are two aspects to this problem:

1. The rates of acceptance for correct and incorrect fix acceptance are similar in magnitude. This suggests that the predicted success rate does not provide much information to discriminate between correct and incorrect fixes.
2. Fixes that are accepted have predicted success rates of 0.95 or higher, so it is expected that less than 5% of accepted fixes are “unsuccessful” (i.e. incorrect). This is not the case here: for the **L1 only GPS only** solution, 15% of accepted

fixes are incorrect (i.e. 982 / [982 + 5703]). For the **L1 only GG float GLO** solution, 11% of accepted fixes are incorrect (i.e. 761 / [761 + 6068]).

Accepting incorrect fixes leads to *undetected position biases*, a major problem for fixed-ambiguity applications where the expectation is to have position accuracies better than 10 cm. This is further illustrated in Figure 41, which shows the distribution of predicted success rates for the **L1 only GPS only** solutions. The predicted success rate probabilities for nearly every fix are greater than 0.98, despite the fact that the aggregate actual success rate probability (from Table 9) is only 0.84.

Conversely, correct fixes do not appear to be rejected very often for this baseline. Rejecting a correct fix induces a *loss of precision* in the position. This is again a function of the predicted success rate being so optimistic; fixes *in general* are not rejected very often.

There is an important consideration regarding the solutions with few incorrect fixes. These solutions either use GLONASS measurements and fix the ambiguities, or use dual-frequency measurement combinations. The actual success rates are so high that there are few incorrect fixes that *could* actually be accepted. Hence, the use of GLONASS or dual-frequency measurements can be partly viewed as a positive contributor to fix reliability, in that they drive the actual success rate higher and remove incorrect fixes that can be potentially accepted.

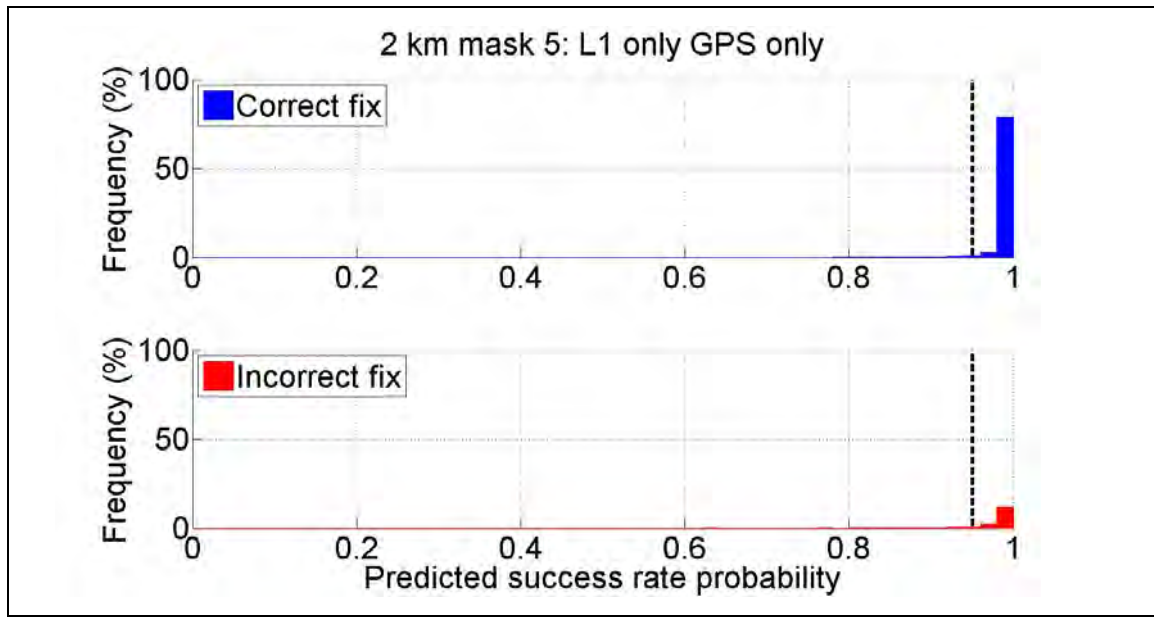


Figure 41 - Distribution of predicted success rate for L1 only GPS only solutions - 2 km baseline under 5° mask

The predicted success rate is an *a priori* statistic, so it is affected by *a priori* parameters like the estimated phase uncertainty. The highly optimistic predicted success rates illustrated by Figure 41 are indicative of unrealistic *a priori* parameters. Processing was done in this environment using an *a priori* undifferenced phase uncertainty of 4 mm (1σ). Figure 42 illustrates that changing the *a priori* uncertainty (to 8, 12, 16 or 20 mm) changes the predicted success rate significantly.

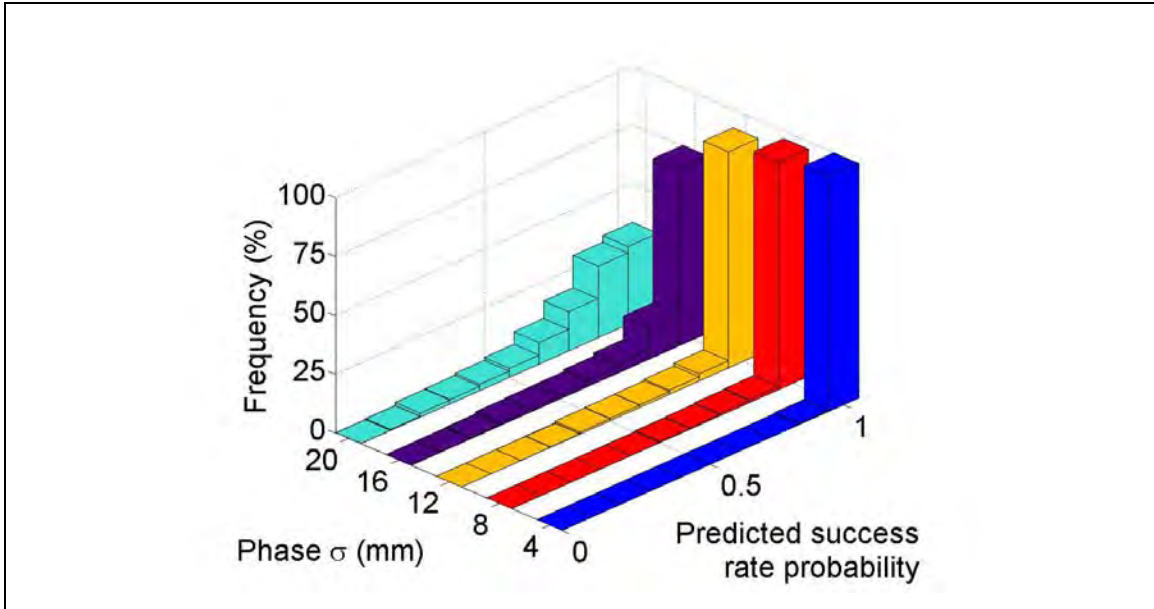


Figure 42 - Predicted success rate as a function of *a priori* phase uncertainty

Ideally the actual phase error distribution would be used to compute the predicted success rates – for the 2 km baseline, the 1σ phase uncertainty is 13 mm in the DD domain (see Figure 20), equivalent to 6.5 mm for undifferenced phase measurements. When this uncertainty is applied *a priori*, the resulting performance of the predicted success rate is shown in Table 15. The numbers of fixes corresponding to each result are highlighted in blue. A comparison with Table 14 reveals that the new predicted success rates are generally more effective at rejecting incorrect fixes, as highlighted in green. For instance less than 50% of the incorrect fixes from the **L1 only GPS only** solution are accepted, as opposed to nearly 90% when the *a priori* phase uncertainty is 4 mm. However there are four considerations regarding changing the *a priori* uncertainty:

1. The reduction in incorrect fix acceptance is not overwhelming – a rate of 50% is still potentially harmful, especially when operating in environments where incorrect fixes are more common.
2. The reduction in incorrect fix acceptance comes at the expense of higher correct fixes *rejection*. This is expected since the predicted success rates decrease (as illustrated by Figure 42) but it means that the ambiguities are resolved less often.
3. The true phase errors are generally not known before a survey is undertaken. Determining them requires precise knowledge of the rover station coordinates, which is often the objective of ambiguity resolution in the first place.
4. Phase error growth is strongly correlated to the level of ionospheric activity. The latter could be automatically assessed in software if dual-frequency measurements are available and adapted accordingly. An investigation of adaptability would require data over different inter-receiver distances and under different ionospheric conditions.

Table 15 - Predicted success rate results for undifferenced phase 1σ of 6.5 mm - 2 km baseline under 5° mask

		Predicted success rate (0.95 threshold) – 2 km baseline			
		Correct fix		Incorrect fix	
		Accept	Reject	Reject	Accept
L1 only	GPS only	85.5% (4811)	14.5% (817)	50.7% (683)	49.3% (664)
	GG float GLO	91.0% (5400)	9.0% (534)	34.8% (362)	65.2% (679)
	GG fixed GLO	96.7% (6682)	3.3% (225)	— —	— —
L1 + L2	GPS only	92.0% (6398)	8.0% (560)	— —	— —
	GG float GLO	92.0% (6410)	8.0% (556)	— —	— —
	GG fixed GLO	90.7% (6324)	9.3% (648)	— —	— —
WL	GPS only	89.9% (6170)	10.1% (695)	— —	— —
	GG float GLO	90.2% (6237)	9.8% (678)	— —	— —
	GG fixed GLO	89.3% (6227)	10.7% (745)	— —	— —

The predicted success rate results from the 18 km baseline are shown in Table 16. The numbers of fixes corresponding to each result are highlighted in blue. All of the solutions from this baseline had more incorrect fixes than the 2 km baseline – hence the impact of GLONASS or dual-frequency measurements on the predicted success rate can finally be evaluated. The main flaw of the predicted success rate becomes clear here: it accepts too many incorrect fixes (as highlighted in red).

The problem is that the predicted success rates are too optimistic (i.e. they are too close to one when expressed as probabilities), because the *a priori* uncertainty is too optimistic. Recall from Figure 20 that the L1 DD phase error standard deviation for this baseline is 3.4 cm. That is equivalent to a 17 mm standard deviation for undifferenced phase

measurements – a full 13 mm more than the *a priori* uncertainty. The *a priori* uncertainty is often optimistic because the differential atmospheric component of the true phase error increases with inter-receiver distance and the level of ionospheric activity.

Table 16 - Predicted success rate results - 18 km baseline under 5° mask

		Predicted success rate (0.95 threshold) – 18 km baseline					
		Correct fix		Incorrect fix			
		Accept	Reject	Reject	Accept	Reject	Accept
L1 only	GPS only	84.4% (271)	15.6% (50)	37.3% (1653)	62.7% (2777)		
	GG float GLO	86.2% (357)	13.8% (57)	26.2% (1138)	73.8% (3199)		
	GG fixed GLO	99.8% (824)	0.2% (2)	0.3% (11)	99.7% (3914)		
L1 + L2	GPS only	99.1% (2511)	0.9% (24)	0.8% (18)	99.2% (2198)		
	GG float GLO	99.1% (2756)	0.9% (26)	0.8% (16)	99.2% (1953)		
	GG fixed GLO	99.0% (2624)	1.0% (27)	0.9% (18)	99.1% (2082)		
WL	GPS only	97.0% (3043)	3.0% (93)	7.3% (118)	92.7% (1497)		
	GG float GLO	97.7% (3310)	2.3% (77)	3.7% (51)	96.3% (1313)		
	GG fixed GLO	97.4% (4050)	2.6% (106)	4.2% (25)	95.8% (570)		

In isolation, the predicted success rate actually becomes *less* useful when GLONASS is added, or when dual-frequency measurements are used. The **L1 only GPS only** solution has the lowest rate of incorrect fix acceptance at just under 63%; this continually increases, up to near 100%, when GLONASS or dual-frequency strategies are implemented.

However, recall from Table 9 that the actual success rate is maximized when using the **GG fixed GLO** strategy with **widelane** measurements. The distributions of the predicted success rates for this solution are shown in Figure 43. With fewer incorrect fixes, there are fewer *total* instances of incorrect fix acceptance. Even though GLONASS and dual-frequency do not improve the ability of the *predicted success rate* to reject incorrect fixes, they do still positively impact fix reliability by driving actual success rates higher.

As well, the rate of correct fix rejection is actually slightly higher for this baseline than for the 2 km baseline. This error is committed most often for the **L1 only GPS only** solution. The use of GLONASS has a positive impact, with the lowest error rate of 0.2% for the **L1 only GG fixed GLO** solution. The dual-frequency solutions are also effective.

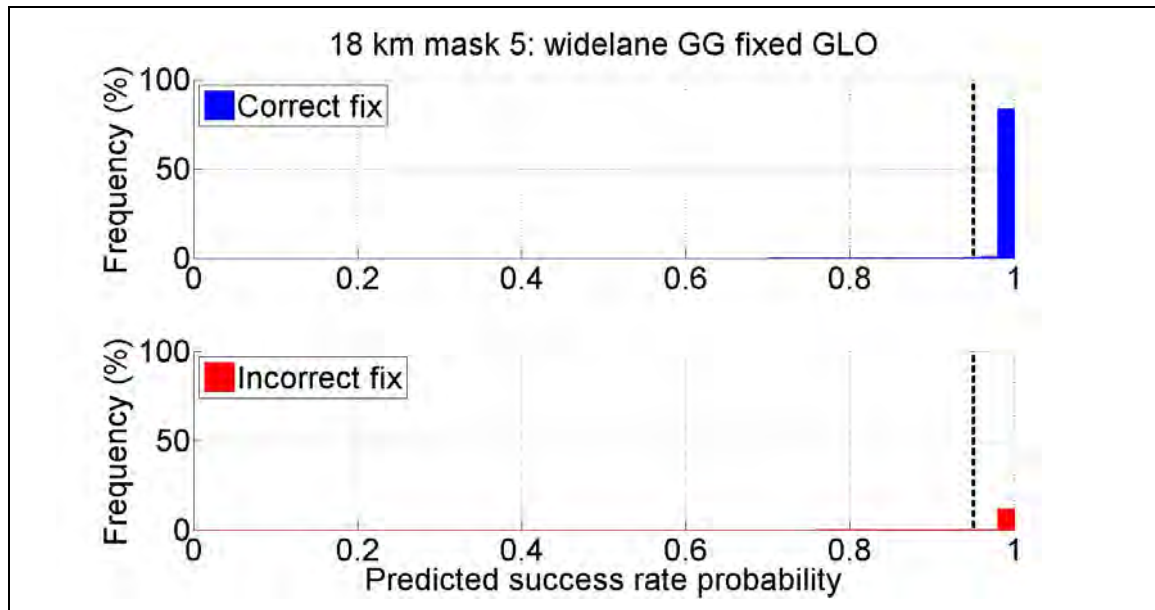


Figure 43 - Distribution of predicted success rate for widelane GG fixed GLO solution - 18 km baseline under 5° mask

4.7 Reliability Testing: F-Test

The performance of the F ratio test (or F-test) is investigated here. The F-test was conducted with a 10% significance level, with the critical value (or threshold) for ratio testing taken from the F probability distribution function. Table 17 shows the results of the F-test from the 2 km baseline. No results are presented for the solutions with too few incorrect fixes to compute meaningful acceptance and rejection rates. The numbers of fixes corresponding to each F-test result are highlighted in **blue**.

Table 17 - F-test results - 2 km baseline under 5° mask

		F-test (10% significance) – 2 km baseline			
		Correct fix		Incorrect fix	
		Accept	Reject	Reject	Accept
L1 only	GPS only	57.4% (3358)	42.6% (2492)	98.0% (1102)	2.0% (23)
	GG float GLO	60.9% (3752)	39.1% (2404)	97.8% (801)	2.2% (18)
	GG fixed GLO	90.8% (6269)	9.2% (632)	— —	— —
L1 + L2	GPS only	87.9% (6119)	12.1% (841)	— —	— —
	GG float GLO	87.7% (6115)	12.3% (854)	— —	— —
	GG fixed GLO	83.6% (5831)	16.4% (1141)	— —	— —
WL	GPS only	83.1% (5770)	16.9% (1170)	— —	— —
	GG float GLO	85.7% (5967)	14.3% (995)	— —	— —
	GG fixed GLO	89.5% (6243)	10.5% (732)	— —	— —

For this baseline, the F-test is more effective than the predicted success rate in terms of *not* accepting incorrect fixes, as highlighted in Table 17 in **green**. For the solutions with meaningful results (**L1 only GPS only** and **L1 only GG float GLO**), the rate of incorrect

fix acceptance is less than 3%. This appears to come at a cost: the F-test rejects correct fixes much more often than the predicted success rate, leading to a loss of precision in the position. This is expected due to the nature of the F-test, which is described below:

- The null and alternative hypotheses for the F-test are described in Section 2.5. The probability of a Type II error is defined by the power of the F-test. For a 10% significance level, Table 18 shows the test powers and corresponding probabilities of Type II error for different numbers of ambiguities. The non-centrality parameter is computed based on the assumption that only one ambiguity is incorrect (and thus biased) – test powers for different biases and uncertainties are also shown in Table 18. The test power varies significantly based on the magnitudes of the ambiguity bias and uncertainty. In some cases, Type II errors occur at probabilities of more than 60%.
- For the two solutions from the 2 km baseline with incorrect fixes to analyze, the occurrence of Type II error (i.e. rejection of correct fix) is 69% for the **L1 only GPS only** solution (i.e. $2492 / [2492 + 1102]$) and 75% for the **L1 only GG float GLO** solution (i.e. $2404 / [2404 + 801]$). These are slightly larger than the theoretical probabilities from Table 18. However much larger probabilities of Type II error can be derived from larger ambiguity biases, smaller ambiguity uncertainties, or multiple incorrect ambiguities.

Table 18 - F-test power as a function of number of ambiguities

Number of ambiguities	Ambiguity bias (cycles)	Ambiguity uncertainty (cycles)	Test power (%)	Probability of Type II error (%)
5	1	1	86.5%	13.5%
	1	0.5	75.3%	24.7%
	2	0.5	36.0%	64.0%
8	1	1	87.0%	13.0%
	1	0.5	77.3%	22.7%
	2	0.5	38.5%	61.5%
12	1	1	87.5%	12.5%
	1	0.5	79.1%	20.9%
	2	0.5	42.4%	57.6%

Rejecting correct fixes is problematic for applications that require ambiguity resolution, although it is generally better to lose precision than to have an undetected bias. The behaviour of the F-test is illustrated by Figure 44, which shows the distribution of the F-test results (pass or fail) for the **L1 only GPS only** solution.

The problem of the F-test rejecting more correct fixes is mitigated by the addition of GLONASS. The lowest rate of correct fix rejection is achieved by the **L1 only GG fixed GLO solution**. The dual-frequency measurement combinations also help in this regard as rejection rates are less than 20%. Since ambiguity resolution can be repeated if not successful the first time, these rejection rates are acceptable. Overall the F-test performs well as a reliability test, for this particular baseline and environment.

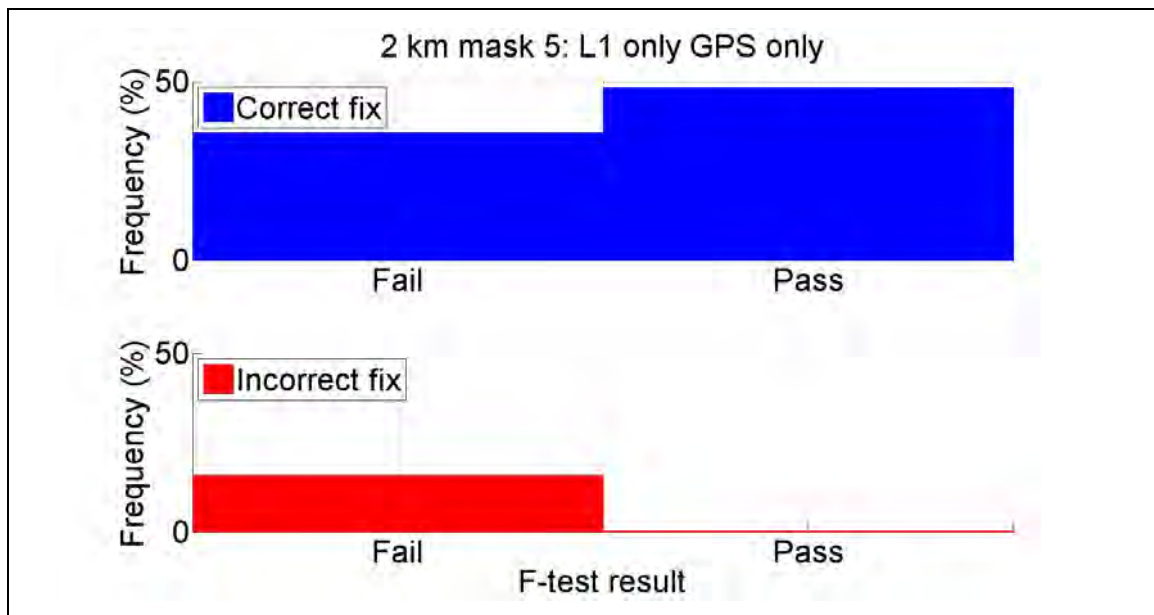
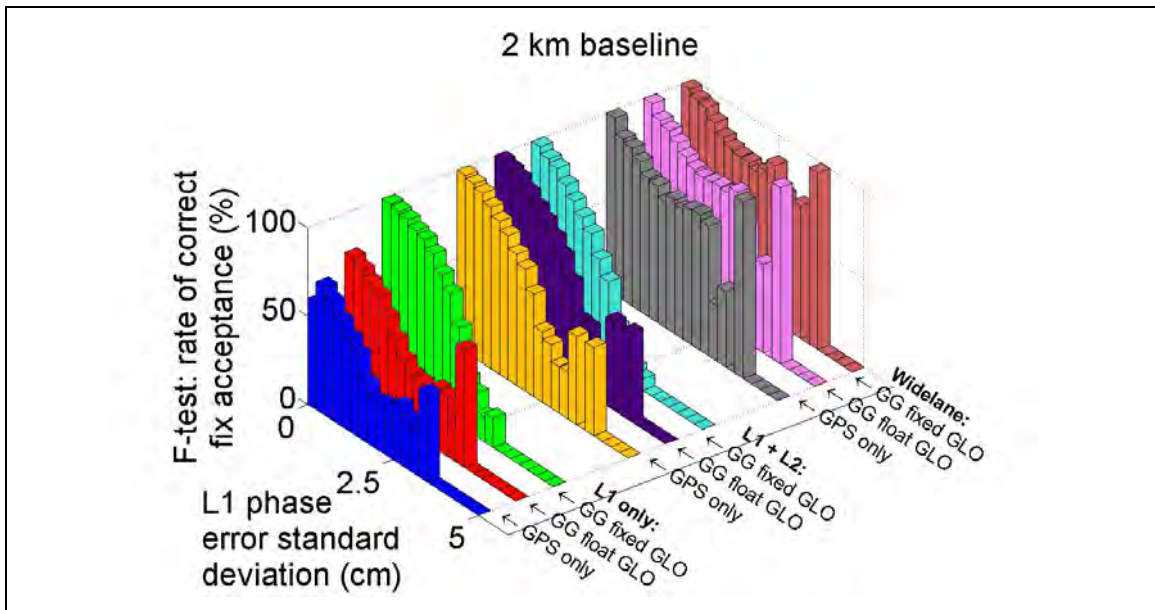


Figure 44 - Distribution of F-test result for L1 only GPS only solution - 2 km baseline under 5° mask

The F-test results from the 18 km baseline are given in Table 19, with the corresponding numbers of fixes highlighted in **blue**. The F-test rejects many more correct fixes for this baseline than it did for the 2 km baseline. The phase errors have an impact on the F-test result, as demonstrated by Figure 45 for the 2 km baseline and Figure 46 for the 18 km baseline. The pattern is obvious: the F-test rejects more correct fixes as the level of phase errors increases. Recall that the phase errors are much larger for the 18 km baseline than the 2 km baseline (1σ of 3.4 cm vs. 1.3 cm, respectively) – this accounts for the higher rate of correct fix rejection.

Table 19 - F-test results - 18 km baseline under 5° mask

		F-test (10% significance) – 18 km baseline			
		Correct fix		Incorrect fix	
		Accept	Reject	Reject	Accept
L1 only	GPS only	8.7% (28)	91.3% (293)	96.3% (4264)	3.7% (166)
	GG float GLO	9.9% (41)	90.1% (373)	96.6% (4188)	3.4% (149)
	GG fixed GLO	24.0% (198)	76.0% (628)	98.3% (3858)	1.7% (67)
L1 + L2	GPS only	45.5% (1153)	54.5% (1381)	99.6% (2208)	0.4% (9)
	GG float GLO	46.2% (1286)	53.8% (1496)	99.8% (1965)	0.2% (4)
	GG fixed GLO	44.7% (1185)	55.3% (1466)	100.0% (2100)	0.0% (0)
WL	GPS only	38.7% (1214)	61.3% (1922)	93.4% (1509)	6.6% (106)
	GG float GLO	42.0% (1423)	58.0% (1964)	92.4% (1261)	7.6% (103)
	GG fixed GLO	62.0% (2578)	38.0% (1578)	82.2% (489)	17.8% (106)

**Figure 45 - F-test correct fix acceptance vs. phase error standard deviation - 2 km baseline under 5° mask**

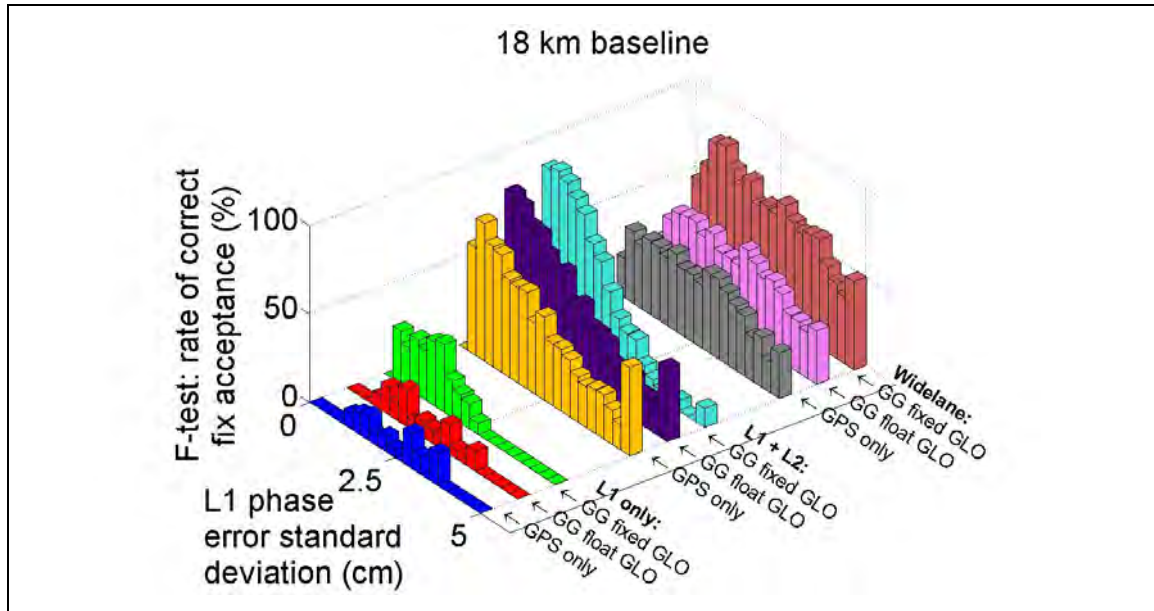


Figure 46 - F-test correct fix acceptance vs. phase error standard deviation - 18 km baseline under 5° mask

There are significant differences in the F-test correct fix acceptance rates between different estimation strategies. For instance, both the **GG fixed GLO** strategy and the **L1 + L2** measurement combination produce higher acceptance rates. These are investigated in greater detail under the reduced visibility scenario. However an interesting feature of the **widelane** combination is discussed here: the distribution of the correct fix acceptance rate is flatter for **widelane** than for either **L1 only** or **L1 + L2**, even when the level of phase errors increases. A similar trend was observed for widelane when analyzing the fixed-ambiguity accuracy and the actual success rate. This suggests that widelane results in general (including F-test correct fix acceptance) are somewhat more robust under increasing phase errors. This is highly useful for longer baselines.

4.8 Combining Reliability Tests

Up to now the predicted success rate and F-test have been analyzed individually; however in practice they can be combined to give the best chance of detecting and rejecting incorrect fixes. If one of the reliability tests would reject a fix, then the fix is rejected. Conversely, the fix is only accepted if *all* of the reliability tests would accept it.

The results of combining the predicted success rate and F-test are shown in Table 20 and Table 21 for the 2 km and 18 km baselines, respectively. The numbers of fixes corresponding to each result are highlighted in blue. The combined testing results are almost the same as the F-test results. This is expected as the F-test rejects many more fixes than the predicted success rate.

Since the combined reliability test and the F-test are nearly identical, it is useful to interpret the combined test as “adding” information from the predicted success rate to the F-test. Doing this very slightly improves (that is, decreases) the rate of incorrect fix acceptance, compared to using the F-test alone. The maximum improvement is 0.4% for the 2 km baseline and 1.5% for the 18 km baseline (both highlighted in green). This suggests that the F-test captures most of the information that the predicted success rate provides. Adding the predicted success rate is not costly – the maximum loss incurred in correct fix acceptance is only 0.2% for both baselines.

Table 20 - Combined reliability testing results - 2 km baseline under 5° mask

		Predicted success rate and F-test – 2 km baseline					
		Correct fix			Incorrect fix		
		Accept	Reject	Reject	Accept	Reject	Accept
L1 only	GPS only	57.3% (3350)	42.7% (2500)	98.2% (1105)	1.8% (20)	—	—
	GG float GLO	60.9% (3749)	39.1% (2407)	98.2% (804)	1.8% (15)	—	—
	GG fixed GLO	90.8% (6269)	9.2% (632)	—	—	—	—
L1 + L2	GPS only	87.9% (6118)	12.1% (842)	—	—	—	—
	GG float GLO	87.7% (6114)	12.3% (855)	—	—	—	—
	GG fixed GLO	83.6% (5831)	16.4% (1141)	—	—	—	—
WL	GPS only	82.9% (5751)	17.1% (1189)	—	—	—	—
	GG float GLO	85.6% (5959)	14.4% (1003)	—	—	—	—
	GG fixed GLO	89.5% (6241)	10.5% (734)	—	—	—	—

Table 21 - Combined reliability testing results - 18 km baseline under 5° mask

		Predicted success rate and F-test – 18 km baseline					
		Correct fix			Incorrect fix		
		Accept	Reject	Reject	Accept	Reject	Accept
L1 only	GPS only	8.7% (28)	91.3% (293)	97.8% (4331)	2.2% (99)	—	—
	GG float GLO	9.7% (40)	90.3% (374)	97.4% (4224)	2.6% (113)	—	—
	GG fixed GLO	24.0% (198)	76.0% (628)	98.3% (3858)	1.7% (67)	—	—
L1 + L2	GPS only	45.5% (1153)	54.5% (1381)	99.6% (2208)	0.4% (9)	—	—
	GG float GLO	46.2% (1286)	53.8% (1496)	99.8% (1965)	0.2% (4)	—	—
	GG fixed GLO	44.7% (1185)	55.3% (1466)	100.0% (2100)	0.0% (0)	—	—
WL	GPS only	38.6% (1209)	61.4% (1927)	93.4% (1509)	6.6% (106)	—	—
	GG float GLO	42.0% (1423)	58.0% (1964)	92.4% (1261)	7.6% (103)	—	—
	GG fixed GLO	62.0% (2578)	38.0% (1578)	82.2% (489)	17.8% (106)	—	—

4.9 Probability of Cycle Slip Detection

It was discussed in Section 2.3 that fix reliability and navigation reliability are analogous, as errors will result in either *loss of precision* or *undetected biases* in the position. The concept of the *marginally detectable blunder* (MDB) is discussed in Lachapelle (2008). This concept has been extended in Petovello (2003): an MDB of one cycle yields a test power for fault detection that is essentially the probability of detecting that one-cycle blunder. In other words, it is the probability of detecting a cycle slip. This is critical for ambiguity resolution since a cycle slip induces a change in the integer value of the ambiguity; any previously resolved and stored integers will actually induce measurement biases. It is also important in the float estimation of the position and ambiguities. Measurements from multiple epochs is often incorporated to estimate the float ambiguities; if there is a cycle slip, phase measurements before the cycle slip cannot be combined with phase measurements after the cycle slip.

The properties of the probability of cycle slip detection are illustrated by the time series in Figure 47 and the frequency distributions in Figure 48, for the **L1 only GPS only solution** from the 2 km baseline. Results from the other solutions are presented later. The probabilities appear to be heavily skewed towards one. However, there are many fixes for which the probability of cycle slip detection is much lower; for instance, 14% of the epochs in Figure 47 have a probability of cycle slip detection of less than 0.50. At these epochs, the user cannot have more than 50% confidence that the position solution is not affected by a one-cycle phase measurement bias. This gives rise to a reliability problem,

even if the user chooses to use a float solution to avoid potentially unreliable integer fixes. The time series in Figure 47 also indicates that the probability of cycle slip detection is time-correlated, which is expected since they are ultimately dependent on the slowly-changing satellite geometry. The probability of cycle slip detection tends to converge to a maximum value; in this case, the maximum is one. The same trend is observed in Petovello (2003).

Both the probability of cycle slip detection and the predicted success rate tend to be very close to one for many fixes (see Figure 41). The relationship between these two parameters is further illustrated in Figure 49, also for the **L1 only GPS only solution** from the 2 km baseline. The pattern is not strong: both parameters are close to one for many fixes, but there are many more fixes with probability of cycle slip detection significantly less than one. Hence, the probability of cycle slip detection is less optimistic than the predicted success rate. There is no correlation observed between the probability of cycle slip detection and the F-test result, as demonstrated in Figure 50.

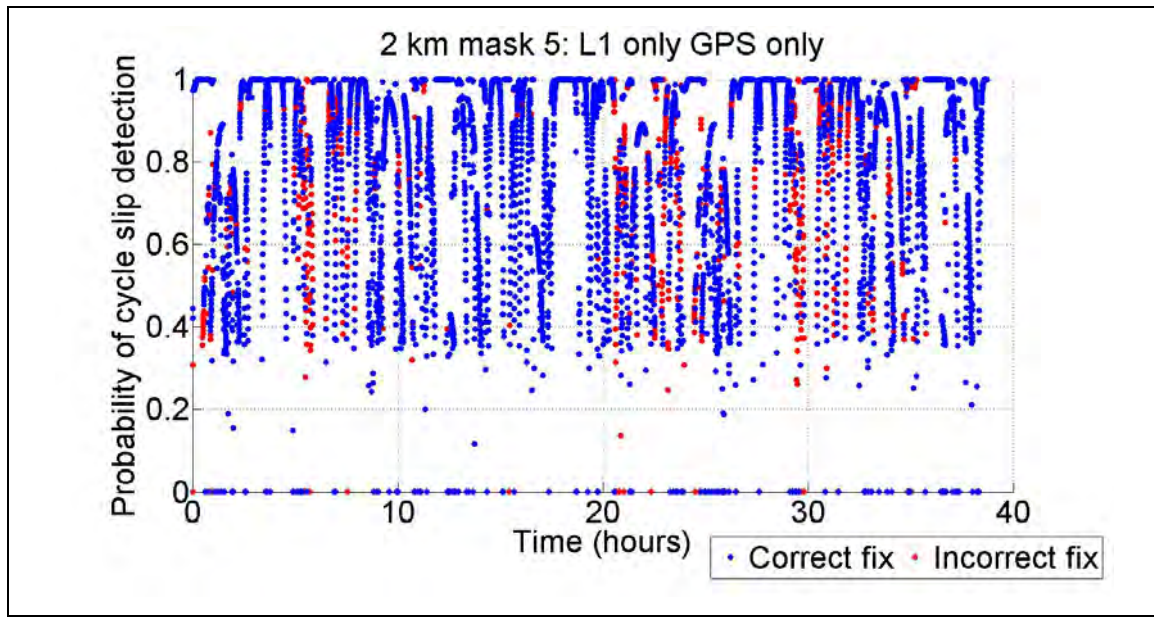


Figure 47 - Time series of probabilities of cycle slip detection for L1 only GPS only solution - 2 km baseline under 5° mask

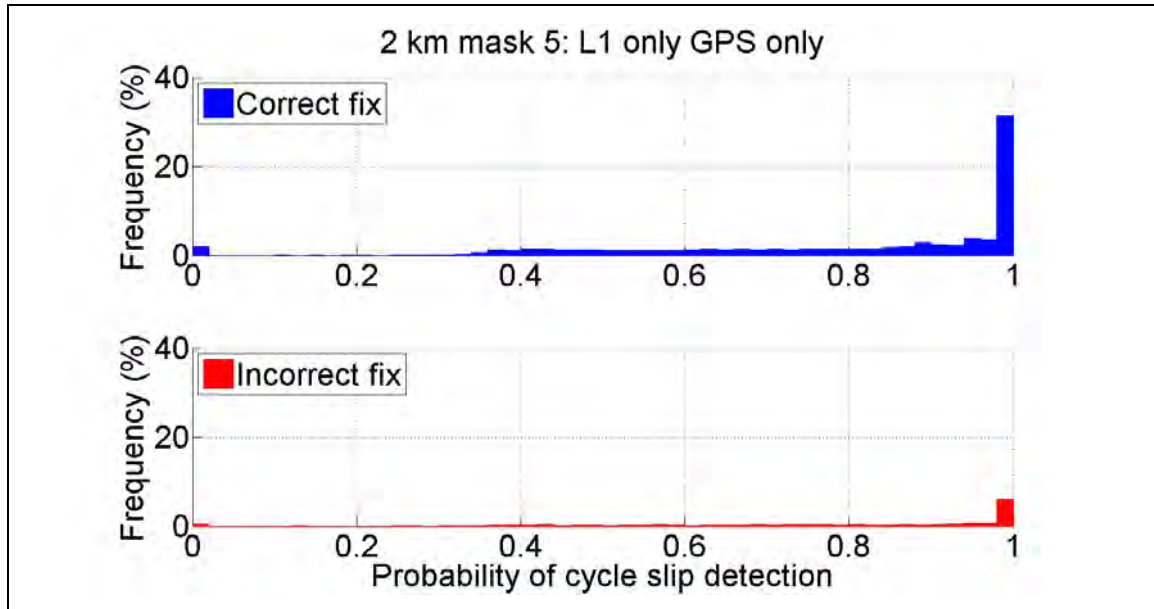


Figure 48 - Distribution of probabilities of cycle slip detection for L1 only GPS only solution - 2 km baseline under 5° mask

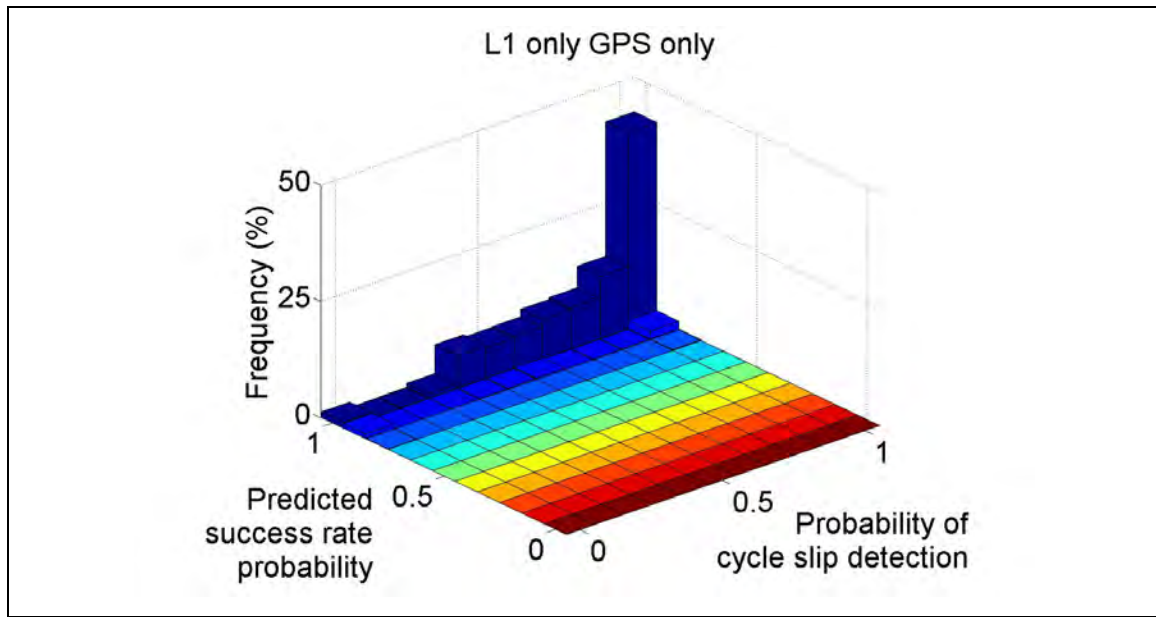


Figure 49 - Relationship between probability of cycle slip detection and predicted success rate for L1 only GPS only solution - 2 km baseline under 5° mask

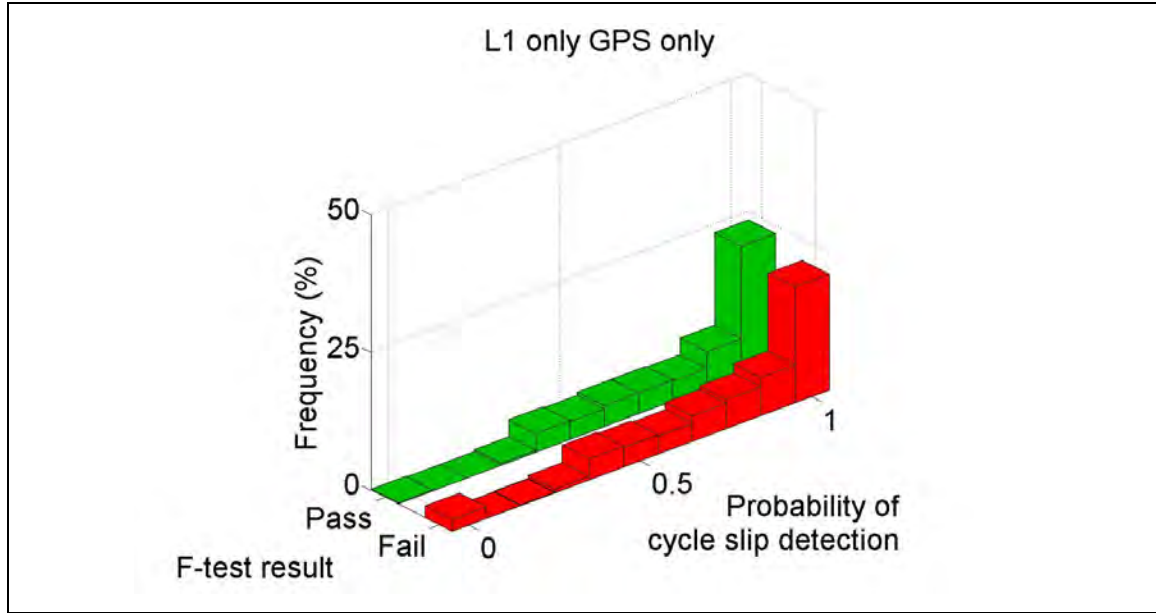


Figure 50 - Relationship between probability of cycle slip detection and F-test result for L1 only GPS only solution - 2 km baseline under 5° mask

Cycle slips are detrimental to ambiguity resolution, so the ability to detect them is crucial. Therefore the probability of cycle slip detection can be implemented like a reliability test. The results of this are shown in Table 22 for the 2 km baseline and Table 23 for the 18 km baseline. The numbers of fixes that correspond to each result are highlighted in **blue**. The probability of cycle slip detection accepts incorrect fixes less often than the predicted success rate, which is expected due to its less optimistic nature. However this comes at a cost, as a high percentage of correct fixes are rejected.

Table 22 - Probability of cycle slip detection results - 2 km baseline under 5° mask

		Cycle slip detection (0.95 threshold) – 2 km baseline			
		Correct fix		Incorrect fix	
		Accept	Reject	Reject	Accept
L1 only	GPS only	44.2% (2583)	55.8% (3267)	55.6% (626)	44.4% (499)
	GG float GLO	34.7% (2137)	65.3% (4019)	64.6% (529)	35.4% (290)
	GG fixed GLO	34.9% (2408)	65.1% (4493)	— —	— —
L1 + L2	GPS only	46.0% (3201)	54.0% (3759)	— —	— —
	GG float GLO	34.4% (2396)	65.6% (4573)	— —	— —
	GG fixed GLO	34.4% (2398)	65.6% (4574)	— —	— —
WL	GPS only	21.8% (1515)	78.2% (5425)	— —	— —
	GG float GLO	10.4% (722)	89.6% (6240)	— —	— —
	GG fixed GLO	10.4% (722)	89.6% (6253)	— —	— —

Table 23 - Probability of cycle slip detection results - 18 km baseline under 5° mask

		Cycle slip detection (0.95 threshold) – 18 km baseline					
		Correct fix			Incorrect fix		
		Accept	Reject	Reject	Accept	Accept	Reject
L1 only	GPS only	76.6% (246)	23.4% (75)	29.7% (1314)	70.3% (3116)		
	GG float GLO	78.0% (323)	22.0% (91)	25.5% (1107)	74.5% (3230)		
	GG fixed GLO	71.9% (594)	28.1% (232)	24.6% (966)	75.4% (2959)		
L1 + L2	GPS only	74.4% (1886)	25.6% (649)	26.4% (586)	73.6% (1630)		
	GG float GLO	67.9% (1888)	32.1% (894)	31.8% (627)	68.2% (1342)		
	GG fixed GLO	65.6% (1740)	34.4% (911)	29.0% (610)	71.0% (1490)		
WL	GPS only	47.3% (1482)	52.7% (1654)	73.0% (1179)	27.0% (436)		
	GG float GLO	47.2% (1600)	52.8% (1787)	58.7% (800)	41.3% (564)		
	GG fixed GLO	46.8% (1944)	53.2% (2212)	63.0% (375)	37.0% (220)		

4.10 Reliability under Simulated Reduced Visibility

The effect of reduced satellite visibility on reliability testing is investigated here. This is the same reduced visibility scenario used to analyze the actual success rates earlier – the circular elevation mask is increased from 5° to 30°. The results of using the predicted success rate as an indicator of reliability are shown in Table 24 and Table 25 for the 2 km and 18 km baselines, respectively. The numbers of fixes corresponding to each result are highlighted in **blue**.

Table 24 - Predicted success rate results - 2 km baseline under 30° mask

		Predicted success rate (0.95 threshold) – 2 km baseline					
		Correct fix			Incorrect fix		
		Accept	Reject	Reject	Accept	Reject	Accept
L1 only	GPS only	50.0% (529)	50.0% (528)	97.6% (4574)	2.4% (114)		
	GG float GLO	53.6% (752)	46.4% (651)	96.1% (5334)	3.9% (215)		
	GG fixed GLO	81.9% (3361)	18.1% (744)	84.2% (2396)	15.8% (451)		
L1 + L2	GPS only	100% (5168)	0.0% (0)	0.0% (0)	100% (577)		
	GG float GLO	100% (6131)	0.0% (0)	0.0% (0)	100% (821)		
	GG fixed GLO	100% (6829)	0.0% (2)	0.0% (0)	100% (121)		
WL	GPS only	81.8% (2715)	18.2% (606)	76.6% (1857)	23.4% (567)		
	GG float GLO	85.0% (3481)	15.0% (614)	58.3% (1666)	41.7% (1191)		
	GG fixed GLO	95.8% (5786)	4.2% (251)	53.1% (486)	46.9% (429)		

Table 25 - Predicted success rate results - 18 km baseline under 30° mask

		Predicted success rate (0.95 threshold) – 18 km baseline					
		Correct fix			Incorrect fix		
		Accept	Reject	Reject	Accept	Reject	Accept
L1 only	GPS only	30.9% (47)	69.1% (105)	89.2% (3443)	10.8% (417)		
	GG float GLO	46.2% (120)	53.8% (140)	84.9% (3799)	15.1% (677)		
	GG fixed GLO	83.5% (515)	16.5% (102)	49.8% (2050)	50.2% (2069)		
L1 + L2	GPS only	99.9% (2489)	0.1% (3)	3.4% (51)	96.6% (1469)		
	GG float GLO	99.8% (2992)	0.2% (7)	2.5% (43)	97.5% (1694)		
	GG fixed GLO	99.8% (3105)	0.2% (7)	2.2% (35)	97.8% (1589)		
WL	GPS only	87.5% (1663)	12.5% (237)	59.1% (1249)	40.9% (863)		
	GG float GLO	92.2% (2155)	7.8% (182)	39.8% (955)	60.2% (1444)		
	GG fixed GLO	97.4% (3400)	2.6% (91)	31.0% (386)	69.0% (859)		

The predicted success rates under the 30° mask appear to be much more effective at rejecting incorrect fixes than under the 5° mask. It was shown in Section 4.5 that the 30° mask reduces the number of ambiguities, which affects the actual success rate. Conceptually, reliable single-epoch ambiguity resolution with less than four DD ambiguities (i.e. less than five phase measurements) is impossible due to the lack of redundancy. While this thesis uses a Kalman filter to incorporate multiple epochs of data, the concept still holds – the actual success rate probability was found to be very low for fixes with less than four ambiguities (see Figure 37 and Figure 38).

The predicted success rate is able to detect this, as Figure 51 and Figure 52 illustrate for the 2 km and 18 km baselines, respectively. For fixes with less than four ambiguities, nearly all of the incorrect fixes are rejected. However, as soon as there are more than four ambiguities, the rate of incorrect fix rejection drops rapidly. Hence, the predicted success rate cannot reject a high rate of those incorrect fixes with a sufficient number of ambiguities. This metric *could* potentially be useful under reduced visibility environments – however its apparent effectiveness in rejecting more incorrect fixes might also be replicated by screening solutions with too few ambiguities.

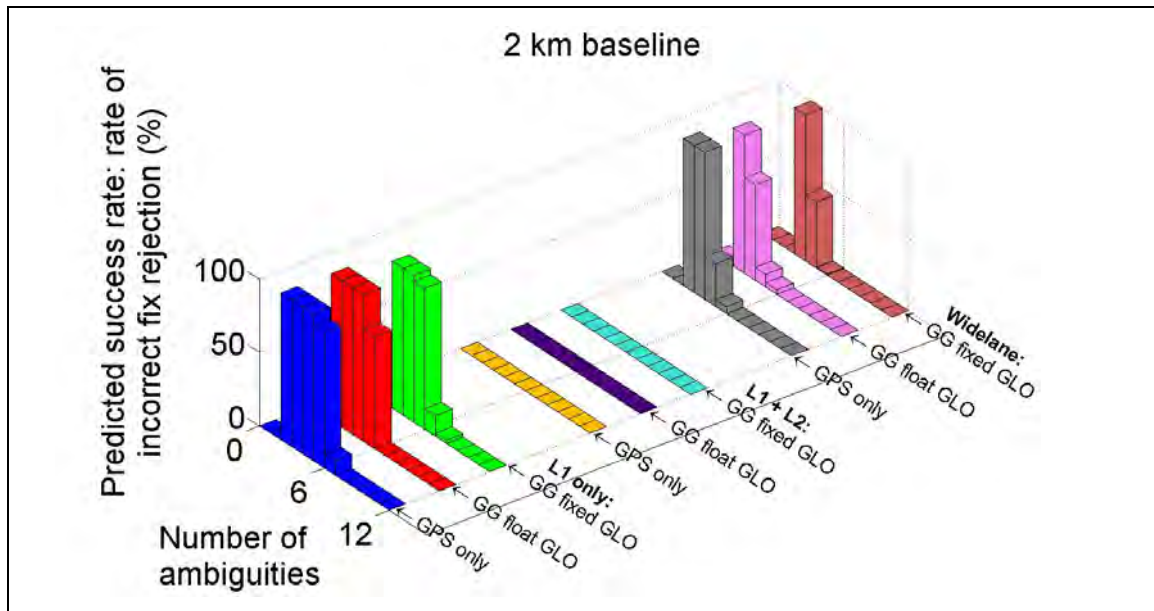


Figure 51 - Predicted success rate incorrect fix rejection vs. number of ambiguities - 2 km baseline under 30° mask

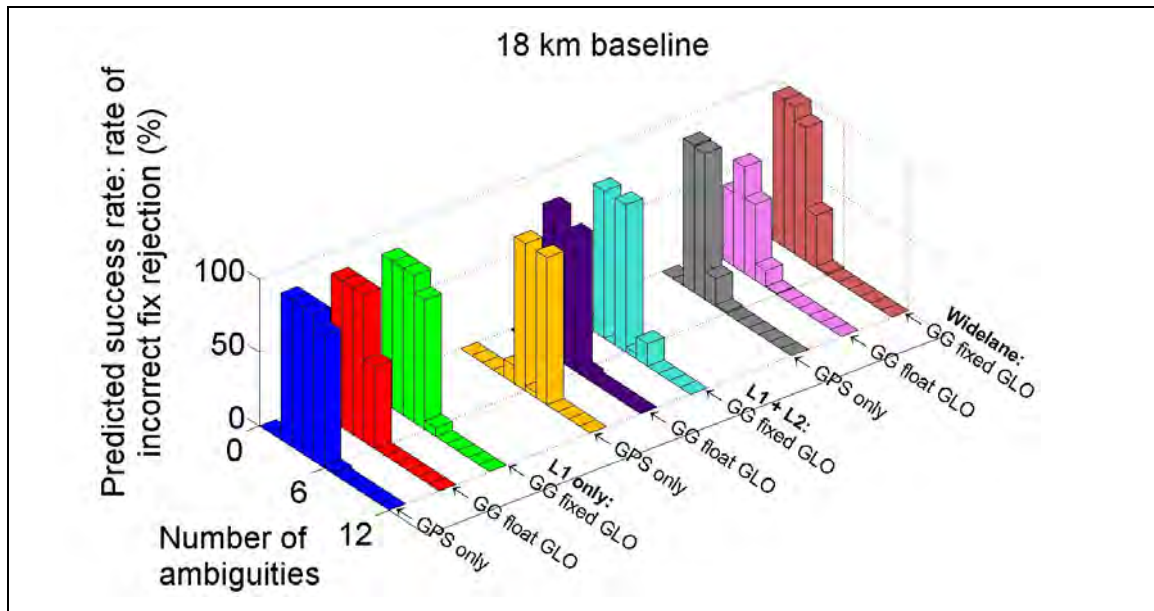


Figure 52 - Predicted success rate incorrect fix rejection vs. number of ambiguities - 18 km baseline under 30° mask

The F-test results under the 30° mask are shown in Table 26 and Table 27 for the 2 km and 18 km baselines, respectively, with the numbers of fixes corresponding with each result highlighted in **blue**. The F-test is once again more effective than the predicted success rate at rejecting incorrect fixes – that is, avoiding *undetected biases* in the position. However, compared to its performance under the 5° mask, the F-test rejects many more correct fixes – that is, *loss of position precision and availability*.

The number of ambiguities again plays a role, as Figure 53 and Figure 54 demonstrate for the 2 km and 18 km baselines, respectively, with all solutions processed under a 30° mask. These are distributions of the F-test rate of correct fix acceptance for various numbers of ambiguities. The more ambiguities there are, the more effective the F-test is at accepting correct fixes. Since there are fewer ambiguities in the reduced visibility scenario, the F-test will obviously be less effective.

However, Table 26 and Table 27 show a strategy (in **green**) that stands out for its ability to detect more correct fixes with the F-test: the **L1 + L2 GG fixed GLO** strategy. These two strategies add ambiguities, and thus improve the F-test performance. This is one of the primary ways that either GLONASS or dual-frequency impact fix reliability.

The dependence of the F-test performance on the geometry of integer estimation is further illustrated in Figure 55 and Figure 56 for the 2 km and 18 km baselines, respectively, with all solutions processed under a 30° mask. These are distributions of the F-test rate of correct fix acceptance for various levels of ADOP. The trend from the

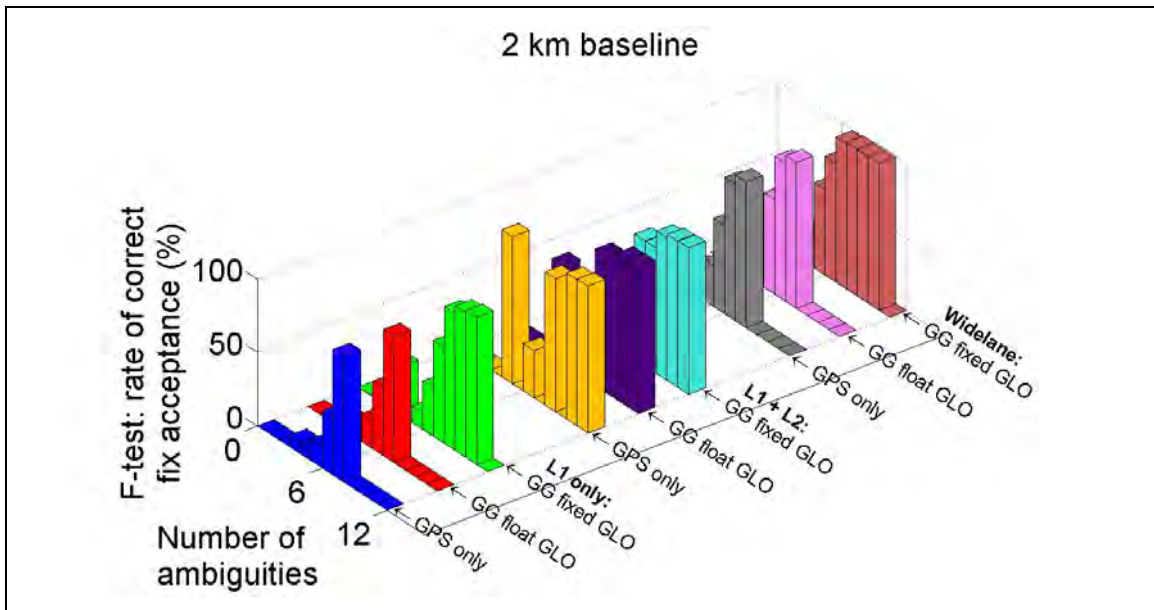
analysis of the number of ambiguities is confirmed – the better the geometry (i.e. the lower the ADOP) the more correct fixes are accepted.

Table 26 - F-test results - 2 km baseline under 30° mask

		F-test (10% significance) – 2 km baseline			
		Correct fix		Incorrect fix	
		Accept	Reject	Reject	Accept
L1 only	GPS only	33.2% (351)	66.8% (706)	90.1% (4224)	9.9% (464)
	GG float GLO	30.5% (428)	69.5% (975)	90.4% (5019)	9.6% (530)
	GG fixed GLO	50.9% (2091)	49.1% (2014)	94.6% (2693)	5.4% (154)
L1 + L2	GPS only	76.3% (3945)	23.7% (1223)	92.4% (533)	7.6% (44)
	GG float GLO	80.3% (4922)	19.7% (1209)	64.2% (527)	35.8% (294)
	GG fixed GLO	95.9% (6553)	4.1% (278)	96.7% (117)	3.3% (4)
WL	GPS only	49.0% (1608)	51.0% (1713)	82.7% (2122)	17.3% (302)
	GG float GLO	49.0% (2007)	51.0% (2088)	82.7% (2362)	17.3% (495)
	GG fixed GLO	71.5% (4316)	28.5% (1721)	90.5% (828)	9.5% (87)

Table 27 - F-test results - 18 km baseline under 30° mask

		F-test (10% significance) – 18 km baseline					
		Correct fix			Incorrect fix		
		Accept	Reject	Accept	Reject	Accept	Reject
L1 only	GPS only	10.5% (16)	89.5% (136)	92.2% (3557)	7.8% (303)		
	GG float GLO	8.1% (21)	91.9% (239)	92.1% (4123)	7.9% (353)		
	GG fixed GLO	16.0% (99)	84.0% (518)	96.5% (3974)	3.5% (145)		
L1 + L2	GPS only	51.2% (1277)	48.8% (1216)	96.2% (1461)	3.8% (58)		
	GG float GLO	54.8% (1642)	45.2% (1357)	90.0% (1563)	10.0% (174)		
	GG fixed GLO	66.5% (2071)	33.5% (1041)	99.1% (1609)	0.9% (15)		
WL	GPS only	31.7% (602)	68.3% (1298)	89.5% (1891)	10.5% (221)		
	GG float GLO	35.2% (823)	64.8% (1514)	86.8% (2083)	13.2% (316)		
	GG fixed GLO	52.0% (1814)	48.0% (1677)	92.2% (1148)	7.8% (97)		

**Figure 53 - F-test correct fix acceptance vs. number of ambiguities - 2 km baseline under 30° mask**

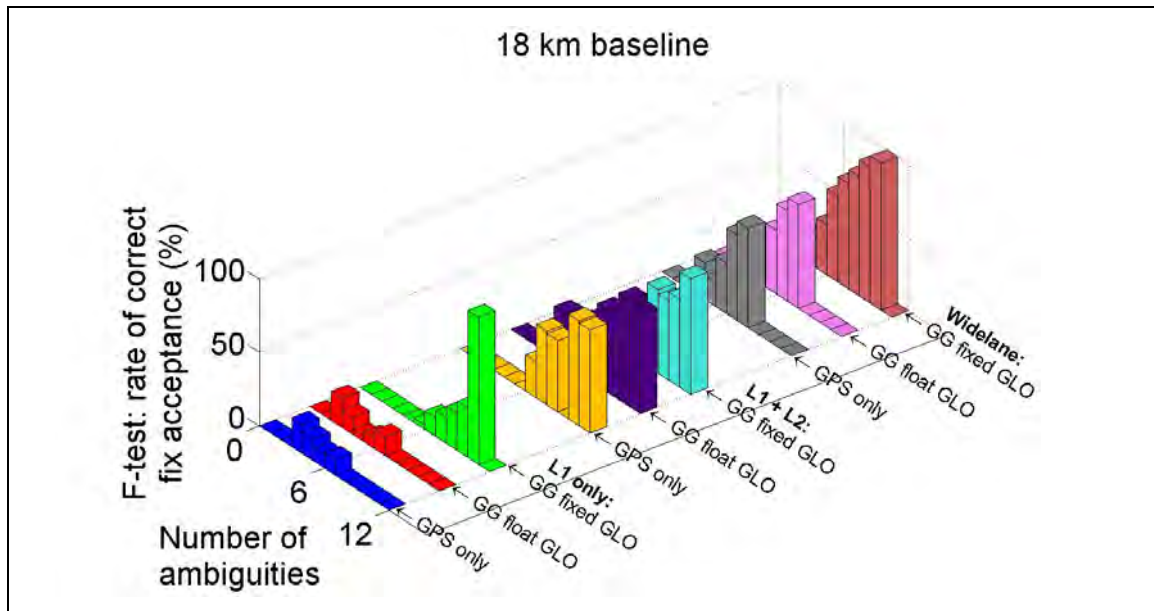


Figure 54 - F-test correct fix acceptance vs. number of ambiguities - 18 km baseline under 30° mask

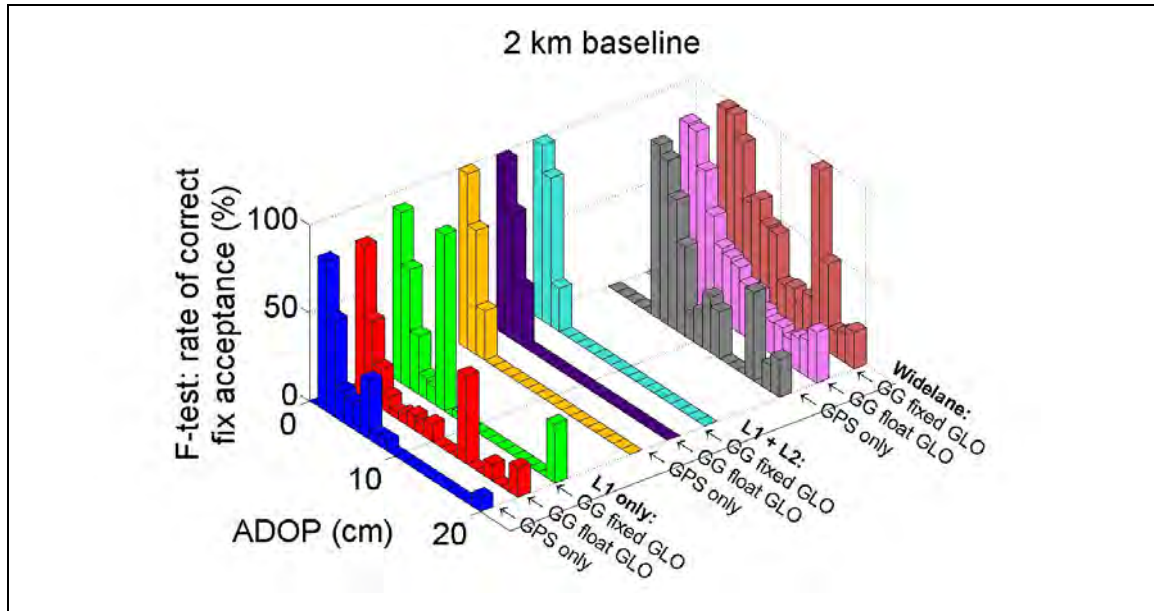


Figure 55 - F-test correct fix acceptance vs. ADOP - 2 km baseline under 30° mask

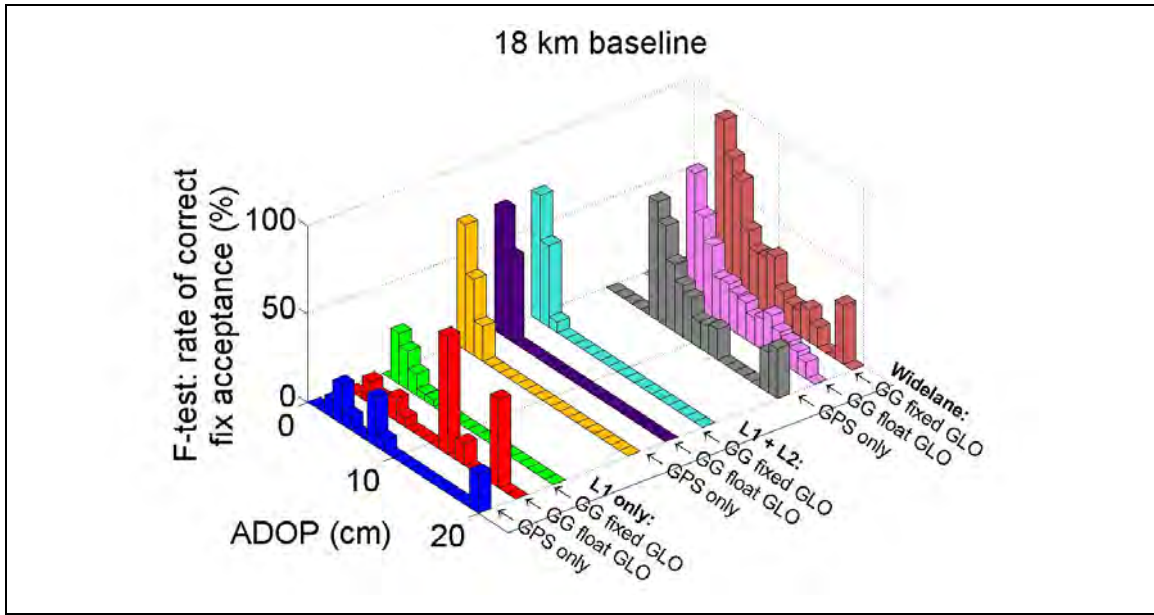


Figure 56 - F-test correct fix acceptance vs. ADOP - 18 km baseline under 30° mask

The results of combining the predicted success rate and F-test under the 30° mask are shown in Table 28 and Table 29 for the 2 km and 18 km baselines, respectively. Under the 5° mask, the combined reliability test was very similar to the F-test, with the predicted success rate adding little information. Under this reduced visibility scenario, the predicted success rate does add a significant amount of information: the rate of incorrect fix rejection improves by up to 11% for the 2 km baseline and 7% for the 18 km baseline. The cost of this is that more correct fixes are also rejected.

Table 28 - Combined reliability testing results - 2 km baseline under 30° mask

		Predicted success rate and F-test – 2 km baseline					
		Correct fix			Incorrect fix		
		Accept	Reject	Reject	Accept	Reject	Accept
L1 only	GPS only	27.7% (293)	72.3% (764)	99.9% (4683)	0.1% (5)		
	GG float GLO	26.2% (367)	73.8% (1036)	99.9% (5546)	0.1% (3)		
	GG fixed GLO	49.1% (2017)	50.9% (2088)	99.4% (2829)	0.6% (18)		
L1 + L2	GPS only	76.3% (3945)	23.7% (1223)	92.4% (533)	7.6% (44)		
	GG float GLO	80.3% (4922)	19.7% (1209)	64.2% (527)	35.8% (294)		
	GG fixed GLO	95.9% (6553)	4.1% (278)	96.7% (117)	3.3% (4)		
WL	GPS only	45.0% (1494)	55.0% (1827)	98.7% (2392)	1.3% (32)		
	GG float GLO	46.3% (1896)	53.7% (2199)	91.6% (2618)	8.4% (239)		
	GG fixed GLO	70.9% (4281)	29.1% (1756)	95.0% (869)	5.0% (46)		

Table 29 - Combined reliability testing results - 18 km baseline under 30° mask

		Predicted success rate and F-test – 18 km baseline					
		Correct fix			Incorrect fix		
		Accept	Reject	Reject	Accept	Reject	Accept
L1 only	GPS only	2.0% (3)	98.0% (149)	99.4% (3837)	0.6% (23)		
	GG float GLO	4.6% (12)	95.4% (248)	99.3% (4444)	0.7% (32)		
	GG fixed GLO	15.9% (98)	84.1% (519)	98.5% (4058)	1.5% (61)		
L1 + L2	GPS only	51.2% (1277)	48.8% (1216)	96.2% (1462)	3.8% (57)		
	GG float GLO	54.8% (1642)	45.2% (1357)	90.0% (1563)	10.0% (174)		
	GG fixed GLO	66.5% (2071)	33.5% (1041)	99.1% (1609)	0.9% (15)		
WL	GPS only	29.4% (559)	70.6% (1341)	96.8% (2044)	3.2% (68)		
	GG float GLO	34.1% (798)	65.9% (1539)	92.2% (2211)	7.8% (188)		
	GG fixed GLO	51.6% (1802)	48.4% (1689)	95.2% (1185)	4.8% (60)		

Chapter Five: Kinematic Testing Results

This chapter presents the analysis and discussion of the reliability of ambiguity resolution for *kinematic* testing. Two kinematic scenarios are investigated for this thesis: 1.) vehicle-to-vehicle relative navigation conducted under both open sky and foliage; and 2.) downhill ski runs.

5.1 Vehicle-to-Vehicle Relative Navigation

Vehicle-to-vehicle (V2V) relative navigation was conducted for 97 minutes under two types of sky coverage: 1.) open sky (49 minutes); and overhead foliage (49 minutes). The open sky environment was not perfect as there were occasionally trees in view. The overhead foliage environment sometimes resulted in near-total obstruction of the sky.

The inter-vehicle distances did not exceed 300 metres, so residual atmospheric effects were not significant. Regardless, the *K* index on the day of the test (August 17, 2009) did not exceed 1.0, based on observations from the Meanook Geomagnetic Observatory (Space Weather Canada 2009). Therefore there were no significant ionospheric disturbances. Under open sky, between four and eight GPS and three and six GLONASS satellites were available. Under foliage, between three and seven GPS and two and four GLONASS satellites were available. A convergence time of 20 seconds was chosen to generate fixes. Table 30 shows the total number of fixes according to the solution type.

Table 30 - Total number of fixes - V2V all environments under 5° mask

		Total number of fixes	
		V2V open sky	V2V foliage
L1 only	GPS only	141	111
	GG float GLO	141	117
	GG fixed GLO	143	122
L1 + L2	GPS only	141	110
	GG float GLO	141	117
	GG fixed GLO	143	126
Widelane	GPS only	139	103
	GG float GLO	141	117
	GG fixed GLO	143	121

Nine types of solutions are investigated: the **L1 only**, **L1 + L2** and **widelane (WL)** measurement combinations are each combined with the **GPS only**, **GG float GLO** and **GG fixed GLO** fixing strategies. The correctness of the resolved ambiguities is determined by comparing the fixed-ambiguity positions to a reference solution derived from GPS/INS. The fix is taken to be correct with a horizontal agreement of better than 10 cm and incorrect otherwise. The availability of reference solutions with estimated 1σ horizontal accuracies at the sub-decimetre level is 98% under open sky and 72% under foliage.

5.1.1 Actual Success Rates and Reliability Testing

Table 31 shows the actual success rates (expressed as probabilities, i.e. ranging from zero to one) for the V2V testing under both open sky and foliage. The corresponding numbers

of correct fixes are highlighted in **blue**. All of the solutions are processed using a circular elevation mask of 5°. The following trends are observed:

- The impact of GLONASS on the actual success rate in this scenario is the same as the static baseline. Just adding the GLONASS measurements (i.e. switching from **GPS only** to **GG float GLO**) does have a small effect, but actually resolving the GLONASS ambiguities (i.e. switching from **GG float GLO** to **GG fixed GLO**) greatly improves the actual success rate. This is highlighted in **green** in Table 31.
- The impact of dual-frequency on the actual success rate in this scenario is the same as the static baseline. Both **L1 + L2** and **widelane** improve the actual success rate over **L1 only**. Since the inter-vehicle distances are short, **L1 + L2** is more effective than **widelane**. The combination of both dual-frequency and GPS/GLONASS gives the best results, as highlighted in **green** in Table 31.
- The actual success rates achieved under foliage are all much lower than those achieved under open sky. It is demonstrated in Section 5.1.2 that this is likely caused by the increased frequency of cycle slips under foliage.

Table 31 - Actual success rate probabilities - V2V all environments under 5° mask

		Actual success rate probability	
		V2V open sky	V2V foliage
L1 only	GPS only	0.41 (58) ²	0.22 (24)
	GG float GLO	0.46 (65)	0.26 (31)
	GG fixed GLO	0.78 (112)	0.47 (57)
L1 + L2	GPS only	0.82 (115)	0.47 (52)
	GG float GLO	0.85 (120)	0.49 (57)
	GG fixed GLO	0.94 (134)	0.58 (73)
Widelane	GPS only	0.71 (98)	0.39 (40)
	GG float GLO	0.80 (113)	0.46 (54)
	GG fixed GLO	0.87 (124)	0.50 (60)

The effectiveness of the predicted success rate as an indicator of fix reliability is shown in Table 32 and Table 33. These show the results – under open sky and foliage, respectively – of using the predicted success rate probability to accept and reject fixes, with an acceptance threshold of 0.95. The numbers of fixes that correspond to each result are highlighted in blue.

The static baseline analysis in Chapter Four (Section 4.6) suggested that the predicted success rate is too optimistic and thus accepts incorrect fixes too often – that is, there are too many *undetected position biases*. This trend holds in general for the V2V scenario: some solutions (such as **L1 + L2 GG fixed GLO**) accept 100% of the incorrect fixes. Operating under foliage actually *decreases* the rate of incorrect fix acceptance; however

² Number of correct fixes

it also decreases the rate of correct fix acceptance, implying that the predicted success rates are just lower under foliage.

The addition of GLONASS measurements does not *initially* appear to benefit incorrect fix acceptance. For instance, under open sky and using the **L1 only** combination, the rate of incorrect fix acceptance goes from 37% to 42% when GLONASS measurements are added to GPS, and then to 65% when the GLONASS ambiguities are fixed. However, the *total number* of incorrect fixes that are accepted by the predicted success rate decreases when GLONASS is added. The same trend is observed when switching from the L1 only combination to either of the dual-frequency combinations.

The apparent degradation in fix reliability is ultimately due to the fact that switching to GLONASS or to dual-frequency turns some of the fixes that were previously incorrect (and rejected by the predicted success rate) into correct fixes, as demonstrated in Table 32 (highlighted in green). Incorrect fixes that would be rejected because of low predicted success rates are likely to suffer from poor geometry; the connection between the two has been shown in Teunissen (2001a). Furthermore, poor geometry (specifically poor ambiguity dilution of precision, or ADOP) will result in more incorrect fixes, as shown in the static baseline analysis (Section 4.5).

Both GLONASS and dual-frequency ultimately improve the geometry of the integer estimation problem. Thus fixes that are incorrect because of poor geometry (e.g. ADOPs of up to 22 cm under open sky and 29 cm under foliage for **L1 only GPS only**) are more

likely to be correct, leaving behind fixes that are incorrect for another reason. Hence the rate of incorrect fix acceptance goes up, but the total number of incorrect fixes drops.

Table 32 - Predicted success rate results - V2V open sky under 5° mask

		Predicted success rate (0.95 threshold) – V2V open sky					
		Correct fix			Incorrect fix		
		Accept	Reject	Reject	Accept	Reject	Accept
L1 only	GPS only	37.9% (22)	62.1% (36)	62.7% (52)	37.3% (31)		
	GG float GLO	49.2% (32)	50.8% (33)	57.9% (44)	42.1% (32)		
	GG fixed GLO	79.5% (89)	20.5% (23)	35.5% (11)	64.5% (20)		
L1 + L2	GPS only	99.1% (114)	0.9% (1)	19.2% (5)	80.8% (21)		
	GG float GLO	99.2% (119)	0.8% (1)	4.8% (1)	95.2% (20)		
	GG fixed GLO	100.0% (134)	0.0% (0)	0.0% (0)	100.0% (9)		
WL	GPS only	89.8% (88)	10.2% (10)	12.2% (5)	87.8% (36)		
	GG float GLO	96.5% (109)	3.5% (4)	0.0% (0)	100.0% (28)		
	GG fixed GLO	100.0% (124)	0.0% (0)	0.0% (0)	100.0% (19)		

Table 33 - Predicted success rate results - V2V foliage under 5° mask

		Predicted success rate (0.95 threshold) – V2V foliage					
		Correct fix			Incorrect fix		
		Accept	Reject	Reject	Accept	Accept	Reject
L1 only	GPS only	4.2% (1)	95.8% (23)	97.7% (85)	2.3% (2)		
	GG float GLO	9.7% (3)	90.3% (28)	94.2% (81)	5.8% (5)		
	GG fixed GLO	63.2% (36)	36.8% (21)	80.0% (52)	20.0% (13)		
L1 + L2	GPS only	98.1% (51)	1.9% (1)	15.5% (9)	84.5% (49)		
	GG float GLO	98.2% (56)	1.8% (1)	16.7% (10)	83.3% (50)		
	GG fixed GLO	95.9% (70)	4.1% (3)	34.0% (18)	66.0% (35)		
WL	GPS only	75.0% (30)	25.0% (10)	44.4% (28)	55.6% (35)		
	GG float GLO	94.4% (51)	5.6% (3)	25.4% (16)	74.6% (47)		
	GG fixed GLO	96.7% (58)	3.3% (2)	26.2% (16)	73.8% (45)		

The F-test results are shown in Table 34 and Table 35 for the open sky and foliage environments, respectively. A significance level of 10% is used to compute the ratio testing critical value (or threshold) from the F distribution. As with the static baseline analysis, the F-test is more effective than the predicted success rate at rejecting incorrect fixes, but at the cost of rejecting more correct fixes (i.e. accepting *loss of precision*).

Foliage affects the F-test negatively: more correct fixes end up being rejected than under open sky. However, GLONASS helps the F-test accept more correct fixes, especially when the ambiguities are fixed (i.e. when the **GG fixed GLO** strategy is used). Dual-frequency also helps; the most effective solution in terms of accepting correct fixes is **widelane GG fixed GLO** (highlighted in green in both Table 34 and Table 35).

Table 34 - F-test results - V2V open sky under 5° mask

		F-test (10% significance) – V2V open sky					
		Correct fix			Incorrect fix		
		Accept	Reject	Reject	Accept	Reject	Accept
L1 only	GPS only	62.1% (36)	37.9% (22)	85.5% (71)	14.5% (12)		
	GG float GLO	47.7% (31)	52.3% (34)	86.8% (66)	13.2% (10)		
	GG fixed GLO	62.5% (70)	37.5% (42)	87.1% (27)	12.9% (4)		
L1 + L2	GPS only	88.7% (102)	11.3% (13)	50.0% (13)	50.0% (13)		
	GG float GLO	90.8% (109)	9.2% (11)	47.6% (10)	52.4% (11)		
	GG fixed GLO	88.8% (119)	11.2% (15)	33.3% (3)	66.7% (6)		
WL	GPS only	76.5% (75)	23.5% (23)	36.6% (15)	63.4% (26)		
	GG float GLO	81.4% (92)	18.6% (21)	25.0% (7)	75.0% (21)		
	GG fixed GLO	96.0% (119)	4.0% (5)	31.6% (6)	68.4% (13)		

Table 35 - F-test results - V2V foliage under 5° mask

		F-test (10% significance) – V2V foliage					
		Correct fix			Incorrect fix		
		Accept	Reject	Reject	Accept	Reject	Accept
L1 only	GPS only	33.3% (8)	66.7% (16)	81.6% (71)	18.4% (16)		
	GG float GLO	25.8% (8)	74.2% (23)	81.4% (70)	18.6% (16)		
	GG fixed GLO	59.6% (34)	40.4% (23)	87.7% (57)	12.3% (8)		
L1 + L2	GPS only	88.5% (46)	11.5% (6)	48.3% (28)	51.7% (30)		
	GG float GLO	87.7% (50)	12.3% (7)	46.7% (28)	53.3% (32)		
	GG fixed GLO	89.0% (65)	11.0% (8)	62.3% (33)	37.7% (20)		
WL	GPS only	82.5% (33)	17.5% (7)	46.0% (29)	54.0% (34)		
	GG float GLO	83.3% (45)	16.7% (9)	54.0% (34)	46.0% (29)		
	GG fixed GLO	93.3% (56)	6.7% (4)	50.8% (31)	49.2% (30)		

The predicted success rate and F-test are combined into one reliability test, the results of which are shown in Table 36 and Table 37 for open sky and foliage, respectively. The combined reliability test is set up such that a fix is only accepted if both of the individual tests would accept it; conversely a fix is rejected if either test would reject it. The numbers of fixes corresponding to each combined test result are highlighted in Table 36 and Table 37 in **blue**.

In the static baseline analysis (Section 4.8), the combined reliability test was demonstrated to be very similar to the F-test, with marginal information added to it by the predicted success rate. For both V2V scenarios, the predicted success rate adds an enormous amount of information when only *single-frequency* data is used (i.e. the **L1 only** combination). This is highlighted in **green** in both Table 36 and Table 37. For instance, under open sky the rate of incorrect fix acceptance drops by up to 11%, and under foliage it drops by up to 18%.

The improvements gained by adding the predicted success rate when using **L1 only** come at a major cost: correct fix acceptance. Combining the tests severely decreases the number of correct fixes that are accepted; this is most noticeable in the **L1 only GPS only** solution under foliage (highlighted in **red** in Table 37), for which *no* correct fixes are accepted. While it is important to detect and reject incorrect fixes, not being able to get an integer fix at all may be too detrimental for some applications.

Table 36 - Combined reliability testing results - V2V open sky under 5° mask

		Predicted success rate and F-test – V2V open sky					
		Correct fix			Incorrect fix		
		Accept	Reject	Reject	Accept	Accept	Reject
L1 only	GPS only	27.6% (16)	72.4% (42)	96.4% (80)	3.6% (3)	3.6% (3)	96.4% (80)
	GG float GLO	30.8% (20)	69.2% (45)	93.4% (71)	6.6% (5)	6.6% (5)	93.4% (71)
	GG fixed GLO	55.4% (62)	44.6% (50)	93.5% (29)	6.5% (2)	6.5% (2)	93.5% (29)
L1 + L2	GPS only	87.8% (101)	12.2% (14)	57.7% (15)	42.3% (11)	42.3% (11)	57.7% (15)
	GG float GLO	90.8% (109)	9.2% (11)	47.6% (10)	52.4% (11)	52.4% (11)	47.6% (10)
	GG fixed GLO	88.8% (119)	11.2% (15)	33.3% (3)	66.7% (6)	66.7% (6)	33.3% (3)
WL	GPS only	70.4% (69)	29.6% (29)	36.6% (15)	63.4% (26)	63.4% (26)	36.6% (15)
	GG float GLO	77.9% (88)	22.1% (25)	25.0% (7)	75.0% (21)	75.0% (21)	25.0% (7)
	GG fixed GLO	96.0% (119)	4.0% (5)	31.6% (6)	68.4% (13)	68.4% (13)	31.6% (6)

Table 37 - Combined reliability testing results - V2V foliage under 5° mask

		Predicted success rate and F-test – V2V foliage					
		Correct fix			Incorrect fix		
		Accept	Reject	Reject	Accept	Accept	Reject
L1 only	GPS only	0.0% (0)	100.0% (24)	100.0% (87)	0.0% (0)	0.0% (0)	100.0% (87)
	GG float GLO	6.5% (2)	93.5% (29)	100.0% (86)	0.0% (0)	0.0% (0)	100.0% (86)
	GG fixed GLO	47.4% (27)	52.6% (30)	96.9% (63)	3.1% (2)	3.1% (2)	96.9% (63)
L1 + L2	GPS only	88.5% (46)	11.5% (6)	48.3% (28)	51.7% (30)	51.7% (30)	48.3% (28)
	GG float GLO	87.7% (50)	12.3% (7)	50.0% (30)	50.0% (30)	50.0% (30)	50.0% (30)
	GG fixed GLO	89.0% (65)	11.0% (8)	66.0% (35)	34.0% (18)	34.0% (18)	66.0% (35)
WL	GPS only	67.5% (27)	32.5% (13)	66.7% (42)	33.3% (21)	33.3% (21)	66.7% (42)
	GG float GLO	83.3% (45)	16.7% (9)	58.7% (37)	41.3% (26)	41.3% (26)	58.7% (37)
	GG fixed GLO	93.3% (56)	6.7% (4)	54.1% (33)	45.9% (28)	45.9% (28)	54.1% (33)

5.1.2 Positioning Accuracy

The accuracies of the positions derived from the integer ambiguity fixes is briefly analyzed herein. The position errors under open sky are represented in 2D for all the fixes (Figure 57) and only the correct fixes (Figure 58). The same errors under foliage are shown in Figure 59 for all the fixes and Figure 60 for only the correct fixes. The spread of position errors between the open sky and foliage environments appears to be similar. This is due to the fact that the code and phase errors are almost the same between the two environments, as demonstrated later in Section 5.1.3. It is shown in that section that the two main effects of foliage over open sky are the lower availability of fixes (approximately 110 instead of 140 despite the same duration) and the higher rate of cycle slips and subsequently negative effect on actual success rate.

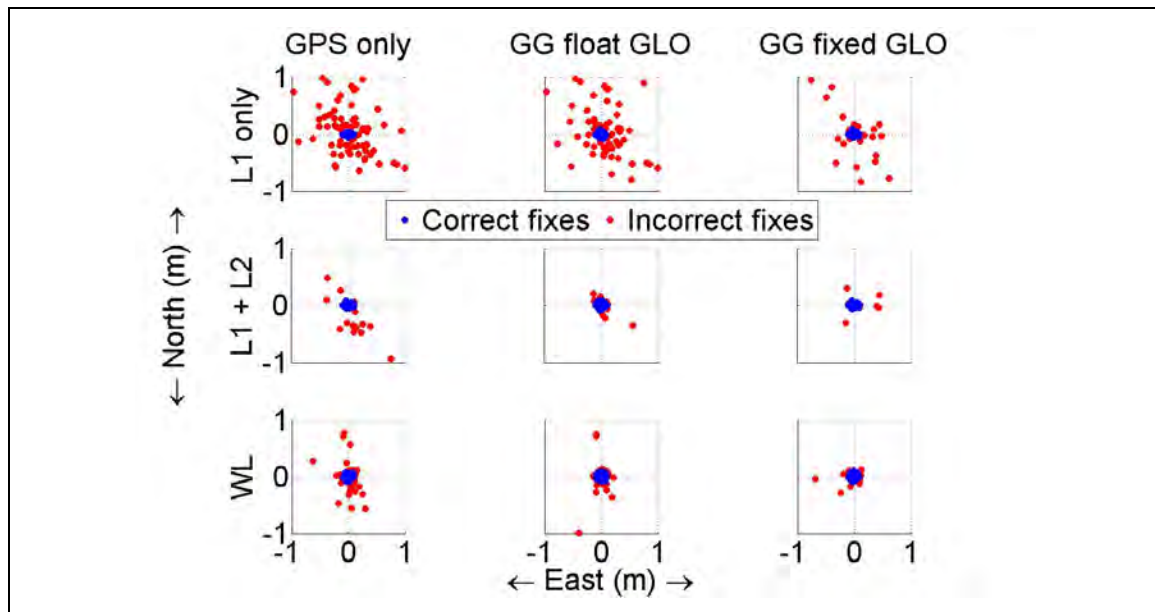


Figure 57 - 2D view of position errors, all fixes - V2V open sky under 5° mask

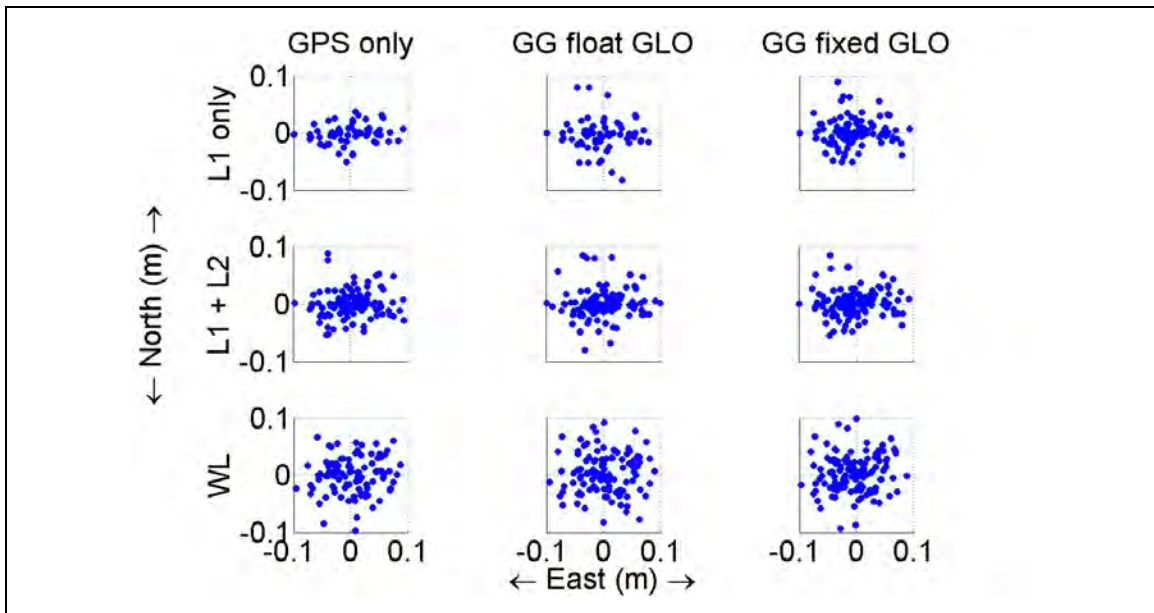


Figure 58 - 2D view of position errors, correct fixes - V2V open sky under 5° mask

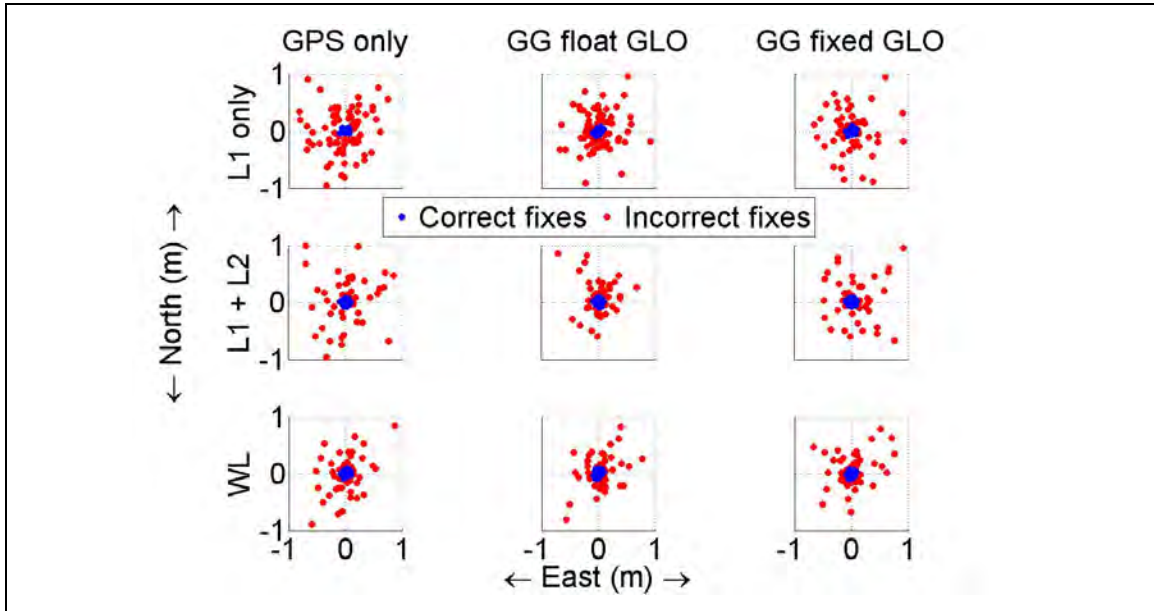


Figure 59 - 2D view of position errors, all fixes - V2V foliage under 5° mask

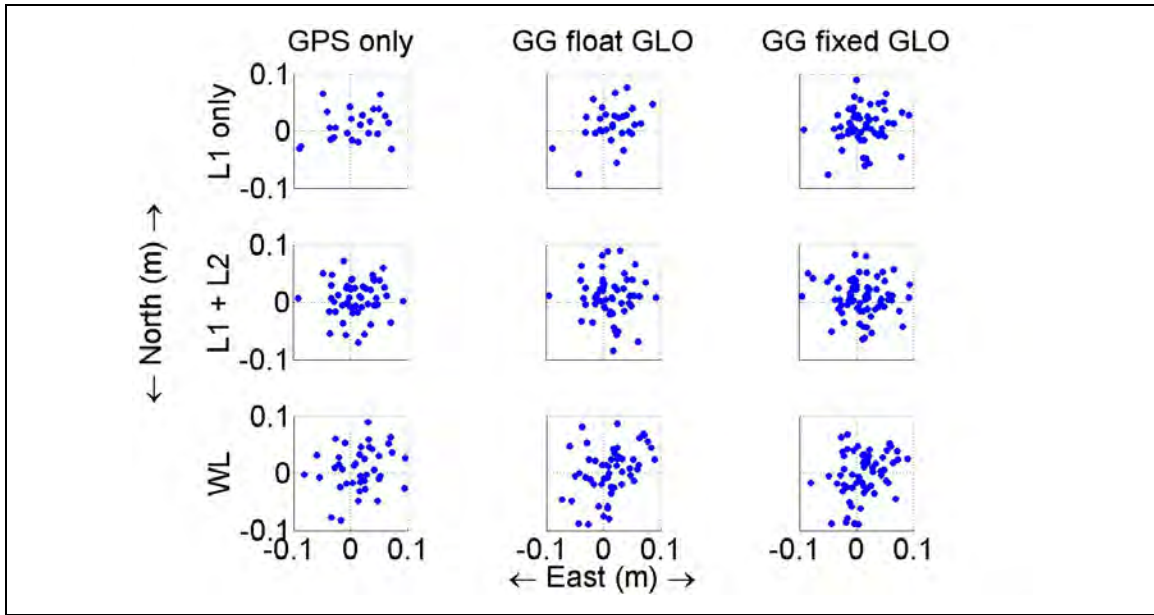


Figure 60 - 2D view of position errors, correct fixes - V2V foliage under 5° mask

The position errors from the correct fixes are summarized in Table 38 and Table 39 (median and RMS errors under open sky) and Table 40 and Table 41 (median and RMS errors under foliage). The corresponding actual success rates and numbers of correct fixes are also given, with the latter highlighted in **blue**.

The impact on the fixed-ambiguity positioning accuracy of using GLONASS or dual-frequency over the standard single-frequency GPS solution (i.e. **L1 only GPS only**) is minimal. The use of GLONASS does reduce the RMS vertical errors under foliage, but since the median vertical error remains approximately the same, this only indicates the removal of a few larger vertical errors. What GLONASS (or dual-frequency) *does* do is increase the actual success rate, and thus the availability of fixed-accuracy solutions.

Table 38 - Median position errors from correct fixes - V2V open sky under 5° mask

		Median errors from correct fixes (cm) – V2V open sky					Actual success rate probabilities	
		East	North	Up	2D	3D		
L1 only	GPS only	3.0	0.8	1.2	3.7	4.5	0.41	(58)
	GG float GLO	2.9	1.2	1.1	3.9	4.5	0.46	(65)
	GG fixed GLO	2.5	1.1	1.0	3.2	3.8	0.78	(112)
L1 + L2	GPS only	2.3	1.1	1.1	3.0	3.7	0.82	(115)
	GG float GLO	2.2	1.0	1.1	3.1	3.7	0.85	(120)
	GG fixed GLO	2.1	1.2	1.0	2.9	3.6	0.94	(134)
WL	GPS only	2.9	2.1	3.7	4.4	6.7	0.71	(98)
	GG float GLO	3.2	2.7	3.9	4.7	7.1	0.80	(113)
	GG fixed GLO	3.2	2.3	3.7	4.3	6.4	0.87	(124)

Table 39 - RMS position errors from correct fixes - V2V open sky under 5° mask

		RMS errors from correct fixes (cm) – V2V open sky					Actual success rate probabilities	
		East	North	Up	2D	3D		
L1 only	GPS only	4.2	1.8	3.9	4.6	6.0	0.41	(58)
	GG float GLO	4.0	2.8	6.4	4.8	8.1	0.46	(65)
	GG fixed GLO	3.8	2.3	4.6	4.5	6.4	0.78	(112)
L1 + L2	GPS only	3.8	2.3	4.0	4.4	6.0	0.82	(115)
	GG float GLO	3.8	2.6	4.9	4.6	6.7	0.85	(120)
	GG fixed GLO	3.8	2.3	3.9	4.4	5.9	0.94	(134)
WL	GPS only	4.1	3.2	7.1	5.2	8.8	0.71	(98)
	GG float GLO	4.1	3.6	7.7	5.4	9.4	0.80	(113)
	GG fixed GLO	4.0	3.3	8.1	5.2	9.6	0.87	(124)

Table 40 - Median position errors from correct fixes - V2V foliage under 5° mask

		Median errors from correct fixes (cm) – V2V foliage					Actual success rate probabilities	
		East	North	Up	2D	3D		
L1 only	GPS only	3.5	2.0	1.8	4.0	6.1	0.22	(24)
	GG float GLO	3.1	2.4	1.8	4.2	5.1	0.26	(31)
	GG fixed GLO	2.0	2.1	1.8	3.9	5.3	0.47	(57)
L1 + L2	GPS only	2.5	2.2	1.6	4.0	5.1	0.47	(52)
	GG float GLO	2.3	2.1	1.2	3.9	5.1	0.49	(57)
	GG fixed GLO	2.0	1.9	1.5	3.9	5.3	0.58	(73)
WL	GPS only	2.7	2.7	4.5	5.1	8.4	0.39	(40)
	GG float GLO	2.6	2.5	4.6	4.6	8.4	0.46	(54)
	GG fixed GLO	2.2	2.6	4.1	4.3	8.0	0.50	(60)

Table 41 - RMS position errors from correct fixes - V2V foliage under 5° mask

		RMS errors from correct fixes (cm) – V2V foliage					Actual success rate probabilities	
		East	North	Up	2D	3D		
L1 only	GPS only	4.5	2.9	32.6	5.4	33.0	0.22	(24)
	GG float GLO	3.9	3.4	17.6	5.2	18.3	0.26	(31)
	GG fixed GLO	3.5	3.3	5.8	4.8	7.6	0.47	(57)
L1 + L2	GPS only	3.5	3.1	33.9	4.7	34.2	0.47	(52)
	GG float GLO	3.5	3.7	7.8	5.1	9.3	0.49	(57)
	GG fixed GLO	3.8	3.2	5.7	5.0	7.5	0.58	(73)
WL	GPS only	4.2	3.9	16.0	5.7	17.0	0.39	(40)
	GG float GLO	4.0	4.2	11.1	5.8	12.5	0.46	(54)
	GG fixed GLO	3.6	3.9	8.6	5.3	10.1	0.50	(60)

5.1.3 Signal Tracking and Cycle Slips under Foliage

The foliage environment affects the ambiguity resolution process negatively: ambiguities are correctly fixed less often, and identifying fixes as correct or incorrect is harder. In fact, foliage does impact *signal tracking* significantly – this was first demonstrated in Chapter Three (Section 3.1.2) and is reiterated in Table 42. The quality of the phase measurements was also discussed in Chapter Three where it was shown that the phase noise under open sky is at the millimetre level. The foliage does not impact the C/N₀ of the signals that are tracked. One would expect that the C/N₀ would be lower under foliage; however the hardware used in this thesis is geodetic grade, not high-sensitivity. The average number of satellites under foliage is lower, suggesting that the weaker signals were simply not tracked.

Table 42 - Signal tracking for V2V in all environments

		V2V open sky		V2V foliage	
		L1	L2	L1	L2
Mean C/N₀ (dB-Hz)	GPS	47	40	47	40
	GLONASS	46	40	47	42
Mean signal lock time (min:sec)	GPS	7:36	7:38	0:57	1:03
	GLONASS	8:20	8:08	1:46	1:52
Rate of cycle slips detected	GPS	0.01%	0.00%	0.05%	0.01%
	GLONASS	0.06%	0.04%	0.02%	0.11%
Mean number of satellites tracked	GPS	7		6	
	GLONASS	4		3	
Mean number of satellites available above 5° elevation	GPS	7		5	
	GLONASS	4		3	

The code and phase errors under both open sky and foliage are represented by the histograms in Figure 61. These are derived from the DD code and phase residuals corresponding to correct ambiguity fixes (i.e. positions with sub-decimetre accuracy). The error distributions are very similar under open sky and foliage. This is expected since the signal strength (specifically the C/N₀) is the same in both environments.

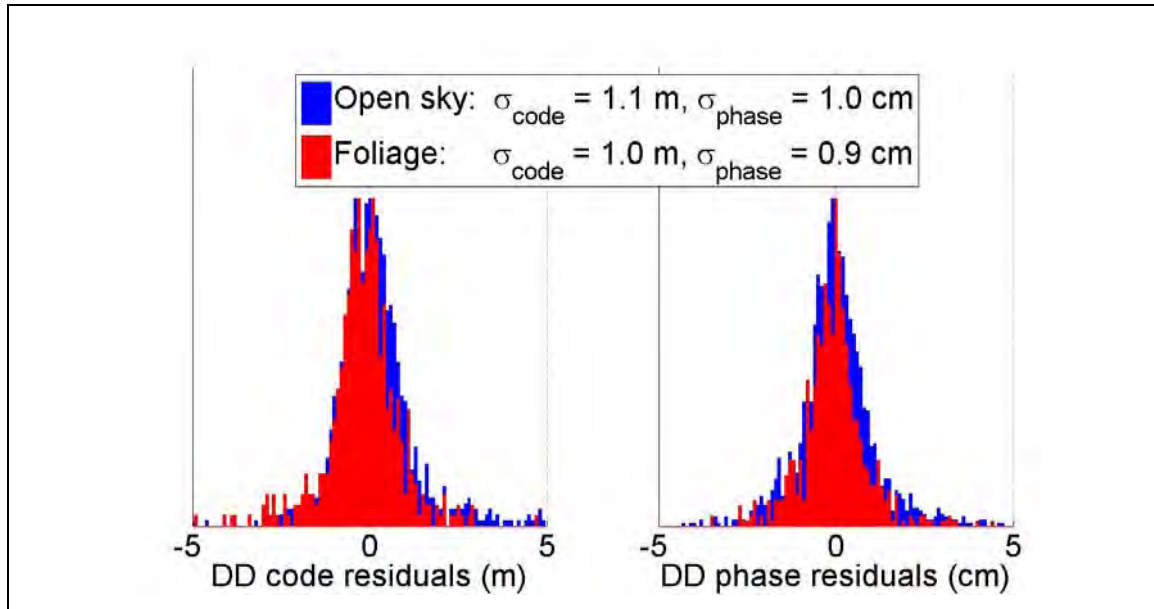


Figure 61 - L1 DD code and phase errors - V2V all environments

Where the foliage *does* impact signal tracking is in the frequency of cycle slips. On the surface this does not appear to be the case, as the rate of *detected* cycle slips is significantly less than 1% for all signals in all environments. However, these are only cycle slips detected by the *phase velocity trend method* (Lachapelle 2008). The disagreement between the actual change in phase and the change predicted by the Doppler frequency is defined by

$$\Delta\phi = (\phi_k - \phi_{k-1}) - \left(\frac{d_k + d_{k-1}}{2} (t_k - t_{k-1}) \right)$$

where ϕ_k is the phase at the k^{th} epoch,

d_k is the Doppler at the k^{th} epoch, and

t_k is the time of the k^{th} epoch.

A cycle slip is detected if the disagreement in the change in phase exceeds a certain threshold (usually on the order of cycles). However, this method only operates on measurements that have already been output by the receiver. The receiver does not output phase measurements on which cycle slips (or more generally, loss of phase lock) are detected during signal processing. Frequent loss of phase lock is indicated by short durations of signal lock, or *lock times*. Table 42 shows that the lock times under foliage are much shorter than those under open sky. Therefore foliage induces more frequent loss of phase lock and consequently more frequent cycle slips.

Signal tracking under foliage has a definite impact on the ability to fix the ambiguities correctly. Table 43 breaks down the average C/N₀ values and lock times for the correct and incorrect fixes under foliage. These are generated using the **L1 + L2 GG fixed GLO** solution, so that signal tracking parameters for each system and frequency are available; results for all of the solutions are presented later. The impact of the C/N₀ appears to be small: about 1 dB-Hz higher for correct fixes than incorrect fixes. However the impact of the lock time is significant: for correct fixes, about 15 seconds longer for GPS and one minute longer for GLONASS.

Table 43 - Signal tracking parameters for correct and incorrect L1 + L2 GG fixed GLO fixes - V2V foliage under 5° mask

		Correct fix	Incorrect fix
Mean C/N₀ (dB-Hz)	GPS L1	47	46
	GPS L2	41	40
	GLONASS L1	47	46
	GLONASS L2	42	41
Mean signal lock time (min:sec)	GPS L1	1:04	0:47
	GPS L2	1:09	0:56
	GLONASS L1	2:13	1:18
	GLONASS L2	2:15	1:10

The effect of lock time on the actual success rate is further illustrated in Figure 62. These are the distributions of the actual success rate probability for various lock times; each epoch is associated with one aggregate measure of lock time, which is the average of the individual lock times of the signals at that epoch. The trend is obvious: as the average lock time increases, so does the actual success rate.

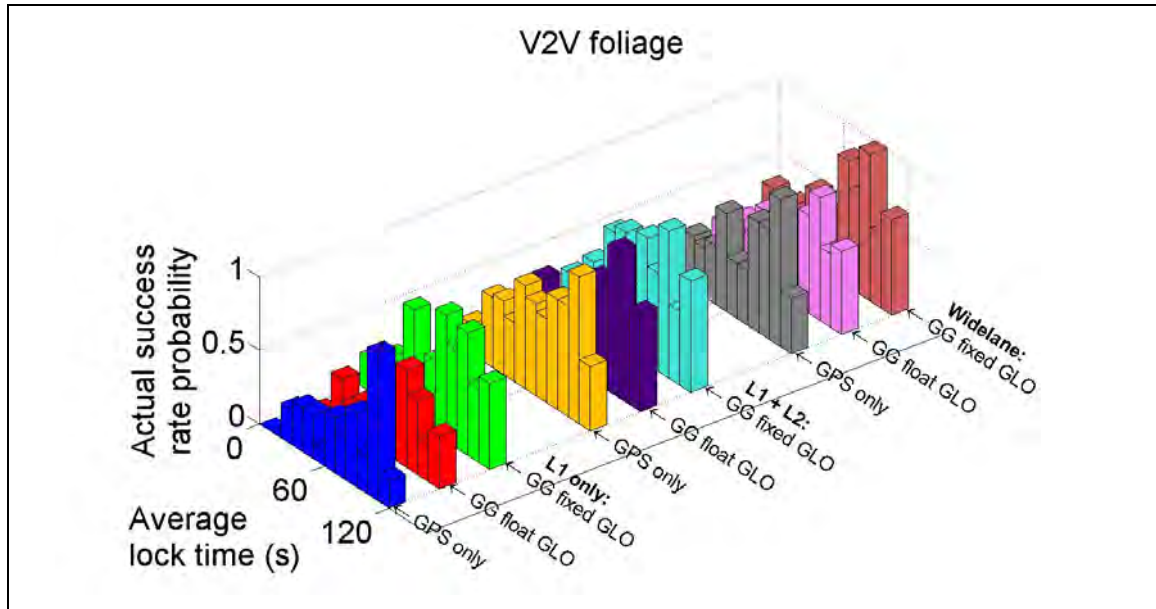


Figure 62 - Actual success rate vs. lock time - V2V foliage under 5° mask

Conceptually, short lock times, and more frequent cycle slips, negatively affect the convergence of the float estimate: because the value of the phase ambiguity changes, it has to be estimated anew and fewer epochs of code and phase measurements can be incorporated. Hence, the amount of convergence time available for that particular ambiguity is lower. The relationship between the available convergence time and the ADOP is illustrated in Figure 63 (for the **L1 only GPS only** solution), Figure 64 (for the **L1 only GG fixed GLO** solution) and Figure 65 (for the **L1 + L2 GPS only** solution). For all three solutions, the ADOP decreases as the ambiguities are given more time to converge. The static baseline analysis demonstrated that the actual success rate increases as the ADOP decreases; hence, the connection between short lock times and low actual success rates is established.

Another pattern established here is that the ADOP decreases when one adds GLONASS (i.e. switching from **GPS only** to **GG fixed GLO**) or dual-frequency (i.e. switching from **L1 only** to **L1 + L2**). The trend is much more obvious when dual-frequency is added. This relates to what is illustrated in Figure 62; there are improvements in the distributions of actual success rate (for various lock times) when one adds GLONASS or dual-frequency, with the bigger improvements when dual-frequency is added.

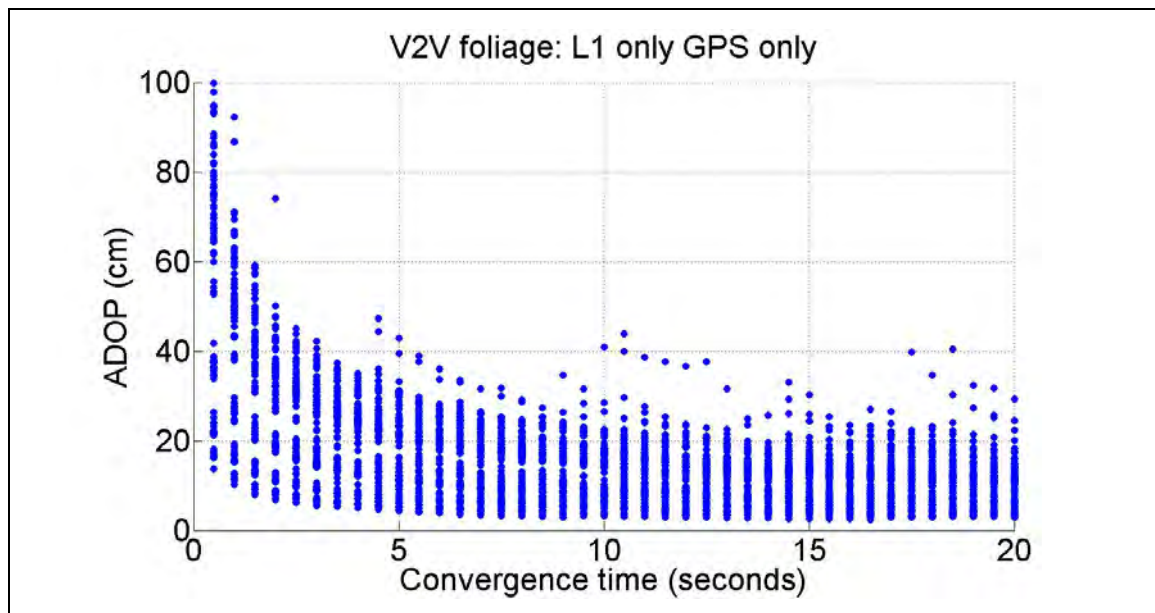


Figure 63 - Relationship between ADOP and convergence time for L1 only GPS only solution - V2V foliage under 5° mask

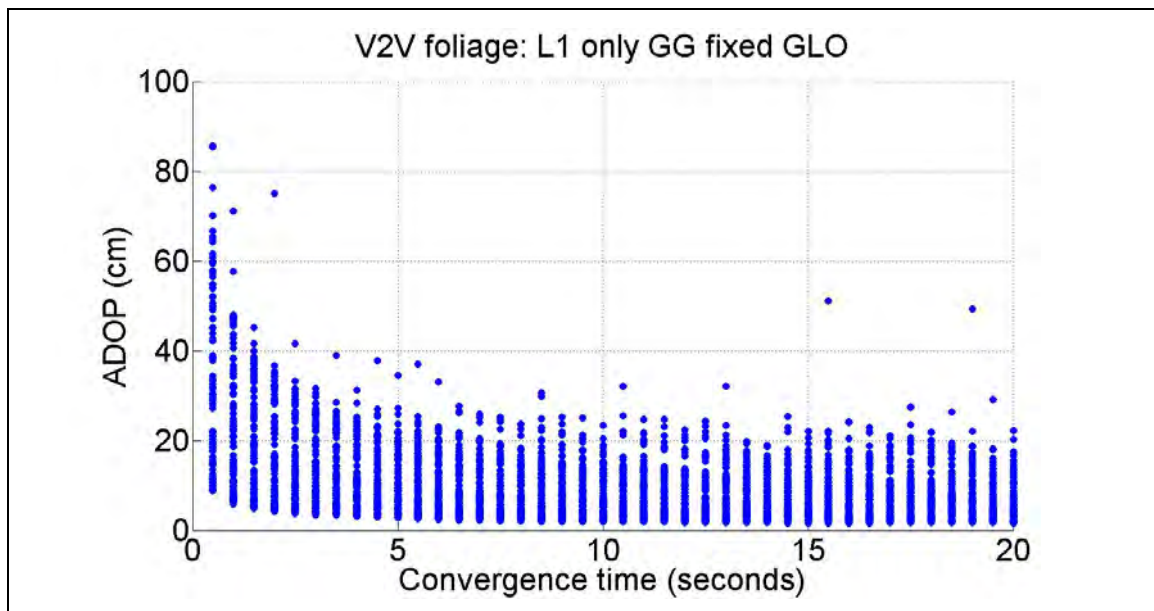


Figure 64 - Relationship between ADOP and convergence time for L1 only GG fixed GLO solution - V2V foliage under 5° mask

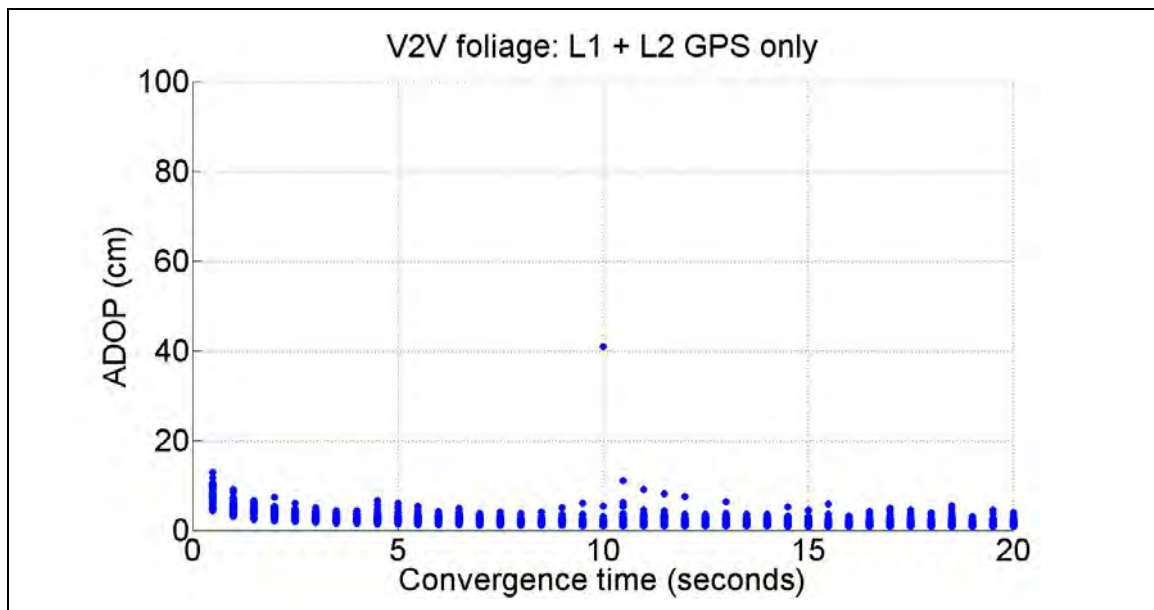


Figure 65 - Relationship between ADOP and convergence time for L1 + L2 GPS only solution - V2V foliage under 5° mask

The effect of foliage on the signal lock time also impacts fix reliability. It was established in the static baseline analysis from Chapter Four (Sections 4.6 and 4.7) that the weakness of the predicted success rate is its limitation in rejecting incorrect fixes, and the weakness of the F-test is its rate of acceptance of correct fixes. For the V2V foliage environment, Figure 66 shows the rate of incorrect fix rejection for the predicted success rate, for various levels of signal lock time.

Unfortunately, Figure 66 indicates that the predicted success rate rejects *less* incorrect fixes as the lock time increases, when the **L1 + L2** and **widelane** combinations are used. Although this is a surprising result, it was demonstrated in Section 3.5 that predicted success rate increases with convergence time. Figure 67 further illustrates that the predicted success rate probabilities under foliage increase convergence to one faster than the actual success rates from Figure 66, when dual-frequency is used. When **L1 only** is used, the predicted success rate probabilities do not converge to one, so most of the incorrect fixes are rejected. This comes at a cost as demonstrated in Section 5.1.1; many correct fixes are *also* rejected. Overall, the predicted success rate does not reject incorrect fixes very effectively, corroborating the conclusions from the static baseline analysis.

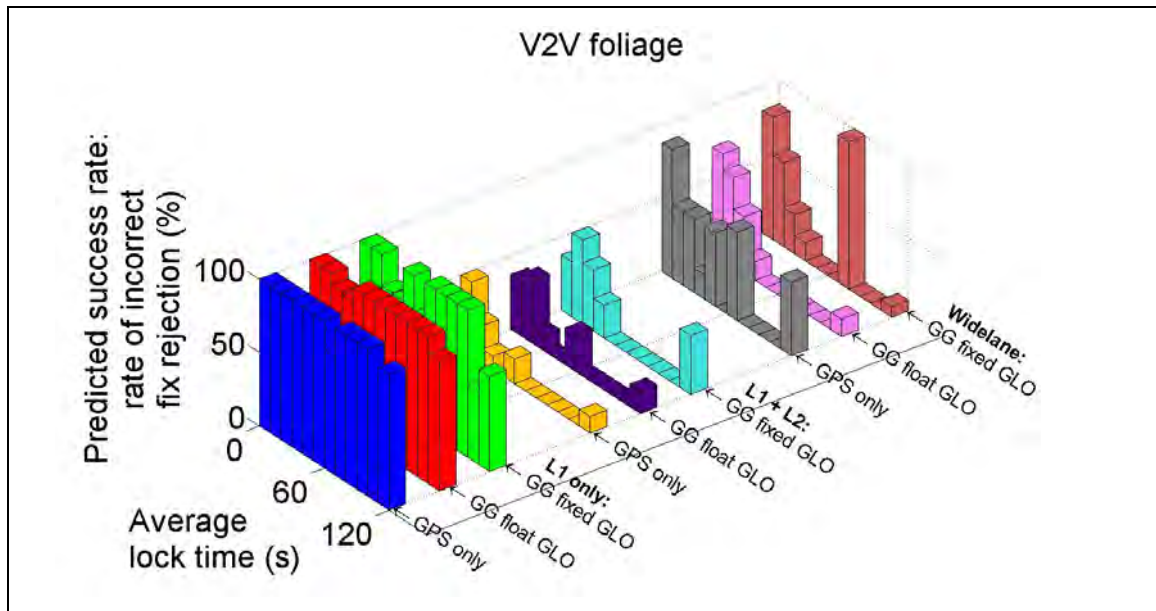


Figure 66 - Predicted success rate incorrect fix rejection vs. lock time - V2V foliage under 5° mask

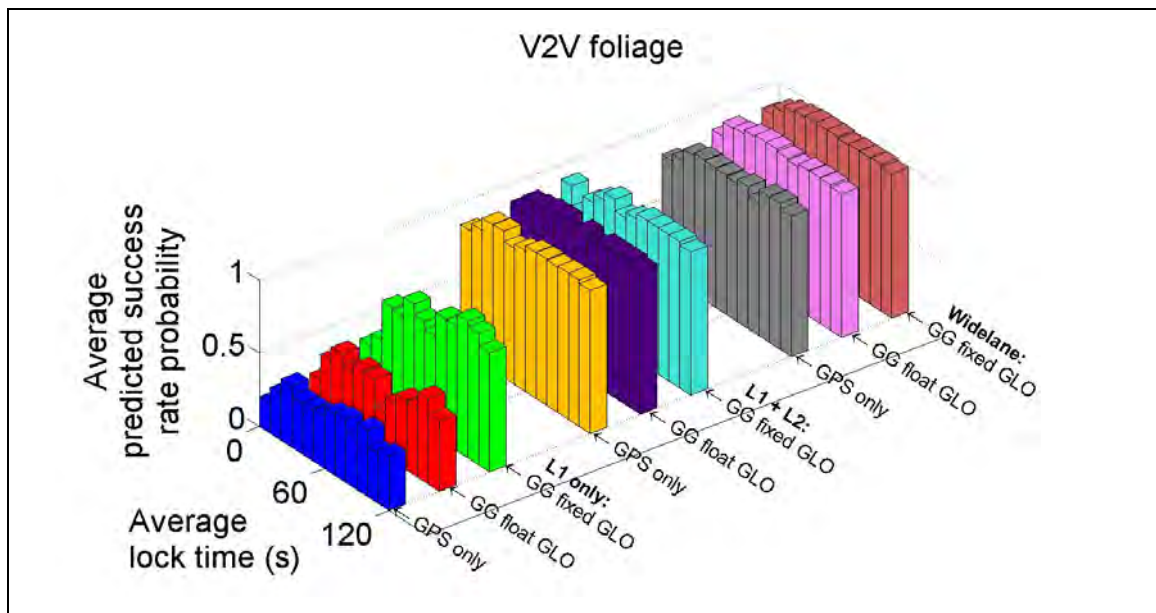


Figure 67 - Predicted success rate probability vs. lock time - V2V foliage under 5° mask

The dependency of the F-test rate of correct fix acceptance on the lock time is illustrated in Figure 68. For the solutions that use the **L1 only** combination, the rate of correct fix acceptance increases as the lock time increases. For the dual-frequency combinations, the rate of correct fix acceptance is very close to 100% for a wide range of lock times. This illustrates the positive impact of dual frequency on fix reliability in environments with many cycle slips.

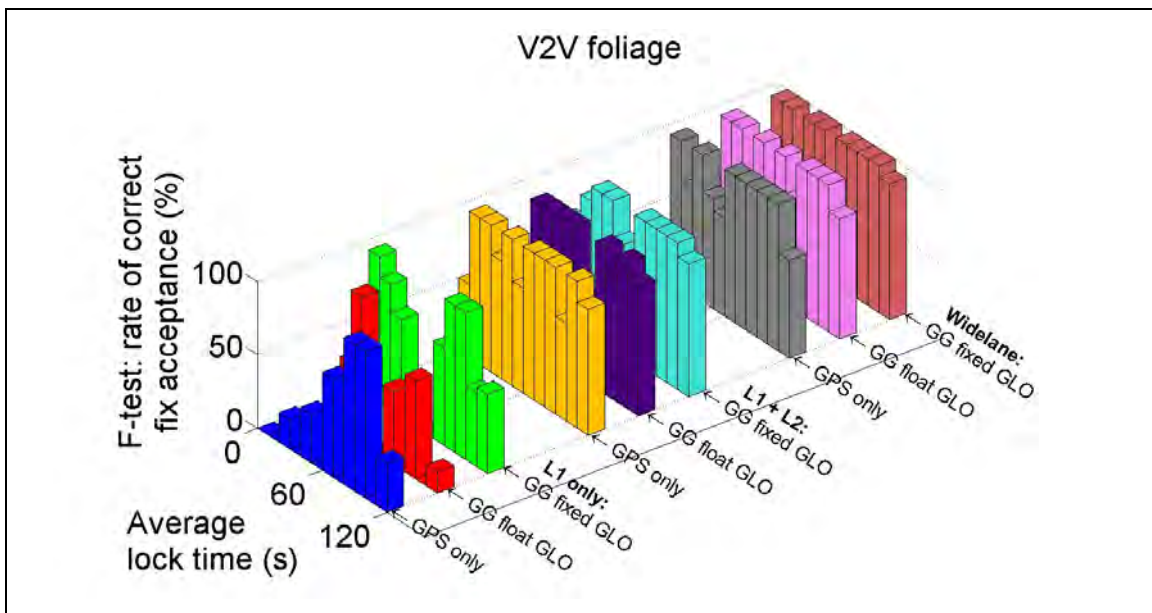


Figure 68 - F-test correct fix acceptance vs. lock time - V2V foliage under 5° mask

5.2 Downhill Ski Runs

Downhill ski testing was conducted at the Nakiska ski resort under open sky on February 9, 2010. Mask angles of up to 20° were encountered due to the slope itself; however these were not always present. Seven runs were conducted, each lasting four to eight minutes. Between seven and 11 GPS and three and five GLONASS satellites were available. The

same GNSS hardware used in the static and V2V tests was used for the downhill testing (dual-frequency GPS/GLONASS NovAtel OEMV2-G receivers and GPS-702-GG antennas). A convergence time of five seconds was used to generate fixes for this test. This is different from the previous two tests (which used 20 seconds) and was chosen by trial and error so that there would be incorrect fixes to analyze. Table 44 shows the total number of fixes, which are the same for all solutions under a circular 5° elevation mask but varies under a 30° mask if GLONASS is used.

Table 44 - Total number of fixes - downhill ski runs with all masks

		Total number of fixes
Under 5° mask		418
Under 30° mask	GPS only	410
	<i>Availability relative to 5° mask</i>	98.1%
	GPS/GLONASS	417
	<i>Availability relative to 5° mask</i>	99.8%

A static base station was set up for the differential processing, less than 2 km from the ski slope. Differential atmospheric effects over such a small inter-receiver distance are expected to be negligible. Regardless, the geomagnetic *K* index on the day of the test did not exceed 1.0. Therefore there were no significant ionospheric disturbances.

Nine types of solutions are investigated: the **L1 only**, **L1 + L2** and **widelane** measurement combinations are each combined with the **GPS only**, **GG float GLO** and **GG fixed GLO** fixing strategies. The correctness of the resolved ambiguities is

determined by comparing the fixed-ambiguity positions to a reference solution derived from GPS/GLONASS RTK with forward-backward smoothing applied. The fix is taken to be correct with a horizontal agreement of better than 10 cm and incorrect otherwise. The precision of the reference solution was evaluated by the vertical consistency at physical checkpoints that the skier occupied at the beginning and end of each run. The vertical range of the reference solution at these checkpoints (i.e. maximum minus minimum height) did not exceed 5 cm either at the top or bottom of the hill.

Table 45 shows the actual success rate probabilities for downhill skiing. The numbers of correct fixes that correspond to the success rates are highlighted in **blue**. Two scenarios are investigated, namely the use of a standard circular elevation mask angle of 5° , and then a circular mask angle of 30° . The latter approximately simulates downhill skiing on a steeper hill where the mask angles from the slopes themselves are more severe. Such mask angles could realistically be encountered in all directions (i.e. like a circular mask) when skiing in mountainous valleys with steep slopes and trees along ski runs. The following trends are observed:

- For both downhill scenarios, the impact of GLONASS on the actual success rate is the same as for the static and V2V analyses. The actual success rate effectively does not change when the GLONASS measurements are simply added to float estimation. However, significant improvement is observed when *fixing* the GLONASS ambiguities.

- Because of the short inter-receiver distances (and consequently the smaller phase errors), switching from **L1 only** to **L1 + L2** improves the actual success rate more than switching to **widelane**, as highlighted in **green** in Table 45. As with the analyses of previous scenarios, either dual-frequency combination benefits the actual success rate over L1 alone.
- The higher elevation mask has a negative impact on the actual success rate, which is completely expected. However it is noteworthy that when GLONASS is fully incorporated (even with **L1 only**), the ambiguities are more likely than not to be fixed correctly. For the specific application of tracking skiers, single-frequency ambiguity resolution can be useful even under high elevation masks, if GLONASS is also used. In fact this has already been demonstrated for Olympic alpine skiing (Lachapelle et al 2009).

Table 45 - Actual success rate probabilities - downhill ski runs with all masks

		Actual success rate probability	
		Downhill 5°	Downhill 30°
L1 only	GPS only	0.83 (347) ³	0.22 (91)
	GG float GLO	0.82 (344)	0.21 (87)
	GG fixed GLO	0.94 (395)	0.51 (214)
L1 + L2	GPS only	0.99 (415)	0.92 (378)
	GG float GLO	0.99 (415)	0.91 (380)
	GG fixed GLO	1.00 (417)	0.98 (408)
Widelane	GPS only	0.87 (363)	0.51 (211)
	GG float GLO	0.89 (374)	0.55 (229)
	GG fixed GLO	0.94 (393)	0.71 (298)

The results of using the predicted success rate as an indicator of fix reliability are shown in Table 46 and Table 47, for the 5° and 30° mask scenarios, respectively. Fixes are accepted if they exceed the threshold of 0.95, and are otherwise rejected. No incorrect fix results are presented for the solutions with actual success rates of 0.98 and above, as there are too few incorrect fixes to compute meaningful acceptance and rejection rates.

For the 5° mask scenario, the predicted success rate is very optimistic, as it accepts almost all of the fixes whether they are correct or incorrect. This implies that the predicted success rate provides almost no information about the fix reliability. For the 30° mask scenario, the predicted success rates are less optimistic.

³ Number of correct fixes

The addition of GLONASS does not consistently improve the rate of incorrect fix acceptance. The same trend was observed in the V2V analysis. As GLONASS measurements or dual-frequency are added to the basic single-frequency GPS solution, the geometry of the integer ambiguity estimation improves and the fixes that were incorrect due to poor geometry have a better chance of becoming correct. The fixes that are incorrect for another reason are left behind: the predicted success rate, which was established by Teunissen (2001a) to be connected to the ambiguity dilution of precision, will reflect the improved geometry of those fixes, and thence will *not* indicate that they are incorrect.

Table 46 - Predicted success rate results - downhill ski runs with 5° mask

		Predicted success rate (0.95 threshold) – Downhill 5°			
		Correct fix		Incorrect fix	
		Accept	Reject	Reject	Accept
L1 only	GPS only	88.2% (306)	11.8% (41)	45.1% (32)	54.9% (39)
	GG float GLO	92.2% (317)	7.8% (27)	43.2% (32)	56.8% (42)
	GG fixed GLO	99.2% (392)	0.8% (3)	8.7% (2)	91.3% (21)
L1 + L2	GPS only	100.0% (415)	0.0% (0)	—	—
	GG float GLO	100.0% (415)	0.0% (0)	—	—
	GG fixed GLO	100.0% (417)	0.0% (0)	—	—
WL	GPS only	97.8% (355)	2.2% (8)	9.1% (5)	90.9% (50)
	GG float GLO	97.9% (366)	2.1% (8)	4.5% (2)	95.5% (42)
	GG fixed GLO	99.2% (390)	0.8% (3)	4.0% (1)	96.0% (24)

Table 47 - Predicted success rate results - downhill ski runs with 30° mask

		Predicted success rate (0.95 threshold) – Downhill 30°					
		Correct fix			Incorrect fix		
		Accept	Reject	Reject	Accept	Reject	Accept
L1 only	GPS only	48.4% (44)	51.6% (47)	87.5% (279)	12.5% (40)		
	GG float GLO	54.0% (47)	46.0% (40)	78.5% (259)	21.5% (71)		
	GG fixed GLO	74.8% (160)	25.2% (54)	69.0% (140)	31.0% (63)		
L1 + L2	GPS only	92.1% (348)	7.9% (30)	28.1% (9)	71.9% (23)		
	GG float GLO	93.7% (356)	6.3% (24)	56.8% (21)	43.2% (16)		
	GG fixed GLO	100.0% (408)	0.0% (0)	–	–	–	–
WL	GPS only	70.6% (149)	29.4% (62)	60.8% (121)	39.2% (78)		
	GG float GLO	76.9% (176)	23.1% (53)	53.2% (100)	46.8% (88)		
	GG fixed GLO	85.6% (255)	14.4% (43)	43.7% (52)	56.3% (67)		

The F-test results are shown in Table 48 and Table 49 for the 5° and 30° mask scenarios, respectively. The numbers of fixes corresponding to each result are highlighted in blue. A significance level of 10% is used to compute the ratio testing critical value (or threshold) from the F distribution. Similar to the static and V2V analyses, the F-test is more effective than the predicted success rate at rejecting incorrect fixes. However, more correct fixes are rejected: the ambiguities are less likely to be fixed in a timely manner, resulting in a *loss of precision* in the position.

The problem of excessive correct fix rejection appears to be addressed by using either GLONASS or dual-frequency, as highlighted in green in both Table 48 and Table 49). In the 5° mask scenario, it appears that using GLONASS is sufficient, as the **L1 only GG fixed GLO** solution accepts four out of every five correct fixes. However, under the more

restrictive 30° mask, the **L1 + L2** dual-frequency combination is most effective, as at least three out of every four correct fixes are accepted even if GPS is used alone.

Table 48 - F-test results - downhill ski runs with 5° mask

		F-test (10% significance) – Downhill 5°					
		Correct fix			Incorrect fix		
		Accept	Reject	Reject	Accept	Reject	Accept
L1 only	GPS only	50.4% (175)	49.6% (172)	98.6% (70)	1.4% (1)	—	—
	GG float GLO	57.6% (198)	42.4% (146)	97.3% (72)	2.7% (2)	—	—
	GG fixed GLO	81.8% (323)	18.2% (72)	100.0% (23)	0.0% (0)	—	—
L1 + L2	GPS only	95.9% (398)	4.1% (17)	—	—	—	—
	GG float GLO	95.9% (398)	4.1% (17)	—	—	—	—
	GG fixed GLO	95.7% (399)	4.3% (18)	—	—	—	—
WL	GPS only	71.9% (261)	28.1% (102)	69.1% (38)	30.9% (17)	—	—
	GG float GLO	74.3% (278)	25.7% (96)	56.8% (25)	43.2% (19)	—	—
	GG fixed GLO	87.3% (343)	12.7% (50)	24.0% (6)	76.0% (19)	—	—

Table 49 - F-test results - downhill ski runs with 30° mask

		F-test (10% significance) – Downhill 30°					
		Correct fix			Incorrect fix		
		Accept	Reject	Reject	Accept	Reject	Accept
L1 only	GPS only	24.2% (22)	75.8% (69)	95.9% (306)	4.1% (13)		
	GG float GLO	19.5% (17)	80.5% (70)	96.7% (319)	3.3% (11)		
	GG fixed GLO	36.4% (78)	63.6% (136)	93.1% (189)	6.9% (14)		
L1 + L2	GPS only	73.5% (278)	26.5% (100)	90.6% (29)	9.4% (3)		
	GG float GLO	75.0% (285)	25.0% (95)	94.6% (35)	5.4% (2)		
	GG fixed GLO	91.9% (375)	8.1% (33)	–	–	–	–
WL	GPS only	46.0% (97)	54.0% (114)	93.5% (186)	6.5% (13)		
	GG float GLO	44.5% (102)	55.5% (127)	95.2% (179)	4.8% (9)		
	GG fixed GLO	55.4% (165)	44.6% (133)	84.0% (100)	16.0% (19)		

The results of combining the predicted success rate and F-test into *one* test are shown in Table 50 and Table 51 for the 5° and 30° mask scenarios, respectively. The combined reliability test rejects a fix if either the predicted success rate or F-test would reject it. Conversely a fix is only accepted if both individual tests would accept it. The numbers of fixes corresponding to each result are highlighted in **blue**.

The static baseline analysis demonstrated that the combined reliability test can be thought of as the F-test with information added from the predicted success rate. The V2V analysis showed that the predicted success rate *can*, for some solutions, add a significant amount of information to the F-test – that is, the predicted success rate can reject a significant number of incorrect fixes that the F-test would accept.

However, it was established earlier in the analysis of the downhill ski test that the predicted success rate contains little information on its own. For instance, Table 46 had shown that almost all fixes are accepted, correct or not, when using the **widelane** combination under the 5° mask. Consequently, the predicted success rate appears to contribute very little information to the combined reliability test. The maximum improvement in the rate of incorrect fix acceptance when going from the F-test to the combined test is 4% for the 5° mask scenario and 5% for the 30° mask scenario.

Table 50 - Combined reliability testing results - downhill ski runs with 5° mask

		Predicted success rate and F-test – Downhill 5°			
		Correct fix		Incorrect fix	
		Accept	Reject	Reject	Accept
L1 only	GPS only	48.4% (168)	51.6% (179)	100.0% (71)	0.0% (0)
	GG float GLO	56.4% (194)	43.6% (150)	98.6% (73)	1.4% (1)
	GG fixed GLO	81.8% (323)	18.2% (72)	100.0% (23)	0.0% (0)
L1 + L2	GPS only	95.9% (398)	4.1% (17)	– –	– –
	GG float GLO	95.9% (398)	4.1% (17)	– –	– –
	GG fixed GLO	95.7% (399)	4.3% (18)	– –	– –
WL	GPS only	71.4% (259)	28.6% (104)	69.1% (38)	30.9% (17)
	GG float GLO	73.3% (274)	26.7% (100)	59.1% (26)	40.9% (18)
	GG fixed GLO	87.3% (343)	12.7% (50)	28.0% (7)	72.0% (18)

Table 51 - Combined reliability testing results - downhill ski runs with 30° mask

		Predicted success rate and F-test – Downhill 30°					
		Correct fix			Incorrect fix		
		Accept	Reject	Reject	Accept	Reject	Accept
L1 only	GPS only	14.3% (13)	85.7% (78)	99.4% (317)	0.6% (2)		
	GG float GLO	12.6% (11)	87.4% (76)	100.0% (330)	0.0% (0)		
	GG fixed GLO	32.7% (70)	67.3% (144)	97.5% (198)	2.5% (5)		
L1 + L2	GPS only	70.9% (268)	29.1% (110)	93.7% (30)	6.3% (2)		
	GG float GLO	73.9% (281)	26.1% (99)	100.0% (37)	0.0% (0)		
	GG fixed GLO	91.9% (375)	8.1% (33)	–	–	–	–
WL	GPS only	38.9% (82)	61.1% (129)	97.0% (193)	3.0% (6)		
	GG float GLO	40.2% (92)	59.8% (137)	97.3% (183)	2.7% (5)		
	GG fixed GLO	53.0% (158)	47.0% (140)	85.7% (102)	14.3% (17)		

Chapter Six: Conclusions and Recommendations

This thesis has examined the impact of combining GPS and GLONASS on the reliability of carrier phase ambiguity resolution, or ambiguity fixing. *Reliability* in this context refers to the ability to identify and reject incorrectly fixed ambiguities, as these lead to undetected position biases. The ability to generate more correct fixes (and subsequently identify and accept them) was also investigated, as the objective of ambiguity resolution is to obtain sub-decimetre level position accuracy. Three key concepts related to fix reliability were investigated herein: the *actual* success rate (i.e. the rate of correct fix); the *predicted* success rate (i.e. an *a priori* indicator of the likelihood of a fix being correct); and the F ratio test or *F-test* (i.e. a discriminator of correct and incorrect fixes).

The PLANSOFT™ real-time kinematic (RTK) processing software was developed by the author to perform GPS/GLONASS ambiguity resolution. The impact of GLONASS was examined in two contexts: partial fixing (i.e. only the GPS ambiguities are resolved) and full fixing (i.e. both GPS and GLONASS ambiguities are resolved). Single- and dual-frequency measurement combinations were also investigated.

Three tests were conducted to investigate ambiguity resolution. *Static baselines* were analyzed over distances of 2 km and 18 km, with the static surveys exceeding 24 hours to provide statistically significant data. *Vehicle-to-vehicle (V2V) relative navigation* was conducted over inter-receiver distances of up to a few hundred metres. A series of *downhill ski runs* was tracked using a base station less than 2 km away from the ski slope.

Geodetic-grade GPS/GLONASS dual-frequency hardware (NovAtel OEMV2-G receivers and GPS-702-GG antennas) were used to collect the data. No significant ionospheric disturbances were encountered during these data collections.

6.1 Conclusions

The following conclusions are based on the data used in the thesis and should be interpreted in this context. The use of additional data sets under different atmospheric conditions could impact these conclusions, as noted in the next section on recommendations.

Impact of GLONASS: The main effect of adding the GLONASS measurements is that the accuracy of the float estimate of the position improves. This is expected since adding GLONASS measurements improves the geometry of the float position estimation. However, the float position error just prior to ambiguity resolution is only weakly correlated with the correctness of the resulting fixed ambiguities. Hence GLONASS with *partial* fixing does not significantly improve the actual success rate.

GLONASS with *full* fixing improves the actual success rate significantly. The additional ambiguities from GLONASS improve the geometry of the integer ambiguity estimation (represented by the ambiguity dilution of precision, or ADOP). Both the number of ambiguities and the ADOP are strongly correlated with actual success rate.

GLONASS has a small effect on the fixed position accuracies that correspond with *correct* fixes. However since GLONASS (with full fixing) provides many *more* correct fixes, the availability of precise (sub-decimetre) positioning accuracy is higher in general. One of the other major benefits of GLONASS is increased solution availability under certain scenarios where the satellite visibility is reduced. Tests under elevation mask angles of 30° have shown that a GPS/GLONASS solution maintains nearly 100% solution availability, while GPS-only availability was as low as 80% for some tests. The effect of GLONASS in other reduced-visibility scenarios (such as urban canyons) has not been explored and may not produce results that are as successful.

GLONASS with full fixing also improves the reliability of ambiguity resolution, as it generally maximizes both incorrect fix rejection and correct fix acceptance (over GPS alone or GLONASS with partial fixing) when the predicted success rate and F-test are both used to identify correct and incorrect fixes. The performance of the F-test has a strong correlation with the integer estimation geometry (i.e. both the number of ambiguities and the ADOP) which GLONASS with full fixing improves substantially.

Impact of dual-frequency: Incorporating L1 and L2 phase measurements (as separate measurements) is a similar strategy to adding GLONASS with full fixing. The main effect of L1 and L2 is the improvement in the geometry of the integer estimation (but not the geometry of the satellites), which comes about from the additional L2 ambiguities. The better geometry results in higher success rates and better fix reliability when the F-test is applied.

Combining the L1 and L2 phase measurements into *widelane* measurements widens the wavelength of the phase ambiguities from approximately 19 cm to 86 cm. The benefits of using widelane are two-fold. The widelane ambiguities are easier to fix than L1 due to the wider wavelength. As well, the effect of phase errors on a single widelane *cycle* is less than half the effect on an L1 cycle. The actual success rate and fix reliability are both negatively affected by the magnitude of the phase errors. Hence, widelane could potentially be useful for longer inter-receiver distances where the phase errors are larger. However this conclusion can only be made for static baselines under open sky. No significant ionospheric disturbances were encountered, so widelane could not be evaluated with phase errors exceeding half a cycle. Using widelane comes at a cost: positions derived from correct widelane fixes tend to be much less precise than when L1 or L2 are used.

Cycle slips: A higher frequency of cycle slips was found to negatively impact the actual success rate. This is expected because a cycle slip resets the corresponding ambiguity to a new value and shortens the available convergence time for that ambiguity. The geometry of the integer estimation problem is affected: a negative relationship was demonstrated between convergence time and ADOP. This result only applies for the foliage portion of the vehicle-to-vehicle test conducted herein. However this is also expected to be true under more severe signal environments.

The probability of cycle slip detection was also investigated. When used as an *a priori* indicator of reliability, it is similar to the predicted success rate but accepts less fixes in general (and consequently accepts less incorrect fixes).

6.2 Recommendations

In order to expand upon the results and conclusions derived from this thesis, the following recommendations are made:

1. The hardware used in this thesis is geodetic-grade and is calibrated to minimize GLONASS inter-frequency biases. The effect of those inter-frequency biases can exceed one half-cycle and should be investigated with lower-quality receivers.
2. The testing scenarios can be expanded. Reduced satellite visibility was investigated using a 30° circular elevation mask, and overhead foliage was used to investigate cycle slips. An environment that induces multipath and lower signal strength could be investigated.
3. The analysis of the effect of phase errors in this thesis can be expanded. Single- and dual-frequency solutions can be analyzed over a number of inter-receiver distances and under different ionospheric conditions to validate and/or update the findings described in this thesis. Ionospheric effects can potentially be investigated during the next two years as the sunspot number increases.

4. An analysis of the effect of convergence time should be done. In this thesis convergence times were chosen such that there would be enough incorrect fixes to analyze. Convergence times can be added as a variable in the analysis of (for instance) the rate of incorrect fix acceptance for the predicted success rate and the F-test.

References

- Boriskin, A. and G. Zyryanov (2008). "Algorithms to Calibrate and Compensate for GLONASS Biases in GNSS RTK Receivers Working with 3rd Party Networks", in *Proceedings of ION GNSS 2008*, September 16-19, Savannah, GA, pp. 376-384.
- Chen, D., and G. Lachapelle (1995). "A Comparison of the FASF and Least-Squares Search Algorithms for Ambiguity Resolution On The Fly", in *Navigation*, vol. 42, no. 2, pp. 371-390.
- Conley, R., R. Cosentino, C. J. Hegarty, E. D. Kaplan, J. L. Leva, M. U. de Haag and K. Van Dyke (2006). "Performance of Stand-Alone GPS", chapter 7 in *Understanding GPS Principles and Applications*, 2nd edition, Kaplan, E. D. and Hegarty, C. J., ed. Artech House, Norwood MA.
- Cosentino, R. J., D. W. Diggle, M. U. de Haag, C. J. Hegarty, D. Milbert and J. Nagle (2006). "Differential GPS", chapter 8 in *Understanding GPS Principles and Applications*, 2nd edition, Kaplan, E. D. and Hegarty, C. J., ed. Artech House, Norwood MA.
- Counselman, C. C. and S. A. Gourevitch (1981). "Miniature Interferometer Terminals for Earth Surveying: Ambiguity and Multipath with Global Positioning System", in *IEEE Transactions on Geoscience and Remote Sensing*, vol. GE-19, no. 4, pp. 244-252.
- Euler H. J. and B. Schaffrin (1990) "On a Measure of the Discernibility between Different Ambiguity Solutions in the Static-Kinematic GPS-Mode", in *IAG*

- Symposium No. 107, Kinematic Systems in Geodesy, Surveying, and Remote Sensing*, September 10-13, Banff, AB, pp 285-295.
- Fenton, P. and J. Jones (2005). “The Theory and Performance of NovAtel Inc.’s Vision Correlator” in *Proceedings of ION GNSS 2005*, September 13-16, Long Beach, CA, Institute of Navigation, pp. 2178-2186.
- Frei, E. and G. Beutler (1990). “Rapid Static Positioning Based on the Fast Ambiguity Resolution Approach ‘FARA’: Theory and First Results”, in *Manuscripta Geodaetica*, vol. 15, pp. 325-356.
- Habrich, H., Beutler, G., Gurtner, W. and Rothacher, M. (1999). “Double Difference Ambiguity Resolution for GLONASS/GPS Carrier Phase”, in *Proceedings of ION GPS 1999*, September 14-17, Nashville, TN, Institute of Navigation, pp. 1609-1618.
- Han, S. and C. Rizos (1996). “Integrated Method for Instantaneous Ambiguity Resolution Using New Generation GPS Receivers”, in *IEEE Position, Location and Navigation Symposium (PLANS) 1996*, April 22-26, Atlanta, GA, pp. 254-261.
- Keong, J. H. and G. Lachapelle (2000). “Heading and Pitch Determination Using GPS/GLONASS”, in *GPS Solutions*, vol. 3, no. 3, pp. 26-36.
- Kozlov, D. and M. Tkachenko (1998). “Centimeter-Level Real-Time Kinematic Positioning with GPS + GLONASS C/A Receivers”, in *Navigation*, vol. 45, no. 2, pp. 137-147.
- Kozlov, D., M. Tkachenko and A. Tochilin (2000). “Statistical Characterization of Hardware Biases in GPS+GLONASS Receivers”, in *Proceedings of ION GPS 2000*, September 19-22, Salt Lake City, UT, pp. 817-826.

- Lachapelle, G. (2008). *Advanced GNSS Theory and Applications*. ENGO 625 lecture notes, Department of Geomatics Engineering, University of Calgary.
- Lachapelle, G., A. Morrison and R. Ong (2009). "Ultra-Precise Sport Positioning for Sport Applications", in *Proceedings of the 13th International Association of Institutes of Navigation*, October 27-30, Stockholm, Sweden, 11 pages.
- Landau, H. and H. J. Euler (1992). "On-the-Fly Ambiguity Resolution for Precise Differential Positioning", in *Proceedings of ION GPS 1992*, September 16-18, Albuquerque, NM, pp. 607-613.
- Leick, A. (2004). *GPS Satellite Surveying*. 3rd edition, John Wiley and Sons, Hoboken, NJ.
- Leick, A. (1998). "GLONASS Satellite Surveying", in *Journal of Surveying Engineering*, vol. 124, no. 2, pp. 91-99.
- Leick, A., J. Beser, P. Rosenboom and B. Wiley (1998). "Assessing GLONASS Observation", in *Proceedings of ION GPS 1998*, September 15-18, Nashville, TN, pp. 1605-1612.
- Mader, G. L. (1992). "Rapid Static and Kinematic Global Positioning System Solutions Using the Ambiguity Function Technique", in *Journal of Geophysical Research*, vol. 97, no. B3, pp. 3271-3283.
- O'Keefe, K., M. G. Petovello, W. Cao, G. Lachapelle and E. Guyader (2009). "Comparing of Multi-Carrier Ambiguity Resolution Methods for Geometry-Based GPS and Galileo Low Earth Orbiting Satellite Attitude Determination", in *International Journal of Navigation and Observation*, volume 2009, article ID 592073, 15 pages.

- O'Keefe, K., M. G. Petovello, G. Lachapelle and M. E. Cannon (2006). "Assessing Probability of Correct Ambiguity Resolution in the Presence of Time Correlated Errors", in *Navigation*, vol. 53, no. 4, pp. 269-282.
- Petovello, M. G. (2003). "Real-Time Integration of a Tactical-Grade IMU and GPS for High-Accuracy Positioning and Navigation". PhD thesis, Report 20173, Department of Geomatics Engineering, University of Calgary, Calgary, Canada.
- Rossbach, U. (2000). "GLONASS Double Difference Ambiguity Resolution in Real-Time" in *Proceedings of ION GPS 2000*, September 19-22, Salt Lake City, UT, pp. 163-171.
- Space Weather Canada (2009). "Indices", retrieved on May 26, 2010 from <http://www.spaceweather.gc.ca/si-eng.php>.
- Takac, F. (2009). "GLONASS inter-frequency biases and ambiguity resolution", in *Inside GNSS*, vol. 2, no. 4, March/April 2009, pp. 24-28.
- Teunissen, P. J. G. (2003). "Towards a Unified Theory of GNSS Ambiguity Resolution", in *Journal of Global Positioning Systems*, vol. 2, no. 1, pp. 1-12.
- Teunissen, P. J. G. (2001a). "Statistical GNSS Carrier Phase Ambiguity Resolution: A Review", in *Proceedings of the 11th IEEE Signal Processing Workshop on Statistical Signal Processing (2001)*, August 6-8, Singapore, Japan, pp. 4-12.
- Teunissen, P. J. G. (2001b). "Integer Estimation in the Presence of Biases", in *Journal of Geodesy*, vol. 75, nos. 7-8, pp. 399-407.
- Teunissen, P. J. G. (2000a). "The success rate and precision of GPS ambiguities", in *Journal of Geodesy*, vol. 74, nos. 3-4, pp. 321-326.

- Teunissen, P. J. G. (2000b). "The GPS Integer Least-Squares Statistics" in *Physics and Chemistry of the Earth, Part A: Solid Earth and Geodesy*, vol. 25, nos. 9-11, pp. 673-677.
- Teunissen, P. J. G. (1998). "Success probability of integer GPS ambiguity rounding and bootstrapping", in *Journal of Geodesy*, vol. 72, no. 10, pp. 606-612.
- Teunissen, P. J. G. (1995). "The Least-Squares Ambiguity Decorrelation Adjustment: A Method for Fast GPS Integer Ambiguity Estimation", in *Journal of Geodesy*, vol. 70, nos. 1-2, pp. 65-82.
- Teunissen, P. J. G. and S. Verhagen (2004). "On the Foundation of the Popular Ratio Test for GNSS Ambiguity Resolution", in *Proceedings of ION GNSS 2004*, September 21-24, Long Beach, CA, pp. 2529-2540.
- Teunissen, P. J. G., P. Joosten and D. Odijk (1999). "The Reliability of GPS Ambiguity Resolution", in *GPS Solutions*, vol. 2, no. 3, pp. 63-69.
- USNOAA – United States National Oceanic and Atmospheric Administration (2005). "NOAA Space Weather Scales", retrieved on May 26, 2010 from <http://www.swpc.noaa.gov/NOAAscales/index.html>.
- Van Diggelen, F. (1997). "GPS and GPS+GLONASS RTK", in *Proceedings of ION GPS 1997*, September 16-19, Kansas City, MO, pp. 139-144.
- Verhagen, S. (2005). "On the Reliability of Ambiguity Resolution", in *Navigation*, vol. 52, no. 2, pp. 99-110.
- Verhagen, S. (2004). "Integer Ambiguity Validation: An Open Problem?", in *GPS Solutions*, vol. 8, no. 1, pp. 36-43.

Wang, J. (2000). "An Approach to GLONASS ambiguity resolution", in *Journal of Geodesy*, vol. 74, no. 5, July 2000, pp. 421-430.

Yang, Y., R. T. Sharpe and R. R. Hatch (2006). "A Fast Ambiguity Resolution Technique for RTK Embedded Within a GPS Receiver". NavCom Technology white paper, October 2006, retrieved on April 25, 2010 from
<http://www.navcomtech.com/Support/DownloadCenter.cfm?category=whitepapers>.